63

403

KIEL, Otis Gerald, 1931–
THEORETICAL INVESTIGATION OF GAS WELL TRANSIENT PHENOMENA AND ITS EFFECTS ON CONVENTIONAL WELL-TEST DATA INTERPRETATIONS.

The University of Oklahoma, Ph.D., 1963
Engineering, general

University Microfilms, Inc., Ann Arbor, Michigan

THE UNIVERSITY OF OKLAHOMA

GRADUATE COLLEGE

THEORETICAL INVESTIGATION OF GAS WELL TRANSIENT PHENOMENA AND ITS EFFECTS ON CONVENTIONAL WELL-TEST DATA INTERPRETATIONS

A DISSERTATION

SUBMITTED TO THE GRADUATE FACULTY

in partial fulfillment of the requirements for the

degree of

DOCTOR OF PHILOSOPHY

BY

OTIS GERALD KIEL

Norman, Oklahoma

1963

THEORETICAL INVESTIGATION OF GAS WELL TRANSIENT

PHENOMENA AND ITS EFFECTS ON CONVENTIONAL

WELL-TEST INTERPRETATIONS

APPROVED BY

J. Campbell

S. D. Christian

F. M. Townsend

William C. Orthwein

R. V. Andree

DISSERTATION COMMITTEE

ACKNOWLEDGMENT

Special appreciation is expressed to Dr. John M. Campbell for serving as research director during this work.

Particular thanks are due John N. Dew and George C. Clark, Continental Oil Company, Ponca City, Oklahoma, for their guidance.

The author gratefully acknowledges the management of Continental for providing support of the thesis work and permission to release portions of the work included.

Financial support for the work on campus was furnished by the Phillips Petroleum Company. With this aid and that furnished under the Veterans' G.I. Bill, this work was made possible.

The author is indebted to his family for their patient endurance.

Otis Gerald Kiel

TABLE OF CONTENTS

Page

LIST OF TABLES

LIST OF ILLUSTRATIONS

Figure | Page

THEORETICAL INVESTIGATION OF GAS WELL TRANSIENT PHENOMENA AND ITS EFFECTS ON CONVENTIONAL WELL-TEST DATA INTERPRETATIONS

CHAPTER I

INTRODUCTION AND PROBLEM FORMULATION

There has been considerable effort expended in the development of multi-dimensional mathematical reservoir models. (11,12,13,16, 19,23,29,33,34,35,40,43) Nevertheless, no work has been published wherein an adequate description for the area in the immediate vicinity of the wellbore and its effects on transient behavior has been included. More recent studies (19,29,34) have included two uniform layers of different permeabilities for studying the effects of crossflow in a single-well model. However, the authors limited their analyses to open-hole completions with a constant terminal pressure as the wellbore boundary condition. Multiple-layer reservoirs have been studied through use of a heat model (30); however, this work was also limited to analogies for open-hole completions and uniform permeabilities within each layer.

Limited analyses of cased-hole completions wherein a short interval is opened for production have been presented for homogeneous formations. (3,15,26) Attempts at describing flow in fractured systems have been restricted to steady-state solutions (16) or one-dimensional analysis where the fracture is described as a zone of ultra-high conductivity. (44)

The purpose of this investigation is three-fold. First, we intend to develop a two-dimensional mathematical model for unsteady-state isothermal gas flow that is capable of including detailed descriptions of the localized reservoir geometry about any individual well. These descriptions will include such details as the conductivity, radial extent and vertical location of a horizontal fracture; length and location of the completion interval; and, unrestricted radial and vertical permeability distributions. Second, we intend to use the model to show the effects of this geometry on the pressure calculations for any predetermined production rate schedule. Particular emphasis will be placed on how this geometry affects our data interpretations of short-term flow tests for gas wells. Sample calculations for other pertinent reservoir problems will also be presented. Finally, through the study of these more sophisticated calculations, we hope to better define the limitations and/or the utility of one-dimensional analysis as it is currently used.

An increasing number of reservoirs having very low permeabilities are being found. As our technology on well stimulation has improved, it has become economically feasible to produce these reservoirs. Along with our ability to produce tight reservoirs, we must be capable of making accurate predictions about their behavior. This capability is extremely important in the economic evaluation that serves as a basis for decision-making on additional investments; in the contractual arrangements for selling the gas (producer-pipeline regulatory requirements); and in the physical system design to process and transport the gas. Although much work has been done in this area and several interpretative schemes have been presented in the literature (8,31,32, 36), none are entirely satisfactory as witnessed by the continued effort toward refinement of existing techniques. (5,6,18,36,37)

The first widely used predictive technique was developed by Rawlins and Schellhardt and is known as the back-pressure or flow-after-flow test. (32) This method is based on obtaining stabilized flow at successively larger flow rates in order to determine the coefficients C_1 and n_p of the empirical equation:

$$Q = C_1 \left(P_d^2 - P_w^2 \right)^{n_p} \tag{1}$$

The time duration for a well to stabilize in low-permeability reservoirs is measured in days or months in many instances. Therefore, this method of back-pressure testing is often unsatisfactory for analyzing data from this category of wells. (8,31,36) The uninterrupted changing of rates, excluding the short time interval for changing orifice plates, results in the creation of complex gradients which do not dampen out rapidly. (36) Accounting for these complex gradients exceeds the capabilities of the back-pressure method.

Generally speaking, the back-pressure method has been replaced by isochronal testing (8) in low-permeability reservoirs. This method is based on the premise that the transient or radius of drainage (1) moves radially outward at the same speed regardless of the producing rate. Also, the pressure gradient must be a simple one unencumbered by the super-positioning of transient effects from multiple rates. A period of no-flow is required wherein the pressure builds back to its original value, between changes in flow rate. Previous work (8,31,38) has shown that the coefficient C_1 in equation (1) varies with time until the well stabilizes and remains constant thereafter. It has also been shown with the isochronal testing that C_1 is constant at any particular time and independent of rate. A well-known method for predicting the stabilized value of coefficient C_1 from short-term test data is now widely used. (31) Although it seemingly provides a sound basis for short-term test interpretation, experience has shown that this method is not entirely satisfactory.

When the formation permeability is very low, well test periods of a few hours duration provide us with an even more limited insight into the properties of the producing formation. By analyzing Aronofsky and Jenkins' (1) equation expressing the radius of drainage as a function of time, we see that as the permeability decreases the radius of drainage moves more slowly. Under these conditions, the results of our short-term test interpretations are flow-capacity values based on a smaller sampling of the reservoir. The confidence limits for using this data as representative of the entire drainage area are necessarily much lower. We know that longer test periods will provide better data because of the increased areal "insight" into the formation properties. However, the most important testing usually occurs in the early life of the well before pipeline connections are available, which requires the venting of gas. Economics as well as conservation dictates that the duration of flow tests made under these circumstances be limited to the minimum time required to obtain reliable data.

Because of the slowly moving transients in low permeability reservoirs, we are measuring in situ properties of a very limited area in the immediate vicinity of the wellbore. Through knowledge of the usual existence of permeability stratifications and varieties of well completion and stimulation practices, we sense the need for a more definitive model to describe the effects of this area. While improvements to the original one-dimensional model (including variable compressibility and viscosity and accounting for non-Darcy flow) have increased the accuracy of the resulting predictions, the limits of sophistication are close, if not at hand. There is little possibility of improving the geometrical description of completion practices, variations in horizontal and vertical permeability, and well stimulation techniques over the presently used zone of increased (or decreased) permeability (or effective wellbore radius) without resorting to additional space dimensions. Currently, it is assumed that any such effects converge to an equivalent skin-effect value within the first few minutes of a test. There is a definite need for a model that will clarify the significance of these effects.

Suppose we examine a productive system consisting of different permeability layers with no vertical communication between them. (21) Then, for an open-hole completion where the entire interval is opened to flow, we would expect the radius of drainage to move at different speeds through the different layers. That is, at the time the drainage radius has reached an arbitrary radial distance r in the layer having the largest permeability, no layers of lower permeability would have experienced a pressure drop at that point. Now assume that a measurable vertical permeability exists between these layers. Then, once a pressure gradient is established in one layer at the point r, contiguous layers will start producing via crossflow. In turn, other contiguous layers will produce. For this case, it is apparent that the higher permeability layers act as carriers for some of the gas from the low permeability areas. Too, the gradients in the low permeability layers contiguous to high permeability layers move more rapidly than predicted through use of Aronofsky and Jenkins' equation because of the continuous initiation of crossflow along the high permeability layers. It is evident that the presence of vertical permeability tends to smooth out the irregular advance of the drainage radius.

Next, consider the same system completed by opening only a fraction of the total interval at the wellbore. Here a significant portion of the reserves must contribute to the production only by crossflow as no other mechanism or flow channel is available. Upon initiating production, the bulk of the gas must come from the layers in the opened interval. (3) Hence, the initial capacity would reflect only these layers. As the gradient moves outward, continguous intervals contribute to production as a result of the establishment of pressure gradients in the vertical direction at a rate dependent on the vertical permeability. These layers, in turn, establish horizontal gradients in those layers and vertical gradients with more remote contiguous layers. The two components of the pressure gradient will move radially outward and vertically upward and downward.

Obviously, we cannot hope that our one-dimensional analysis, wherein we attempt to describe the pressure behavior with only a radial component, will accurately describe this period of the flow regime.

In the higher permeability formations we depended upon the disappearance of these effects in a very short time. In moderately thick low-permeability reservoirs containing fractures, this time period may extend beyond the time limits currently used for obtaining well-test information. Therefore, in the interest of a more enlightened interpretation of the various contributing factors to the measured pressure behavior, we are most interested in developing a model to account for variable permeability distributions in the immediate vicinity of the wellbore. Further, we want to be able to better describe the effects of having either the entire producing formation opened to flow, a partially penetrating well, or a cased hole with a single-plane fracture or perforated interval. It is necessary to know the limiting horizontal-to-vertical permeability ratio where cross-flow continues as a significant contributor to the flow mechanism in order to decide whether it is better to obtain a single-plane fracture or multiple fractures of smaller size, or whether it is necessary to perforate very low permeability sections within a heterogeneous formation in order to effectively drain them.

The ability to describe fractures as localized areas of extraordinarily high permeability should give us more information on the importance of getting very high capacity fractures such as those propped by a partial monolayer. (9) For example, if we have a 100 psi pressure drop across the entire face of the fracture and only a 5 psi drop within the fracture from its extremity to the wellbore, it is then apparent that we will not significantly increase the flow capacity of the system by reducing the pressure drop in the fracture to 1 psi. In artificially fractured systems, vertical permeability plays a very important role in the resulting system's efficiency because of the large surface area subject to vertical flow. If we can show that a fracture of 25-foot radius will provide the productive capacity required for permissible production with a reasonable margin of safety and show that a fracture twice as large does not improve performance substantially, we are then capable of optimizing fracture treatments for given producing conditions.

Finally, and most important, from a better understanding of the flow mechanisms described in two-dimensional analysis we may find the means to improve our current one-dimensional techniques. For example, it may tell us something of the time duration of flow tests and what data we can interpret using current techniques. This is the goal of the work to be presented.

CHAPTER II

THE MATHEMATICAL MODEL

In selecting a model, we shall restrict ourselves to a single well reservoir in order that a more detailed description of this localized area is possible. Consider a finite cylindrical reservoir having an outer boundary radius, r_e, and uniform height, H, with a producing well of radius, r_w, at its center. The equations necessary to describe gas flow in this system comes from invoking the principles of conservation of mass and momentum. The conservation of mass (continuity equation) expressed in cylindrical coordinates is:

$$\frac{1}{r}\frac{\partial}{\partial r}(\gamma r \bar{V}_r) + \frac{1}{r}\frac{\partial}{\partial \theta}(\gamma \bar{V}_\theta) + \frac{\partial}{\partial z}(\gamma \bar{V}_z) = -\phi \frac{\partial \gamma}{\partial t} \qquad (2)$$

The equation of motion which serves as a macroscopic expression for the conservation of momentum is Darcy's Law. Neglecting gravitational forces, it may be written:

$$\bar{V} = -\frac{k}{\mu}\nabla P$$

$$\bar{V} = \bar{V}_r + \bar{V}_\theta + \bar{V}_z$$

where:

$$\bar{V}_r = -\frac{k_r}{\mu}\frac{\partial P}{\partial r}$$

$$\bar{V}_\theta = -\frac{k_\theta}{\mu}\frac{\partial P}{\partial \theta}$$

$$\bar{V}_z = -\frac{k_z}{\mu}\frac{\partial P}{\partial z} \qquad (3)$$

Radial symmetry will be assumed; i.e., $\bar{V}_\theta = 0$. Combining equations (3) with equation (2) gives:

$$\frac{1}{r}\frac{\partial}{\partial r}\left(-\gamma r \frac{k_r}{\mu}\frac{\partial P}{\partial r}\right) + \frac{\partial}{\partial z}\left(-\gamma \frac{k_z}{\mu}\frac{\partial P}{\partial z}\right) = -\phi \frac{\partial \gamma}{\partial t} \quad (4)$$

By assuming the reservoir contains an ideal gas at constant temperature and has a viscosity, μ, independent of pressure, equation (4) becomes

$$\frac{1}{r}\frac{\partial}{\partial r}\left(r k_r \frac{\partial P^2}{\partial r}\right) + \frac{\partial}{\partial z}\left(k_z \frac{\partial P^2}{\partial z}\right) = 2\mu\phi \frac{\partial P}{\partial t} \quad (5)$$

Equation (5) is the differential equation for describing flow within the proposed model.

Coupled to this equation must be equations for describing flow conditions at the upper and lower boundaries, the outer drainage boundary, and the wellbore. Initial conditions must also be specified. At the upper and lower boundaries and the outer drainage boundary we assume no-flow conditions, i.e.,

$$\left(\frac{\partial P^2}{\partial z}\right)_{z=0,\, z=H} = 0$$
$$\left(\frac{\partial P^2}{\partial r}\right)_{r=r_e} = 0 \quad (6)$$

Boundary equations at the wellbore must properly describe flow and cased- or open-hole completions. Let h_1 be the top of the slot representing the opened producing interval and h_2 be the bottom. Then, all production will be from the interval h_1 - h_2 where

$$0 \le h_1 < h_2 \le H$$

This means that the interval opened to production can be anywhere from a small finite thickness corresponding to a single-plane fracture to the entire interval for representing open-hole completions. Because of the assumed radial symmetry, perforated intervals must be treated as opened-producing intervals having a special permeability function for simulating the flow mechanism. The boundary equations for this interval are:

$$\left.\begin{matrix} 0-h_1 \\ h_2-H \end{matrix}\right\} \quad \left(\frac{\partial P^2}{\partial r}\right)_{r=r_w} = 0$$

$$h_1-h_2 \begin{cases} q = (k_{r_w})_{h_1-h_2} \dfrac{2\pi r(h_2-h_1)}{\mu RT} P\dfrac{\partial P}{\partial r} \\ \text{or } P_{r_w}^2 = \text{CONSTANT} \end{cases} \tag{7}$$

It is easy to generalize this set of equations to include more than one interval, $h_1 - h_2$; however, this investigation is restricted to one interval. The initial conditions will be a uniform pressure over the entire drainage area:

$$P = P_0 \tag{8}$$

Permeability functions in the horizontal and vertical directions are represented respectively by k_r and k_z. Each may be expressed as a function of two dimensions

$$\begin{aligned} k_r &= f(r,z) \\ k_z &= g(r,z) \end{aligned} \tag{9}$$

In the model, these functions will be represented by a matrix of values located at each mid-point between pressure grid points as shown in Figure 2. Thus, formations having uniform permeability, stratified layers of different permeability, or pseudo-random permeability functions, may be simulated through the proper selection of model divisions and values assigned to the permeability matrix. Once these values are assigned, they remain unchanged throughout the calculations. There will be no assumptions made concerning these functions other than that they are everywhere non-negative, the first partials exist and are piecewise continuous, and higher-order derivatives may be neglected without causing serious error. We expect to describe flow through fractures by creating localized areas of extraordinarily high permeability, through damaged zones by creating localized areas of reduced permeability, through layered formations by assigning $k_r = f(\text{constant}, z)$, and production by crossflow through non-zero values of k_z.

There are no known analytical solutions to the most general form of the above-described system of equations. Therefore, we must resort to the application of numerical techniques to obtain approximate answers. To accomplish this, a rectangular grid network having equally-spaced points in each dimension, but with Δr not necessarily equal to Δz, is superimposed over a radial slice from our cylindrical model. A sample permeability distribution and wellbore completion geometry is shown in Figure 1. The boundaries of the system will occur at the mid-point between the pressure nodes in columns 1 and 2, rows 1 and 2, the lower-most 2 rows, and the outer-most two columns as shown in Figure 2. A finite-difference equation is written that approximates equation (5) for each interior grid point (i,j) in Figure 2. Other difference approximations representing the boundary equations (6) and (7) are written at each external grid point to complete the system of equations. Simultaneous solution of these equations for each time step through some computational scheme, wherein the error residuals are maintained at a satisfactory level, will provide an approximate solution.

We must wisely choose the location of the grid-points in our model through proper coordinate transformations or non-uniform grid network spacing because of the large number of points necessary to adequately describe this system in detail. Because of the more nearly logarithmic pressure distribution in the radial direction, the logarithmic transformation

$$V = \ln(r/r_e) \tag{10}$$

has been found to be most satisfactory as verified in one-dimensional model studies. (4,36) This transformation permits a clustering of the equally-spaced mesh points in the vicinity of the wellbore where the gradients are steepest. Substituting equation (10) into equation (5),

$$\frac{1}{r_e^2 e^{2v}} \frac{\partial}{\partial v}\left(k_v \frac{\partial P^2}{\partial v}\right) + \frac{\partial}{\partial z}\left(k_z \frac{\partial P^2}{\partial z}\right) = 2\phi\mu \frac{\partial P}{\partial t} \tag{11}$$

where k_v is assumed to represent the same surface as k_r but the matrix of values corresponds to different (v_i, z_j).

Careful consideration must be given to the objectives established for the model before selecting a useful transformation for the vertical dimension. For open-hole completions, a linear transformation should be quite satisfactory since we are interested only in a proper description of the permeability distribution. In this case, the number of model divisions would be governed by the variations found in the permeability distribution and the detailed description sought. This would correspond to the concept of layered zones of different permeability with one or more rows of matrix points representing each layer.

In fractured formations, a linear transformation has the disadvantage of not permitting the location of many grid points within the area of steepest gradients without having an unreasonable number of grid points. In the case of fractional-interval (slot) completions, the vertical pressure gradients would be more nearly logarithmic than linear so the linear transformation would make the problem of finding a convergent iterative scheme more difficult. On the other hand a logarithmic transformation would put more of the mesh points in the immediate area of the fracture. However, this transformation seemingly creates more problems than it solves. The logarithmic transformation would require that three model segments be tied together; one describing the fractured area; the others describing the areas above and below the fracture. In order to calculate the effects of moving the vertical location of the fracture upon the production efficiency, some method, presently considered unjustifiably complicated, would have to be devised to insure the equivalent native formation permeability in each set of calculations for comparative purposes. This would be extremely difficult for all but the uniform permeability matrix. Since we are interested in alternative type completion comparisons, the choice was a linear transformation

$$y = z/H$$

Then equation (11) becomes

$$\frac{1}{r_a^2 e^{2v}} \frac{\partial}{\partial v}\left(k_v \frac{\partial P^2}{\partial v}\right) + \frac{1}{H^2}\frac{\partial}{\partial y}\left(k_y \frac{\partial P^2}{\partial y}\right) = 2\phi\mu \frac{\partial P}{\partial t} \tag{12}$$

Normalize the variables to form a dimensionless equation by multiplying both sides of equation (12) by the factor (1 ft^2) and letting

$$\begin{aligned} P &= P/P_o \\ K_v &= k_v/K_{AVG} \\ K_y &= k_y/K_{AVG} \\ \theta &= \frac{P_o K_{AVG}\, t}{2\phi\mu} \end{aligned} \tag{13}$$

Substitution in equation (12) gives the differential equation in final normalized form

$$\frac{1}{r_e^2 e^{2v}} \frac{\partial}{\partial v}\left(K_v \frac{\partial P^2}{\partial v}\right) + \frac{1}{H^2}\frac{\partial}{\partial y}\left(K_y \frac{\partial P^2}{\partial y}\right) = \frac{\partial P}{\partial \theta} \tag{14}$$

The transformed boundary equations are:

upper boundary: $$\left(\frac{\partial P^2}{\partial y}\right)_{y=0} = 0$$

lower boundary: $$\left(\frac{\partial P^2}{\partial y}\right)_{y=1} = 0$$

drainage radius: $$\left(\frac{\partial P^2}{\partial v}\right)_{v=0} = 0$$

wellbore:

$$\left.\begin{matrix} 0-y_1 \\ y_2-1 \end{matrix}\right\} \left(\frac{\partial P^2}{\partial v}\right)_{v=\ln r_w/r_e} = 0$$

$$y_1 - y_2 \quad (K_v)_{y_1-y_2}\left(\frac{\partial P^2}{\partial v}\right) = \frac{\bar{Q}}{2} \tag{15}$$

where:

$$\bar{Q} = \frac{2q\mu RT}{\pi P_0^2 K_{AVG}(h_2-h_1)} \tag{16}$$

An enormous amount of work was expended in trying to find a satisfactory iterative scheme to approximate the solution of this system of equations. Literature investigations revealed a lack of published information on the solution of difference equations for multi-dimensional systems in cylindrical coordinates. Although casual reference to this problem was made in one paper (12), the published work has been for Cartesian coordinate systems. (2,7,10,11,14,28,42) A satisfactory scheme is defined here as one that will remain stable with increasing time steps, and one that can provide a reliable answer in an <u>economical amount</u> of computer time. Additionally, much effort was expended in obtaining satisfactory finite-difference approximations that would account for the wide variations in coefficients encountered in describing flow through fractured systems. The presentation in this chapter is limited to the final results obtained both for the difference equations developed and the iterative scheme used. A discussion of some of the less successful efforts may be found in Appendix A.

We shall assume the pressure function throughout the region in question to be analytic and, therefore, can be represented by a convergent power series about any mesh point, (i,j). The general formulation of Taylor's expansion (20) in two dimensions is:

$$
\begin{aligned}
P^2(v,y) = {} & P^2_{i,j} + \left(\frac{\partial P^2}{\partial v}\right)_{i,j} \Delta v + \left(\frac{\partial P^2}{\partial y}\right)_{i,j} \Delta y + \frac{1}{2!}\left[\left(\frac{\partial^2 P^2}{\partial v^2}\right)_{i,j} \overline{\Delta v}^2 \right. \\
& \left. + 2\left(\frac{\partial^2 P^2}{\partial v \partial y}\right)_{i,j} \Delta v \Delta y + \left(\frac{\partial^2 P^2}{\partial y^2}\right)_{i,j} \overline{\Delta y}^2\right] + \frac{1}{3!}\left[\left(\frac{\partial^3 P^2}{\partial v^3}\right)_{i,j} \overline{\Delta v}^3 \right. \\
& \left. + \left(\frac{\partial^3 P^2}{\partial v^2 \partial y}\right)_{i,j} \overline{\Delta v}^2 \Delta y + \left(\frac{\partial^3 P^2}{\partial v \partial y^2}\right)_{i,j} \Delta v \overline{\Delta y}^2 + \left(\frac{\partial^3 P^2}{\partial y^3}\right)_{i,j} \overline{\Delta y}^3\right] \\
& + \cdots\cdots + \frac{1}{n!}\left[\left(\frac{\partial^n P^2}{\partial v^n}\right)_{i,j} \overline{\Delta v}^n + \left(\frac{\partial^n P^2}{\partial v^{n-1} \partial y}\right)_{i,j} \overline{\Delta v}^{n-1} \Delta y \right. \\
& \left. + \cdots\cdots + \left(\frac{\partial^n P^2}{\partial v \partial y^{n-1}}\right)_{i,j} \Delta v \overline{\Delta y}^{n-1} + \left(\frac{\partial^n P^2}{\partial y^n}\right)_{i,j} \overline{\Delta y}^n\right] + R_m \qquad (17)
\end{aligned}
$$

where R_m is the remainder term. In this rectangular grid network system, we will restrict ourselves to a selection of pressures from eight neighboring points in order to evaluate the function at any point. For the (i,j) mesh point, these would be (i,j+1), (i,j-1), i+1,j), (i-1,j), (i+1,j+1), (i-1,j+1), (i+1,j-1), and (i-1,j-1). When using the first four points, the product $(\Delta v)^m(\Delta y)^{n-m}$ is zero. Then equation (17) reduces to

$$P^2(v,y) = P^2_{i,j} + \left(\frac{\partial P^2}{\partial v}\right)_{i,j}\Delta v + \left(\frac{\partial P^2}{\partial y^2}\right)_{i,j}\Delta y + \frac{1}{2!}\left[\left(\frac{\partial^2 P^2}{\partial v^2}\right)_{i,j}\overline{\Delta v}^2 + \left(\frac{\partial^2 P^2}{\partial y^2}\right)_{i,j}\overline{\Delta y}^2\right] + \frac{1}{3!}\left[\left(\frac{\partial^3 P^2}{\partial v^3}\right)_{i,j}\overline{\Delta v}^3 + \left(\frac{\partial^3 P^2}{\partial y^3}\right)_{i,j}\overline{\Delta y}^3\right]$$

$$+ \cdots + \frac{1}{n!}\left[\left(\frac{\partial^n P^2}{\partial v^n}\right)_{i,j}\overline{\Delta v}^n + \left(\frac{\partial^n P^2}{\partial y^n}\right)_{i,j}\overline{\Delta y}^n\right] + R_m \qquad (18)$$

We can write these equations. First in the y-direction ($\Delta v = 0$)

$$P^2_{i+1,j} = P^2_{i,j} + \left(\frac{\partial P^2}{\partial y}\right)_{i,j}\Delta y + \left(\frac{\partial^2 P^2}{\partial y^2}\right)_{i,j}\frac{\overline{\Delta y}^2}{2!} + \left(\frac{\partial^3 P^2}{\partial y^3}\right)_{i,j}\frac{\overline{\Delta y}^3}{3!} + \cdots\cdots \qquad (19)$$

$$P^2_{i-1,j} = P^2_{i,j} - \left(\frac{\partial P^2}{\partial y}\right)_{i,j}\Delta y + \left(\frac{\partial^2 P^2}{\partial y^2}\right)_{i,j}\frac{\overline{\Delta y}^2}{2!} - \left(\frac{\partial^3 P^2}{\partial y^3}\right)_{i,j}\frac{\overline{\Delta y}^3}{3!} + \cdots\cdots \qquad (20)$$

and then in the v-direction ($\Delta y = 0$)

$$P^2_{i,j+1} = P^2_{i,j} + \left(\frac{\partial P^2}{\partial v}\right)_{i,j}\Delta v + \left(\frac{\partial^2 P^2}{\partial v^2}\right)_{i,j}\frac{\overline{\Delta v}^2}{2!} + \left(\frac{\partial^3 P^2}{\partial v^3}\right)_{i,j}\frac{\overline{\Delta v}^3}{3!} + \cdots\cdot \qquad (21)$$

$$P^2_{i,j-1} = P^2_{i,j} - \left(\frac{\partial P^2}{\partial v}\right)_{i,j}\Delta v + \left(\frac{\partial^2 P^2}{\partial v^2}\right)_{i,j}\frac{\overline{\Delta v}^2}{2!} - \left(\frac{\partial^3 P^2}{\partial v^3}\right)_{i,j}\frac{\overline{\Delta v}^3}{3!} + \cdots\cdot \qquad (22)$$

The number of terms used in the Taylor's expansion as shown in equation (19) to (22) will determine the magnitude of the truncation error. However, every additional higher-order derivative will require several additional pressure points for a central-difference approximation in order to evaluate the function at the (i,j)th mesh point. Therefore, in the interest of keeping this number of pressure points at a minimum, we want to express the higher-order derivatives in terms of spatial derivatives of the time derivative. After a few attempts (see Appendix A) at developing a finite-difference equation for equation (14), we assumed there exists a function (or constant), σ, that is independent of v and y such that equation (14) can be separated into two equations whose sum is equal to equation (14). The equations are

$$\frac{1}{r_e^2 e^{2v}} \frac{\partial}{\partial v}\left(K_v \frac{\partial P^2}{\partial v}\right) = \sigma \frac{\partial P}{\partial \theta} \tag{23}$$

$$\frac{1}{H^2} \frac{\partial}{\partial y}\left(K_y \frac{\partial P^2}{\partial y}\right) = (1-\sigma) \frac{\partial P}{\partial \theta} \tag{24}$$

First, consider equation (24). Utilizing the assumptions made about K_y, this equation may be written in its expanded form

$$\left(\frac{\partial K_y}{\partial y}\right) \frac{\partial P^2}{\partial y} + K_y \frac{\partial^2 P^2}{\partial y^2} = H^2 (1-\sigma) \frac{\partial P}{\partial \theta} \tag{25}$$

The general form for the (n-2) partial differential of equation (24) is:

$$(n-1)\left(\frac{\partial^{n-1} P^2}{\partial y^{n-1}}\right)\left(\frac{\partial K_y}{\partial y}\right) + K_y \left(\frac{\partial^n P^2}{\partial y^n}\right) = H^2 (1-\sigma) \frac{\partial^{n-1} P}{\partial y^{n-2} \partial \theta} \tag{26}$$

Upon multiplying equation (19) by $K_{y_{i+1/2,j}}$ and equation (20) by $K_{y_{i-1/2,j}}$, adding the results together, and evaluating the derivatives at the point (i,j), we get:

$$\begin{aligned} K_{y_{i+\frac{1}{2},j}}\left(P^2_{i+1,j} - P^2_{i,j}\right) + K_{y_{i-\frac{1}{2},j}}\left(P^2_{i-1,j} - P^2_{i,j}\right) &= \Big(K_{y_{i+\frac{1}{2},j}} \\ - K_{y_{i-\frac{1}{2},j}}\Big)\left[\left(\frac{\partial P^2}{\partial y}\right)_{i,j} \Delta y + \left(\frac{\partial^3 P^2}{\partial y^3}\right)_{i,j} \frac{\overline{\Delta y}^3}{3!} + \cdots\right] &+ \Big(K_{y_{i+\frac{1}{2},j}} \\ + K_{y_{i-\frac{1}{2},j}}\Big)\left[\left(\frac{\partial^2 P^2}{\partial y^2}\right)_{i,j} \frac{\overline{\Delta y}^2}{2!} + \left(\frac{\partial^4 P^2}{\partial y^4}\right)_{i,j} \frac{\overline{\Delta y}^4}{4!} + \cdots\right] \end{aligned} \tag{27}$$

Then, by recognizing that

$$\left(\frac{\partial K_y}{\partial y}\right)_{i,j} \cong \left(\frac{K_{y_{i+\frac{1}{2},j}} - K_{y_{i-\frac{1}{2},j}}}{\Delta y}\right) \tag{28}$$

and

$$(K_y)_{i,j} \cong \frac{1}{2}\left(K_{y_{i+\frac{1}{2},j}} + K_{y_{i-\frac{1}{2},j}}\right) \tag{29}$$

and combining the terms on the right side of equation (27) according to equation (26), we get

$$\frac{1}{H^2 \overline{\Delta y}^2}\left[K_{y_{i+\frac{1}{2},j}}\left(P^2_{i+1,j}-P^2_{i,j}\right)+K_{y_{i-1/2,j}}\left(P^2_{i-1,j}-P^2_{i,j}\right)\right]$$
$$=(1-\sigma)\left[\left(\frac{\partial P}{\partial \theta}\right)_{i,j}+\left(\frac{\partial^3 P}{\partial y^2 \partial \theta}\right)_{i,j}\frac{\overline{\Delta y}^2}{12}\right] \tag{30}$$

by neglecting fifth and higher order partial derivatives and the remainder term

$$\frac{1}{2}\left(K_{y_{i+1/2,j}}-K_{y_{i-1/2,j}}\right)\left(\frac{\partial^3 P^2}{\partial y^3}\right)_{i,j}\frac{\overline{\Delta y}^3}{3!} \tag{31}$$

The left-hand member of equation (30) is equivalent to the central difference approximation for the left-hand member of equation (24). The additional term on the right comes from a higher-order approximation through the utilization of fourth-order partial derivatives. By approximating the remaining derivatives in equation (30) with the equations:

$$\left(\frac{\partial P}{\partial \theta}\right)_{i,j} = \left(P_{i,j,n+1}-P_{i,j,n}\right)/\Delta\theta \tag{32}$$

$$\left(\frac{\partial^3 P}{\partial y^2 \partial \theta}\right)_{i,j} = \left[\left(P_{i+1,j,n+1}-2P_{i,j,n+1}+P_{i-1,j,n+1}\right)-\left(P_{i+1,j,n}\right.\right.$$
$$\left.\left.-2P_{i,j,n}+P_{i-1,j,n}\right)\right]/\overline{\Delta y}^2\Delta\theta \tag{33}$$

the finite difference approximation to equation (24) becomes

$$\frac{1}{H^2 \overline{\Delta y}^2}\left[K_{y_{i+1/2,j}}\left(P^2_{i+1,j}-P^2_{i,j}\right)+K_{y_{i-1/2,j}}\left(P^2_{i-1,j}-P^2_{i,j}\right)\right]$$
$$=\left(\frac{1-\sigma}{\Delta\theta}\right)\left\{P_{i,j,n+1}-P_{i,j,n}+\frac{1}{12\overline{\Delta y}^2}\left[\left(P_{i+1,j,n+1}-2P_{i,j,n+1}\right.\right.\right.$$
$$\left.\left.\left.+P_{i-1,j,n+1}\right)-\left(P_{i+1,j,n}-2P_{i,j,n}+P_{i-1,j,n}\right)\right]\right\} \tag{34}$$

Next, consider equation (23). The expanded form of this equation for the (n-2) partial differentiation is obtained by neglecting terms $\frac{\partial^m p}{\partial y^{m-1}\partial\theta}$, where $m > 3$, is

$$(n-1)\left(\frac{\partial^{n-1}P^2}{\partial v^{n-1}}\right)\left(\frac{\partial K_v}{\partial v}\right) + K_v\frac{\partial^n P^2}{\partial v^n} = \sigma r_e^2 e^{2v}\Big[2^{n-2}\frac{\partial P}{\partial \theta}$$

$$+ 2^{n-3}(n-2)\frac{\partial^2 P}{\partial v \partial \theta} + 2^{n-5}(n-2)(n-3)\frac{\partial^3 P}{\partial v^2 \partial \theta}\Big] \qquad (35)$$

If we multiply equation (21) by $Kv_{i,j+1/2}$, equation (22) by $Kv_{i,j-1/2}$ and add them together, we get

$$Kv_{i,j+\frac{1}{2}}(P^2_{i,j+1} - P^2_{i,j}) + Kv_{i,j-\frac{1}{2}}(P^2_{i,j-1} - P^2_{i,j}) = \Big(Kv_{i,j+\frac{1}{2}}$$

$$+ Kv_{i,j-\frac{1}{2}}\Big)\Big[\left(\frac{\partial^2 P^2}{\partial v^2}\right)_{i,j}\frac{\overline{\Delta v}^2}{2!} + \left(\frac{\partial^4 P^2}{\partial v^4}\right)_{i,j}\frac{\overline{\Delta v}^4}{4!} + \left(\frac{\partial^6 P^2}{\partial v^6}\right)_{i,j}\frac{\overline{\Delta v}^6}{6!}$$

$$+ \left(\frac{\partial^8 P^2}{\partial v^8}\right)_{i,j}\frac{\overline{\Delta v}^8}{8!} + \cdots\Big] + \Big(Kv_{i,j+\frac{1}{2}} - Kv_{i,j-\frac{1}{2}}\Big)\Big[\left(\frac{\partial P^2}{\partial v}\right)_{i,j}\Delta v$$

$$+ \left(\frac{\partial^3 P^2}{\partial v^3}\right)_{i,j}\frac{\overline{\Delta v}^3}{3!} + \left(\frac{\partial^5 P^2}{\partial v^5}\right)_{i,j}\frac{\overline{\Delta v}^5}{5!} + \left(\frac{\partial^7 P^2}{\partial v^7}\right)_{i,j}\frac{\overline{\Delta v}^7}{7!} + \cdots\cdots\Big] \qquad (36)$$

Combine terms in equation (36) according to equation (35) by adding and subtracting terms to get equivalent values for n = 2,4,6,8. Then we get

$$Kv_{i,j+\frac{1}{2}}(P^2_{i,j+1} - P^2_{i,j}) + Kv_{i,j-\frac{1}{2}}(P^2_{i,j-1} - P^2_{i,j}) = \sigma r_e^2 e^{2v_i}\Big\{\left(\frac{\partial P}{\partial \theta}\right)_{i,j}\Delta v$$

$$+ \frac{\overline{\Delta v}^4}{12}\Big[4\left(\frac{\partial P}{\partial \theta}\right)_{i,j} + 4\left(\frac{\partial^2 P}{\partial v \partial \theta}\right)_{i,j} + \left(\frac{\partial^3 P}{\partial v^2 \partial \theta}\right)_{i,j}\Big] + \frac{1}{3}\left(\frac{\overline{\Delta v}^6}{5!}\right)\Big[16\left(\frac{\partial P}{\partial \theta}\right)_{i,j}$$

$$+ 32\left(\frac{\partial^2 P}{\partial v \partial \theta}\right)_{i,j} + 24\left(\frac{\partial^3 P}{\partial v^2 \partial \theta}\right)_{i,j}\Big] + \Big[64\left(\frac{\partial P}{\partial \theta}\right)_{i,j} + 192\left(\frac{\partial^2 P}{\partial v \partial \theta}\right)_{i,j}$$

$$+ 240\left(\frac{\partial^3 P}{\partial v^2 \partial \theta}\right)_{i,j}\Big]\left(\frac{\overline{\Delta v}^8}{7!}\right)/4 \quad + R_m \qquad (37)$$

where:

$$R_m = -\left(\frac{Kv_{i,j+\frac{1}{2}} - Kv_{i,j-\frac{1}{2}}}{\Delta v}\right)\Big[\frac{1}{2}\left(\frac{\partial^3 P^2}{\partial v^3}\right)_{i,j}\frac{\overline{\Delta v}^4}{3!} + \frac{2}{3}\left(\frac{\partial^5 P^2}{\partial v^5}\right)_{i,j}\frac{\overline{\Delta v}^6}{5!} + \frac{3}{4}\left(\frac{\partial^7 P^2}{\partial v^7}\right)_{i,j}\frac{\overline{\Delta v}^8}{7!}\Big] \qquad (38)$$

Then combine terms in R_m by adding and subtracting terms to get equivalent values for n = 3,5,7 in equation (35). R_m can be replaced by

$$R_m = -\frac{2\left(K_{v_{i,j+1/2}} - K_{v_{i,j-1/2}}\right)}{\Delta V\left(K_{v_{i,j+1/2}} + K_{v_{i,j-1/2}}\right)} \Bigg\{ \frac{\sigma}{2} r_e^2 e^{2v_j} \frac{\overline{\Delta V}^4}{3!}\left[2\left(\frac{\partial P}{\partial \theta}\right)_{i,j} + \left(\frac{\partial^2 P}{\partial v \partial \theta}\right)_{i,j}\right]$$

$$+ \frac{2\sigma}{3} r_e^2 e^{2v_j} \frac{\overline{\Delta V}^6}{5!}\left[8\left(\frac{\partial P}{\partial \theta}\right)_{i,j} + 12\left(\frac{\partial^2 P}{\partial v \partial \theta}\right)_{i,j} + 6\left(\frac{\partial^3 P}{\partial v^2 \partial \theta}\right)_{i,j}\right]$$

$$+ \frac{3\sigma}{4} r_e^2 e^{2v_j} \frac{\overline{\Delta V}^8}{7!}\left[32\left(\frac{\partial P}{\partial \theta}\right)_{i,j} + 80\left(\frac{\partial^2 P}{\partial v \partial \theta}\right)_{i,j} + 80\left(\frac{\partial^3 P}{\partial v^2 \partial \theta}\right)_{i,j}\right] + R_{m_1} \Bigg\} \tag{39}$$

where:

$$R_{m_1} = \left(\frac{\partial K_v}{\partial v}\right)_{i,j}\left[-\frac{\overline{\Delta V}^4}{3!}\left(\frac{\partial^2 P^2}{\partial v^2}\right)_{i,j} - \frac{8}{3}\frac{\overline{\Delta V}^6}{5!}\left(\frac{\partial^4 P^2}{\partial v^4}\right)_{i,j} - \frac{9}{2}\frac{\overline{\Delta V}^8}{7!}\left(\frac{\partial^6 P^2}{\partial v^6}\right)_{i,j}\right] \tag{40}$$

If we recognize that

$$\left(\frac{\partial \ln K_v}{\partial v}\right)_{i,j} = \frac{2\left(K_{v_{i,j+1/2}} - K_{v_{i,j-1/2}}\right)}{\Delta V\left(K_{v_{i,j+1/2}} + K_{v_{i,j-1/2}}\right)} \tag{41}$$

we can rewrite equation (37) as

$$K_{v_{i,j+1/2}}\left(P^2_{i,j+1} - P^2_{i,j}\right) + K_{v_{i,j-1/2}}\left(P^2_{i,j-1} - P^2_{i,j}\right) = \sigma r_e^2 e^{2v_j} \overline{\Delta V}^2 \Bigg\{\left(\frac{\partial P}{\partial \theta}\right)_{i,j}$$

$$+ \frac{\overline{\Delta V}^2}{12}\left[4\left(\frac{\partial P}{\partial \theta}\right)_{i,j} + 4\left(\frac{\partial^2 P}{\partial v \partial \theta}\right)_{i,j} + \left(\frac{\partial^3 P}{\partial v^2 \partial \theta}\right)_{i,j}\right] + \frac{\overline{\Delta V}^4}{360}\left[16\left(\frac{\partial P}{\partial \theta}\right)_{i,j} + 32\left(\frac{\partial^2 P}{\partial v \partial \theta}\right)_{i,j}\right.$$

$$\left. + 24\left(\frac{\partial^3 P}{\partial v^2 \partial \theta}\right)_{i,j}\right] + \frac{\overline{\Delta V}^6}{20160}\left[64\left(\frac{\partial P}{\partial \theta}\right)_{i,j} + 192\left(\frac{\partial^2 P}{\partial v \partial \theta}\right)_{i,j} + 240\left(\frac{\partial^3 P}{\partial v^2 \partial \theta}\right)_{i,j}\right]$$

$$- \left(\frac{\partial \ln K_v}{\partial v}\right)_{i,j}\frac{\overline{\Delta V}^2}{12}\left[2\left(\frac{\partial P}{\partial \theta}\right)_{i,j} + \left(\frac{\partial^2 P}{\partial v \partial \theta}\right)_{i,j}\right] - \left(\frac{\partial \ln K_v}{\partial v}\right)_{i,j}\frac{\overline{\Delta V}^4}{180}\left[8\left(\frac{\partial P}{\partial \theta}\right)_{i,j}\right.$$

$$\left. + 12\left(\frac{\partial^2 P}{\partial v \partial \theta}\right)_{i,j} + 6\left(\frac{\partial^3 P}{\partial v^2 \partial \theta}\right)_{i,j}\right] - \left(\frac{\partial \ln K_v}{\partial v}\right)_{i,j}\frac{\overline{\Delta V}^6}{6720}\left[32\left(\frac{\partial P}{\partial \theta}\right)_{i,j}\right.$$

$$\left. + 80\left(\frac{\partial^2 P}{\partial v \partial \theta}\right)_{i,j} + 80\left(\frac{\partial^3 P}{\partial v^2 \partial \theta}\right)_{i,j}\right]\Bigg\} - \left(\frac{\partial \ln K_v}{\partial v}\right)_{i,j} R_{m_1} \tag{42}$$

For the final reduction of the remainder term R_{m1}, we get

$$-\left(\frac{\partial \ln K_v}{\partial v}\right)_{i,j} R_1 = \left(\frac{\partial \ln K_v}{\partial v}\right)^2_{i,j} \sigma\, r_e^2 e^{2v_j}\left\{\frac{\overline{\Delta v}^4}{3!}\left(\frac{\partial P}{\partial \theta}\right)_{i,j} + \frac{8}{3}\frac{\overline{\Delta v}^6}{5!}\left[4\left(\frac{\partial P}{\partial \theta}\right)_{i,j} + 4\left(\frac{\partial^2 P}{\partial v \partial \theta}\right)_{i,j} + \left(\frac{\partial^3 P}{\partial v^2 \partial \theta}\right)_{i,j}\right] + \frac{9}{2}\frac{\overline{\Delta v}^8}{7!}\left[16\left(\frac{\partial P}{\partial \theta}\right)_{i,j} + 32\left(\frac{\partial^2 P}{\partial v \partial \theta}\right)_{i,j} + 24\left(\frac{\partial^3 P}{\partial v^2 \partial \theta}\right)_{i,j}\right]\right\} + R_{m_2} \quad (43)$$

where:

$$R_{m_2} = -\left(\frac{\partial \ln K_v}{\partial v}\right)^2_{i,j}\left(\frac{\partial K_v}{\partial v}\right)_{i,j}\left[\frac{\overline{\Delta v}^4}{3!}\left(\frac{\partial P^2}{\partial v}\right)_{i,j} + 8\frac{\overline{\Delta v}^6}{5!}\left(\frac{\partial^3 P^2}{\partial v^3}\right)_{i,j} + \frac{45}{2}\frac{\overline{\Delta v}^8}{7!}\left(\frac{\partial^5 P^2}{\partial v^5}\right)_{i,j}\right] \quad (44)$$

If we neglect the remainder R_{m2} and substitute equation (43) into equation (42), we obtain the following equation:

$$\frac{1}{r_e^2 e^{2v_j}\overline{\Delta v}^2}\left[K_{v_{i,j+1/2}}\left(P^2_{i,j+1} - P^2_{i,j}\right) + K_{v_{i,j-1/2}}\left(P^2_{i,j-1} - P^2_{i,j}\right)\right] = \sigma\left(\frac{\partial P}{\partial \theta}\right)_{i,j}$$
$$+ \sigma\left\{\frac{\overline{\Delta v}^2}{3} + \frac{2\overline{\Delta v}^4}{45} + \frac{\overline{\Delta v}^6}{315} - \left(\frac{\partial \ln K_v}{\partial v}\right)_{i,j}\left(\frac{\overline{\Delta v}^2}{6} + \frac{2\overline{\Delta v}^4}{45} + \frac{\overline{\Delta v}^6}{210}\right) + \left(\frac{\partial \ln K_v}{\partial v}\right)^2_{i,j}\left(\frac{\overline{\Delta v}^4}{6} + \frac{4\overline{\Delta v}^6}{45} + \frac{\overline{\Delta v}^8}{70}\right)\right\}\left(\frac{\partial P}{\partial \theta}\right)_{i,j}$$
$$+ \sigma\left\{\frac{\overline{\Delta v}^2}{3} + \frac{4\overline{\Delta v}^4}{45} + \frac{\overline{\Delta v}^6}{105} - \left(\frac{\partial \ln K_v}{\partial v}\right)_{i,j}\left(\frac{\overline{\Delta v}^2}{12} + \frac{\overline{\Delta v}^4}{15} + \frac{\overline{\Delta v}^6}{64}\right) + \left(\frac{\partial \ln K_v}{\partial v}\right)^2_{i,j}\left(\frac{4\overline{\Delta v}^6}{45} + \frac{\overline{\Delta v}^8}{35}\right)\right\}\left(\frac{\partial^2 P}{\partial v \partial \theta}\right)_{i,j}$$
$$+ \sigma\left\{\frac{\overline{\Delta v}^2}{12} + \frac{\overline{\Delta v}^4}{15} + \frac{\overline{\Delta v}^6}{84} - \left(\frac{\partial \ln K_v}{\partial v}\right)_{i,j}\left(\frac{\overline{\Delta v}^4}{30} + \frac{\overline{\Delta v}^6}{84}\right) + \left(\frac{\partial \ln K_v}{\partial v}\right)^2_{i,j}\left(\frac{\overline{\Delta v}^6}{45} + \frac{3\overline{\Delta v}^8}{140}\right)\right\}\left(\frac{\partial^3 P}{\partial v^2 \partial \theta}\right)_{i,j} \quad (45)$$

After substituting the appropriate finite difference approximations for the time derivatives:

$$\left(\frac{\partial^2 P}{\partial v \partial \theta}\right)_{i,j} = \left[\left(P_{i,j+1,n+1} - P_{i,j-1,n+1}\right) - \left(P_{i,j+1,n} - P_{i,j-1,n}\right)\right] / 2\Delta v \Delta \theta \quad (46)$$

$$\left(\frac{\partial^3 P}{\partial v^2 \partial \theta}\right)_{i,j} = \left[\left(P_{i,j+1,n+1} - 2P_{i,j,n+1} + P_{i,j-1,n+1}\right) - \left(P_{i,j+1,n} - 2P_{i,j,n} + P_{i,j-1,n}\right)\right] / \overline{\Delta V}^2 \Delta\theta \qquad (47)$$

along with the expression for $\frac{\partial \ln K_v}{\partial v}$, we get the difference approximation for equation (23)

$$\frac{1}{r_e^2 e^{2v_j} \overline{\Delta V}^2}\left[Kv_{i,j+1/2}\left(P^2_{i,j+1} - P^2_{i,j}\right) + Kv_{i,j-1/2}\left(P^2_{i,j-1} - P^2_{i,j}\right)\right] =$$

$$\frac{\sigma}{\Delta\theta}\left(P_{i,j,n+1} - P_{i,j,n}\right) + \sigma\left\{\frac{\overline{\Delta V}^2}{3} + \frac{2\overline{\Delta V}^4}{45} + \frac{\overline{\Delta V}^6}{315} - \frac{2\left(Kv_{i,j+1/2} - Kv_{i,j-1/2}\right)}{\Delta V\left(Kv_{i,j+1/2} + Kv_{i,j-1/2}\right)}\left(\frac{\overline{\Delta V}^2}{6}\right.\right.$$

$$\left.+ \frac{2\overline{\Delta V}^4}{45} + \frac{\overline{\Delta V}^6}{210}\right) + \left[\frac{2\left(Kv_{i,j+1/2} - Kv_{i,j-1/2}\right)}{\Delta V\left(Kv_{i,j+1/2} + Kv_{i,j-1/2}\right)}\right]^2\left.\left(\frac{\overline{\Delta V}^4}{6} + \frac{4\overline{\Delta V}^6}{45} + \frac{\overline{\Delta V}^8}{70}\right)\right\}\left(P_{i,j,n+1}\right.$$

$$\left.- P_{i,j,n}\right)/\Delta\theta + \sigma\left\{\frac{\overline{\Delta V}^2}{3} + \frac{4\overline{\Delta V}^4}{45} + \frac{\overline{\Delta V}^6}{105} - \left[\frac{2\left(Kv_{i,j+1/2} - Kv_{i,j-1/2}\right)}{\Delta V\left(Kv_{i,j+1/2} + Kv_{i,j-1/2}\right)}\right]\left(\frac{\overline{\Delta V}^2}{12}\right.\right.$$

$$\left.+ \frac{\overline{\Delta V}^4}{15} + \frac{\overline{\Delta V}^6}{64}\right) + \left[\frac{2\left(Kv_{i,j+1/2} - Kv_{i,j-1/2}\right)}{\Delta V\left(Kv_{i,j+1/2} + Kv_{i,j-1/2}\right)}\right]^2\left.\left(\frac{4\overline{\Delta V}^6}{45} + \frac{\overline{\Delta V}^8}{35}\right)\right\}\left[P_{i,j+1,n+1}\right.$$

$$\left.- P_{i,j+1,n} + P_{i,j-1,n}\right]/2\Delta V\Delta\theta + \sigma\left\{\frac{\overline{\Delta V}^2}{12} + \frac{\overline{\Delta V}^4}{15} + \frac{\overline{\Delta V}^6}{84}\right.$$

$$- \left[\frac{2\left(Kv_{i,j+1/2} - Kv_{i,j-1/2}\right)}{\Delta V\left(Kv_{i,j+1/2} + Kv_{i,j-1/2}\right)}\right]\left(\frac{\overline{\Delta V}^4}{30} + \frac{\overline{\Delta V}^6}{84}\right) + \left(\frac{\overline{\Delta V}^6}{45}\right.$$

$$\left.\left.+ \frac{3\overline{\Delta V}^8}{140}\right)\left[\frac{2\left(Kv_{i,j+1/2} - Kv_{i,j-1/2}\right)}{\Delta V\left(Kv_{i,j+1/2} + Kv_{i,j-1/2}\right)}\right]^2\right\}\left[\left(P_{i,j+1,n+1} - 2P_{i,j,n+1}\right.\right.$$

$$\left.\left.+ P_{i,j-1,n+1}\right) - \left(P_{i,j+1,n} - 2P_{i,j,n} + P_{i,j-1,n}\right)\right]/\overline{\Delta V}^2\Delta\theta \qquad (48)$$

Combine equations (34) and (48) to get the finite-difference approximation for equation (14)

$$
\begin{aligned}
&\frac{1}{re^2 e^{2v_i}\overline{\Delta v}^2}\Big[Kv_{i,j+\frac{1}{2}}\left(P^2_{i,j+1}-P^2_{i,j}\right)+Kv_{i,j-\frac{1}{2}}\left(P^2_{i,j-1}-P^2_{i,j}\right)\Big] \\
&+\frac{1}{H^2\overline{\Delta y}^2}\Big[Ky_{i+\frac{1}{2},j}\left(P^2_{i+1,j}-P^2_{i,j}\right)+Ky_{i-\frac{1}{2},j}\left(P^2_{i-1,j}-P^2_{i,j}\right)\Big]=\big(P_{i,j,n+1} \\
&-P_{i,j,n}\big)/\Delta\theta+\left(\frac{1-\sigma}{12}\right)\Big[\left(P_{i+1,j,n+1}-2P_{i,j,n+1}+P_{i-1,j,n+1}\right)-\big(P_{i+1,j,n} \\
&-2P_{i,j,n}+P_{i-1,j,n}\big)\Big]+\sigma\left\{\frac{\overline{\Delta v}^2}{3}+\frac{\overline{\Delta v}^4}{22.5}+\frac{\overline{\Delta v}^6}{315}-\left[\frac{2\left(Kv_{i,j+\frac{1}{2}}-Kv_{i,j-\frac{1}{2}}\right)}{\Delta v\left(Kv_{i,j+\frac{1}{2}}+Kv_{i,j-\frac{1}{2}}\right)}\right]\left(\frac{\overline{\Delta v}^2}{6}\right.\right. \\
&\left.+\frac{2\overline{\Delta v}^4}{45}+\frac{\overline{\Delta v}^6}{210}\right)+\left[\frac{2\left(Kv_{i,j+\frac{1}{2}}-Kv_{i,j-\frac{1}{2}}\right)}{\Delta v\left(Kv_{i,j+\frac{1}{2}}+Kv_{i,j-\frac{1}{2}}\right)}\right]^2\left(\frac{\overline{\Delta v}^4}{6}+\frac{4\overline{\Delta v}^6}{45}\right. \\
&\left.\left.+\frac{\overline{\Delta v}^8}{90}\right)\right\}\left(P_{i,j,n+1}-P_{i,j,n}\right)/\Delta\theta+\sigma\left\{\frac{\overline{\Delta v}^2}{3}+\frac{4\overline{\Delta v}^4}{45}+\frac{\overline{\Delta v}^6}{105}-\left(\frac{\overline{\Delta v}^2}{12}\right.\right. \\
&\left.+\frac{\overline{\Delta v}^4}{15}+\frac{\overline{\Delta v}^6}{64}\right)\left[\frac{2\left(Kv_{i,j+\frac{1}{2}}-Kv_{i,j-\frac{1}{2}}\right)}{\Delta v\left(Kv_{i,j+\frac{1}{2}}+Kv_{i,j-\frac{1}{2}}\right)}\right]+\left[\frac{2\left(Kv_{i,j+\frac{1}{2}}-Kv_{i,j-\frac{1}{2}}\right)}{\Delta v\left(Kv_{i,j+\frac{1}{2}}+Kv_{i,j-\frac{1}{2}}\right)}\right]^2\left(\frac{4\overline{\Delta v}^6}{45}\right. \\
&\left.\left.+\frac{\overline{\Delta v}^8}{35}\right)\right\}\Big[P_{i,j+1,n+1}-P_{i,j-1,n+1}-P_{i,j+1,n}+P_{i,j-1,n}\Big]/2\Delta v\Delta\theta+\sigma\left\{\frac{\overline{\Delta v}^2}{12}+\frac{\overline{\Delta v}^4}{15}+\frac{\overline{\Delta v}^6}{84}\right. \\
&-\left[\frac{2\left(Kv_{i,j+\frac{1}{2}}-Kv_{i,j-\frac{1}{2}}\right)}{\Delta v\left(Kv_{i,j+\frac{1}{2}}+Kv_{i,j-\frac{1}{2}}\right)}\right]\left(\frac{\overline{\Delta v}^4}{30}+\frac{\overline{\Delta v}^6}{84}\right)+\left.\left[\frac{2\left(Kv_{i,j+\frac{1}{2}}-Kv_{i,j-\frac{1}{2}}\right)}{\Delta v\left(Kv_{i,j+\frac{1}{2}}+Kv_{i,j-\frac{1}{2}}\right)}\right]^2\left(\frac{\overline{\Delta v}^6}{45}+\frac{3\overline{\Delta v}^8}{190}\right)\right\}\Big[\big(P_{i,j+1,n+1} \\
&-2P_{i,j,n+1}+P_{i,j-1,n+1}\big)-\left(P_{i,j+1,n}-2P_{i,j,n}+P_{i,j-1,n}\right)\Big]/\overline{\Delta v}^2\Delta\theta \qquad (49)
\end{aligned}
$$

There are three general techniques for solving iterative schemes: the forward-difference method in which the derivatives with respect to y and v are evaluated at the time step n and the pressure in the time derivative is calculated for the (n+1) time step; the backward-difference method in which the derivatives with respect to y and v are calculated at the (n+1) time step; and, the Crank-Nicholson method (7) where the calculated values of the spatial derivatives at the (n+1) time step are averaged with the computed values for time step n. The method selected was that of Crank-Nicholson, where the difference expressions on the left-hand side of equation (49) were averaged for time steps n and n+1 to give an implicit equation of the form:

$$
\begin{aligned}
&\frac{1}{2 r_e^2 e^{2v_j}\overline{\Delta v}^2}\Big[Kv_{i,j+\frac{1}{2}}\left(P^2_{i,j+1,n+1}-P^2_{i,j,n+1}+P^2_{i,j+1,n}-P^2_{i,j,n}\right)+Kv_{i,j-\frac{1}{2}}\left(P^2_{i,j-1,n+1}-P^2_{i,j,n+1}\right.\\
&\left.+P^2_{i,j-1,n}-P^2_{i,j,n}\right)\Big]+\frac{1}{2H^2\overline{\Delta y}^2}\Big[Ky_{i+\frac{1}{2},j}\left(P^2_{i+1,j,n+1}-P^2_{i,j,n+1}+P^2_{i+1,j,n}-P^2_{i,j,n}\right)\\
&+Ky_{i-\frac{1}{2},j}\left(P^2_{i-1,j,n+1}-P^2_{i,j,n+1}+P^2_{i-1,j,n}-P^2_{i,j,n}\right)\Big]=\frac{P_{i,j,n+1}-P_{i,j,n}}{\Delta\theta}+\left(\frac{1-\sigma}{12\Delta\theta}\right)\Big[\left(P_{i+1,j,n+1}\right.\\
&\left.-2P_{i,j,n+1}+P_{i-1,j,n+1}\right)-\left(P_{i+1,j,n}-2P_{i,j,n}+P_{i-1,j,n}\right)\Big]+\sigma\Bigg\{\frac{\overline{\Delta v}^2}{3}+\frac{2\overline{\Delta v}^4}{45}+\frac{\overline{\Delta v}^6}{315}\\
&-\left[\frac{2(Kv_{i,j+\frac{1}{2}}-Kv_{i,j-\frac{1}{2}})}{\Delta v(Kv_{i,j+\frac{1}{2}}+Kv_{i,j-\frac{1}{2}})}\right]\left(\frac{\overline{\Delta v}^2}{6}+\frac{2\overline{\Delta v}^4}{45}+\frac{\overline{\Delta v}^6}{210}\right)+\left[\frac{2(Kv_{i,j+\frac{1}{2}}-Kv_{i,j-\frac{1}{2}})}{\Delta v(Kv_{i,j+\frac{1}{2}}+Kv_{i,j-\frac{1}{2}})}\right]^2\left(\frac{\overline{\Delta v}^4}{6}+\frac{4\overline{\Delta v}^6}{45}\right.\\
&\left.+\frac{\overline{\Delta v}^8}{70}\right)\Bigg\}\left(\frac{P_{i,j,n+1}-P_{i,j,n}}{\Delta\theta}\right)+\sigma\Bigg\{\frac{\overline{\Delta v}^2}{3}+\frac{4\overline{\Delta v}^4}{45}+\frac{\overline{\Delta v}^6}{105}-\left[\frac{2(Kv_{i,j+\frac{1}{2}}-Kv_{i,j-\frac{1}{2}})}{\Delta v(Kv_{i,j+\frac{1}{2}}+Kv_{i,j-\frac{1}{2}})}\right]\left(\frac{\overline{\Delta v}^2}{12}\right.\\
&\left.+\frac{\overline{\Delta v}^4}{15}+\frac{\overline{\Delta v}^6}{64}\right)+\left[\frac{2(Kv_{i,j+\frac{1}{2}}-Kv_{i,j-\frac{1}{2}})}{\Delta v(Kv_{i,j+\frac{1}{2}}+Kv_{i,j-\frac{1}{2}})}\right]^2\left(\frac{4\overline{\Delta v}^6}{45}+\frac{\overline{\Delta v}^8}{35}\right)\Bigg\}\Big[P_{i,j+1,n+1}-P_{i,j-1,n+1}\\
&-P_{i,j+1,n}+P_{i,j-1,n}\Big]/2\Delta v\Delta\theta+\sigma\Bigg\{\frac{\overline{\Delta v}^2}{12}+\frac{\overline{\Delta v}^4}{15}+\frac{\overline{\Delta v}^6}{84}-\left[\frac{2(Kv_{i,j+\frac{1}{2}}-Kv_{i,j-\frac{1}{2}})}{\Delta v(Kv_{i,j+\frac{1}{2}}+Kv_{i,j-\frac{1}{2}})}\right]\left(\frac{\overline{\Delta v}^4}{30}\right.\\
&\left.+\frac{\overline{\Delta v}^6}{84}\right)+\left[\frac{2(Kv_{i,j+\frac{1}{2}}-Kv_{i,j-\frac{1}{2}})}{\Delta v(Kv_{i,j+\frac{1}{2}}+Kv_{i,j-\frac{1}{2}})}\right]^2\left(\frac{\overline{\Delta v}^6}{45}+\frac{3\overline{\Delta v}^8}{140}\right)\Bigg\}\Big[\left(P_{i,j+1,n+1}-2P_{i,j,n+1}\right.\\
&\left.+P_{i,j-1,n+1}\right)-\left(P_{i,j+1,n}-2P_{i,j,n}+P_{i,j-1,n}\right)\Big]/\overline{\Delta v}^2\Delta\theta \qquad (50)
\end{aligned}
$$

This equation must be written for each interior point within the network model. In order to obtain an adequate description in the vertical direction, we will need several rows of grid points. This number will depend on the permeability variation and the detailed description required in the completion interval and/or fracture. Similarly, we will need a large number in each row for the radial direction. Therefore, an average model run will probably contain from 300 to 600 matrix points, requiring that equation (50) be written for each point. We must then repeatedly solve this set of equations to get the pressure distribution as a function of time. Simultaneous solution of such a large set of equations for each time step would be prohibitive in computer time requirements. Therefore, several line methods were attempted to obtain a solution for this set of equations coupled with the finite-difference approximations of the boundary equations. The alternating-direction method (28) for multi-dimensional problems, in which one partial derivative is evaluated at the previous time step and the other evaluated at the one being calculated, was never made to work. Likewise, trying to establish a method similar to that of Brian (2), wherein the intermediate values for the pressure were calculated and required a calculational sweep in both spatial directions for one time step, also was unsuccessful.

The technique finally chosen was my own innovation for an iterative line method in solving for both partial derivatives at the (n+1) time step. It is a single-direction line method analogous to the one-dimensional technique described by Bruce, et. al. (4) Pressure equations for the ith row at the (n+1) time step are solved in terms of the required values at the nth time step plus pressure terms in the (n+1/2) time step through an iterative process. Repeated iteration until the convergence, within prescribed bounds, of the calculated pressures with those of the previous trial, constitutes a general description of the technique. We make the definitions

$$\begin{aligned}X_{i,j} = {} & \frac{\overline{\Delta V}^2}{3} + \frac{2\overline{\Delta V}^4}{45} + \frac{\overline{\Delta V}^6}{315} - \left[\frac{2(Kv_{i,j+\frac{1}{2}} - Kv_{i,j-\frac{1}{2}})}{\Delta V(Kv_{i,j+\frac{1}{2}} + Kv_{i,j-\frac{1}{2}})}\right]\left(\frac{\overline{\Delta V}^2}{6} + \frac{2\overline{\Delta V}^4}{45}\right.\\ & \left. + \frac{\overline{\Delta V}^6}{10}\right) + \left[\frac{2(Kv_{i,j+\frac{1}{2}} - Kv_{i,j-\frac{1}{2}})}{\Delta V(Kv_{i,j+\frac{1}{2}} + Kv_{i,j-\frac{1}{2}})}\right]^2\left(\frac{\overline{\Delta V}^4}{6} + \frac{4\overline{\Delta V}^6}{45} + \frac{\overline{\Delta V}^8}{70}\right)\end{aligned} \qquad (51)$$

$$\begin{aligned}Z_{i,j} = {} & \frac{\overline{\Delta V}^2}{3} + \frac{4\overline{\Delta V}^4}{45} + \frac{\overline{\Delta V}^6}{105} - \left[\frac{2(Kv_{i,j+\frac{1}{2}} - Kv_{i,j-\frac{1}{2}})}{\Delta V(Kv_{i,j+\frac{1}{2}} + Kv_{i,j-\frac{1}{2}})}\right]\left(\frac{\overline{\Delta V}^2}{12} + \frac{\overline{\Delta V}^4}{15}\right.\\ & \left. + \frac{\overline{\Delta V}^6}{64}\right) + \left[\frac{2(Kv_{i,j+\frac{1}{2}} - Kv_{i,j-\frac{1}{2}})}{\Delta V(Kv_{i,j+\frac{1}{2}} + Kv_{i,j-\frac{1}{2}})}\right]^2\left(\frac{4\overline{\Delta V}^6}{45} + \frac{\overline{\Delta V}^8}{35}\right)\end{aligned} \qquad (52)$$

$$\begin{aligned}T_{i,j} = {} & \frac{\overline{\Delta V}^2}{12} + \frac{\overline{\Delta V}^4}{15} + \frac{\overline{\Delta V}^6}{84} - \left[\frac{2(Kv_{i,j+\frac{1}{2}} - Kv_{i,j-\frac{1}{2}})}{\Delta V(Kv_{i,j+\frac{1}{2}} + Kv_{i,j-\frac{1}{2}})}\right]\left(\frac{\overline{\Delta V}^4}{30} + \frac{\overline{\Delta V}^6}{84}\right)\\ & + \left[\frac{2(Kv_{i,j+\frac{1}{2}} - Kv_{i,j-\frac{1}{2}})}{\Delta V(Kv_{i,j+\frac{1}{2}} + Kv_{i,j-\frac{1}{2}})}\right]^2\left(\frac{\overline{\Delta V}^6}{45} + \frac{3\overline{\Delta V}^8}{140}\right)\end{aligned} \qquad (53)$$

Then substitute equations (51-53) into equation (50) to get

$$\begin{aligned}& \frac{1}{2r_a^2 e^{2V_i}\overline{\Delta V}^2}\Big[Kv_{i,j+\frac{1}{2}}(P^2_{i,j+1,n+1} - P^2_{i,j,n+1} + P^2_{i,j+1,n} - P^2_{i,j,n})\\ & + Kv_{i,j-\frac{1}{2}}(P^2_{i,j-1,n+1} - P^2_{i,j,n+1} + P^2_{i,j-1,n} - P^2_{i,j,n})\Big] + \frac{1}{2H^2\Delta y^2}\Big[Ky_{i+\frac{1}{2},j}(P^2_{i+1,j,n+1}\\ & - P^2_{i,j,n+1} + P^2_{i+1,j,n} - P^2_{i,j,n}) + Ky_{i-\frac{1}{2},j}(P^2_{i-1,j,n+1} - P^2_{i,j,n+1} + P^2_{i-1,j,n}\\ & - P^2_{i,j,n})\Big] = (P_{i,j,n+1} - P_{i,j,n})/\Delta\theta + \left(\frac{1-\sigma}{12\Delta\theta}\right)\Big[(P_{i+1,j,n+1} - 2P_{i,j,n+1} + P_{i-1,j,n+1})\\ & - (P_{i+1,j,n} - 2P_{i,j,n} + P_{i-1,j,n})\Big] + \sigma\Big\{\frac{X_{i,j}}{\Delta\theta}(P_{i,j,n+1} - P_{i,j,n})\\ & + \frac{Z_{i,j}}{2\Delta V\Delta\theta}\Big[(P_{i,j+1,n+1} - P_{i,j-1,n+1}) - (P_{i,j+1,n} - P_{i,j-1,n})\Big] + E_1\Big\}\end{aligned} \qquad (54)$$

where:

$$E_1 = \frac{T_{i,j}}{\Delta V^2 \Delta\theta}\Big[\left(P_{i,j+1,n+1} - 2P_{i,j,n+1} + P_{i,j-1,n+1}\right) - \left(P_{i,j+1,n} - 2P_{i,j,n} + P_{i,j-1,n}\right)\Big] \tag{55}$$

Now separate terms in equation (54) so that the (n+1)st time step is on the left-hand side of the equality sign:

$$\begin{aligned}
&\frac{-1}{2r_a^2 e^{2V_j}\Delta V^2}\Big[K_{V\,i,j+1/2}\left(P^2_{i,j+1,n+1} - P^2_{i,j,n+1}\right) + K_{V\,i,j-1/2}\left(P^2_{i,j-1,n+1} - P^2_{i,j,n+1}\right)\Big] \\
&+ P_{i,j,n+1}/\Delta\theta + \sigma\Big[\frac{X_{i,j}}{\Delta\theta}P_{i,j,n+1} + \frac{Z_{i,j}}{2\Delta V\Delta\theta}\left(P_{i,j+1,n+1} - P_{i,j-1,n+1}\right) \\
&+ \frac{T_{i,j}}{\Delta V^2\Delta\theta}\left(P_{i,j+1,n+1} - 2P_{i,j,n+1} + P_{i,j-1,n+1}\right)\Big] - \frac{1}{2H^2\Delta y^2}\Big[K_{y\,i+1/2,j}\left(P^2_{i+1,j,n+1}\right. \\
&\left. - P^2_{i,j,n+1}\right) + K_{y\,i-1/2,j}\left(P^2_{i-1,j,n+1} - P^2_{i,j,n+1}\right)\Big] + \left(\frac{1-\sigma}{/2\Delta\theta}\right)\left(P_{i+1,j,n+1} - 2P_{i,j,n+1}\right. \\
&\left. + P_{i,j,n+1}\right) = P_{i,j,n}/\Delta\theta + \left(\frac{1-\sigma}{/2\Delta\theta}\right)\left(P_{i+1,j,n} - 2P_{i,j,n} + P_{i-1,j,n}\right) + \sigma\Big[\frac{X_{i,j}}{\Delta\theta}P_{i,j,n} \\
&+ \frac{Z_{i,j}}{2\Delta V\Delta\theta}\left(P_{i,j+1,n} - P_{i,j-1,n}\right) + \frac{T_{i,j}}{\Delta V^2\Delta\theta}\left(P_{i,j+1,n} - 2P_{i,j,n} + P_{i,j-1,n}\right)\Big] \\
&+ \frac{1}{2r_a^2 e^{2V_j}\Delta V^2}\Big[K_{V\,i,j+1/2}\left(P^2_{i,j+1,n} - P^2_{i,j,n}\right) + K_{V\,i,j-1/2}\left(P^2_{i,j-1,n} - P^2_{i,j,n}\right)\Big] \\
&+ \frac{1}{2H^2\Delta y^2}\Big[K_{y\,i+1/2,j}\left(P^2_{i+1,j,n} - P^2_{i,j,n}\right) + K_{y\,i-1/2,j}\left(P^2_{i-1,j,n} - P^2_{i,j,n}\right)\Big]
\end{aligned} \tag{56}$$

Let

$$\begin{aligned}
D_{i,j,n} = {} & P_{i,j,n}/\Delta\theta + \left(\frac{1-\sigma}{/2\Delta\theta}\right)\left(P_{i+1,j,n} - 2P_{i,j,n} + P_{i-1,j,n}\right) + \sigma\Big[\frac{X_{i,j}}{\Delta\theta}P_{i,j,n} \\
&+ \frac{Z_{i,j}}{2\Delta V\Delta\theta}\left(P_{i,j+1,n} - P_{i,j-1,n}\right) + \frac{T_{i,j}}{\Delta V^2\Delta\theta}\left(P_{i,j+1,n} - 2P_{i,j,n} + P_{i,j-1,n}\right)\Big] \\
&+ \frac{1}{2r_a^2 e^{2V_j}\Delta V^2}\Big[K_{V\,i,j+1/2}\left(P^2_{i,j+1,n} - P^2_{i,j,n}\right) + K_{V\,i,j-1/2}\left(P^2_{i,j-1,n} - P^2_{i,j,n}\right)\Big] \\
&+ \frac{1}{2H^2\Delta y^2}\Big[K_{y\,i+1/2,j}\left(P^2_{i+1,j,n} - P^2_{i,j,n}\right) + K_{y\,i-1/2,j}\left(P^2_{i-1,j,n} - P^2_{i,j,n}\right)\Big]
\end{aligned} \tag{57}$$

Bruce, et. al. (4), showed the more stable of three possible methods for factoring the difference of the P^2 terms on the left-hand side of equation (56) to be

$$P^2_{i,j+1,n+1} - P^2_{i,j,n+1} = \left(P_{i,j+1,n+1/2} + P_{i,j,n+1/2}\right)\left(P_{i,j+1,n+1} - P_{i,j,n+1}\right) \tag{58}$$

where the subscript (n+1/2) denotes the assumed value of P which is obtained from the previous iteration of the current time step. That is, for the first iteration, $P_{i,j,n+1/2}$ assumes the value from the nth time step. For each succeeding iteration, $P_{i,j,n+1/2}$ assumes the last calculated value. At least two iterations per time step are assured through proper computer programming; therefore, $P_{i,j,n+1/2}$ is not equal to $P_{i,j,n}$. By factoring the P^2 terms with radial permeability coefficients having (n+1) for a time subscript and substituting equation (57), we get

$$\begin{aligned}
&-\frac{1}{2 r_e^2 e^{2V_j} \Delta V^2}\Big[K_{V_{i,j+1/2}}\left(P_{i,j+1,n+1} - P_{i,j,n+1}\right)\left(P_{i,j+1,n+1/2} + P_{i,j,n+1/2}\right) \\
&\quad + K_{V_{i,j-1/2}}\left(P_{i,j-1,n+1} - P_{i,j,n+1}\right)\left(P_{i,j-1,n+1/2} + P_{i,j,n+1/2}\right)\Big] + P_{i,j,n+1}/\Delta\theta \\
&\quad + \sigma\Big[\frac{X_{i,j}}{\Delta\theta} P_{i,j,n+1} + \frac{Z_{i,j}}{2\Delta V \Delta\theta}\left(P_{i,j+1,n+1} - P_{i,j-1,n+1}\right) + \frac{T_{i,j}}{\Delta V^2 \Delta\theta}\big(P_{i,j+1,n+1} \\
&\quad - 2P_{i,j,n+1} + P_{i,j-1,n+1}\big)\Big] - \frac{1}{2H^2 \Delta y^2}\Big[K_{y_{i+1/2,j}}\left(P^2_{i+1,j,n+1} - P^2_{i,j,n+1}\right) \\
&\quad + K_{y_{i-1/2,j}}\left(P^2_{i-1,j,n+1} - P^2_{i,j,n+1}\right)\Big] + \left(\frac{1-\sigma}{12\Delta\theta}\right)\big(P_{i+1,j,n+1} \\
&\quad - 2P_{i,j,n+1} + P_{i-1,j,n+1}\big) = D_{i,j,n}
\end{aligned} \tag{59}$$

Since we are interested in maintaining a tri-diagonal matrix, all terms in equation (59) containing $P_{i-1,j,n+1/2}$ and $P_{i+1,j,n+1}$ will be evaluated by the iterative process. Therefore, we will change their subscripts to n+1/2. The remaining terms containing $P^2_{i,j,n+1}$ in the vertical derivatives must be factored in order to be included with similar terms. The factors used are

$$P^2_{i,j,n+1} = P_{i,j,n+\frac{1}{2}}\, P_{i,j,n+1} \tag{60}$$

Then, let

$$A_{i,j} = \frac{-K_{v\,i,j-\frac{1}{2}}}{2r_e^2 e^{2v_j}\overline{\Delta V}^2}\left(P_{i,j-1,n+\frac{1}{2}} + P_{i,j,n+\frac{1}{2}}\right) + \sigma\left(\frac{T_{i,j}}{\overline{\Delta V}^2\Delta\theta} - \frac{Z_{i,j}}{2\Delta V\Delta\theta}\right) \tag{61}$$

$$\begin{aligned} B_{i,j} = {} & \frac{K_{v\,i,j+\frac{1}{2}}}{2r_e^2 e^{2v_j}\overline{\Delta V}^2}\left(P_{i,j+1,n+\frac{1}{2}} + P_{i,j,n+\frac{1}{2}}\right) + \frac{K_{v\,i,j-\frac{1}{2}}}{2r_e^2 e^{2v_j}\overline{\Delta V}^2}\left(P_{i,j-1,n+\frac{1}{2}}\right. \\ & \left. + P_{i,j,n+\frac{1}{2}}\right) + \left(K_{y\,i+\frac{1}{2},j} + K_{y\,i-\frac{1}{2},j}\right) P_{i,j,n+\frac{1}{2}} / 2H^2\overline{\Delta y}^2 \\ & + 1/\Delta\theta - \left(\frac{1-\sigma}{6\Delta\theta}\right) + \sigma\left(\frac{X_{i,j}}{\Delta\theta} - \frac{2T_{i,j}}{\overline{\Delta V}^2\Delta\theta}\right) \end{aligned} \tag{62}$$

$$C_{i,j} = \frac{-K_{v\,i,j+\frac{1}{2}}}{2r_e^2 e^{2v_j}\overline{\Delta V}^2}\left(P_{i,j+1,n+\frac{1}{2}} + P_{i,j,n+\frac{1}{2}}\right) + \sigma\left(\frac{T_{i,j}}{\overline{\Delta V}^2\Delta\theta} + \frac{Z_{i,j}}{2\Delta V\Delta\theta}\right) \tag{63}$$

By making these substitutions, equation (59) becomes

$$\begin{aligned} A_{i,j} P_{i,j-1,n+1} + B_{i,j} P_{i,j,n+1} + C_{i,j} P_{i,j+1,n+1} = {} & D_{i,j,n} \\ & - \frac{(1-\sigma)}{12\Delta\theta}\left(P_{i+1,j,n+\frac{1}{2}} - P_{i-1,j,n+\frac{1}{2}}\right) \\ & + \frac{1}{2H^2\overline{\Delta y}^2}\left(K_{y\,i+\frac{1}{2},j} P^2_{i+1,j,n+\frac{1}{2}} + K_{y\,i-\frac{1}{2},j} P^2_{i-1,j,n+\frac{1}{2}}\right) \end{aligned} \tag{64}$$

Let

$$\begin{aligned} D_{i,j,n+\frac{1}{2}} = {} & D_{i,j,n} - \left(\frac{1-\sigma}{12\Delta\theta}\right)\left(P_{i+1,j,n+\frac{1}{2}} - P_{i-1,j,n+\frac{1}{2}}\right) \\ & + \frac{1}{2H^2\overline{\Delta y}^2}\left(K_{y\,i+\frac{1}{2},j} P^2_{i+1,j,n+\frac{1}{2}} + K_{y\,i-\frac{1}{2},j} P^2_{i-1,j,n+\frac{1}{2}}\right) \end{aligned} \tag{65}$$

Upon substituting equation (65) into equation (64), we get the equation describing the pressure at all interior model points:

$$A_{i,j} P_{i,j-1,n+1} + B_{i,j} P_{i,j,n+1} + C_{i,j} P_{i,j+1,n+1} = D_{i,j,n+1/2} \tag{66}$$

The remaining equations to form the complete set are those for the boundaries. For a model having m-cells in the radial direction, the approximation equation used for the outer drainage boundary is:

$$\left(P_{i,m,n+1/2} + P_{i,m+1,n+1/2}\right)\left(P_{i,m,n+1} - P_{i,m+1,n+1}\right) = 0 \tag{67}$$

At the wellbore, the no-flow intervals ($o-h_1$) and (h_2-H) are described with the equation

$$K_{v_{i,1/2}}\left(P_{i,0,n+1/2} + P_{i,1,n+1/2}\right)\left(P_{i,0,n+1} - P_{i,1,n+1}\right) = 0 \tag{68}$$

For the producing interval (h_1-h_2), the equation is:

$$K_{v_{i,1/2}}\left(P_{i,0,n+1/2} + P_{i,1,n+1/2}\right)\left(P_{i,0,n+1} - P_{i,1,n+1}\right) = -\frac{\bar{Q}\Delta V}{2} \tag{69}$$

At the upper boundary, the equation is

$$\left(P_{0,j,n+1/2} + P_{1,j,n+1/2}\right)\left(P_{0,j,n+1} - P_{1,j,n+1}\right) = 0 \tag{70}$$

and the lower boundary of a model having s-cells in the vertical direction

$$\left(P_{s,j,n+1/2} + P_{s+1,j,n+1/2}\right)\left(P_{s,j,n+1} - P_{s+1,j,n+1}\right) = 0 \tag{71}$$

For the iterative scheme used, equations (70) and (71) are included by imposing the equations

$$\left.\begin{aligned} P_{0,j,n+1} &= P_{1,j,n+1} \\ P_{s+1,j,n+1} &= P_{s,j,n+1} \end{aligned}\right\}, \quad 1 \le j \le m+1 \tag{72}$$

at the end of each iteration for the set of rows i, where $2 \leq i \leq s$.

The iterative scheme used is a simultaneous solution to the proper row-wise combination of equations (66, 67, 68, 69). Starting with row 2 and ending at row s, we obtain a set of equations for each row

$$B_{i,0} P_{i,0,n+1} + C_{i,0} P_{i,1,n+1} = D_{i,0,n+1/2}$$

$$A_{i,j} P_{i,j-1,n+1} + B_{i,j} P_{i,j,n+1} + C_{i,j} P_{i,j+1,n+1} = D_{i,j,n+1/2}, \quad 1 \leq j \leq m$$

$$A_{i,m} P_{i,m,n+1} + B_{i,m} P_{i,m+1,n+1} = 0 \tag{73}$$

To solve these equations, we used the Thomas method (4) which is equivalent to Gaussian elimination but avoids the error growth associated with the back solution of the elimination method. At the beginning of each iteration, the coefficients $A_{i,j}$, $B_{i,j}$, $C_{i,j}$, and $D_{i,j,n+1/2}$ are calculated for each row as it is considered.

Define

$$w_{i,0} = B_{i,0}$$

$$w_{i,j} = B_{i,j} - \frac{C_{i,j} A_{i,j}}{w_{i,j-1}}, \qquad 1 \leq j \leq m \tag{74}$$

and

$$g_{i,0} = D_{i,0,n+1/2} / w_{i,0}$$

$$g_{i,j} = \left(D_{i,j,n+1/2} - A_{i,j}\, g_{i,j-1}\right) / w_{i,j}, \quad 1 \leq j \leq m \tag{75}$$

Then, the solution for the ith row is

$$P_{i,m+1,n+1} = g_{i,m+1}$$

$$P_{i,j,n+1} = g_{i,j} - \frac{C_{i,j}}{w_{i,j}} P_{i,j+1,n+1}, \quad 0 \leq j \leq m \tag{76}$$

Application of this method to rows 2 through s inclusive constitutes one iteration. The values obtained from equations (76) are substituted for the $P_{i,j,n+1/2}$ matrix to insure a better evaluation of the vertical derivatives and a better "initial guess" for the pressures.

Upon completion of the second iteration, the criteria for convergence is checked at every interior pressure point. Let some convergence criteria, Δp, be specified. Then, if

$$\left| P_{i,j,n+1/2} - P_{i,j,n+1} \right| < \Delta p, \quad 1 \leq i \leq s, \quad 1 \leq j \leq m \tag{77}$$

the solution has converged and the calculated pressures ($P_{i,j,n+1}$) form the starting point ($P_{i,j,n}$) for the next time step. Otherwise, this iterative procedure is continued until convergence is obtained; or, until the permissible number of iterations is exceeded. If the number is exceeded, the time increment is reduced and another attempt made to obtain convergence. Exceeding a pre-determined number of successive reductions in time-step size terminates the calculations. By analyzing results obtained through use of various convergence schemes, it was determined that a bi-level convergence criteria worked more satisfactorily than any single-valued schemes tried. In order to describe the bi-level scheme, let the subscripts 1 and 2 respectively represent the more and less restrictive criteria. The relation between the two criteria is given by the equation

$$\Delta p_2 = M \Delta p_1 \tag{78}$$

where M is some integral number between the arbitrarily set limits, $2 \leq M \leq 300$. Usually, Δp, was set at some minimum value, say $0.001/P_o$ (psi/psi). Then, a pre-determined maximum number of iterations to get the solution within this closer tolerance was made a control variable. Failure to converge to this specification caused the comparison to revert to the less stringent criteria. If this criteria was satisfied, then convergence was assumed. Otherwise, one or two more iterations were performed using the less stringent criteria before halving the time step.

While this more relaxed convergence criteria did not significantly affect the material balance error, it did permit a slightly higher maximum time-increment size. In the process of developing the model, the time step was determined to be dependent upon the ratios $\overline{\Delta v}^2/\overline{\Delta y}^2$, r_e^2/H^2, and K_v/K_y as well as the variables found in the dimensionless time coefficient. This dependence on Δv and Δy indicates that the method performs as an explicit forward-difference method whose time step must satisfy the condition

$$\frac{\Delta\theta}{\Delta v^2} + \frac{\Delta\theta}{\Delta y^2} \leq \frac{1}{2} \tag{79}$$

rather than an implicit Crank-Nicholson type method that is stable for all time steps. One or two possible reasons for this behavior can be postulated, but no proof offered. First, the linear transformation of the vertical dimension is not completely satisfactory. All the convergent problems seem to stem from the inability of two successive iterations to converge to the same number. Take a sequence of pressure terms in the jth column, $P_{i-2,j}$, $P_{i-1,j}$, $P_{i,j}$, $P_{i+1,j}$, and $P_{i+2,j}$. Then, perform the customary two initial iterations to give the (n+1) and (n+1/2) matrices. Comparison of these numbers in the two matrices will give

$$\begin{array}{lcrr}
 & & \multicolumn{2}{c}{\text{ITERATION}} \\
 & & \underline{\text{2nd}} & \underline{\text{3rd}} \\
P_{i-2,j,n+1} - P_{i-2,j,n+\frac{1}{2}} & = & \Delta\varepsilon_{-2} & -\Delta\varepsilon'_{-2} \\
P_{i-1,j,n+1} - P_{i-1,j,n+\frac{1}{2}} & = & -\Delta\varepsilon_{-1} & \Delta\varepsilon'_{-1} \\
P_{i,j,n+1} - P_{i,j,n+\frac{1}{2}} & = & \Delta\varepsilon_{0} & -\Delta\varepsilon'_{0} \\
P_{i+1,j,n+1} - P_{i+1,j,n+\frac{1}{2}} & = & -\Delta\varepsilon_{1} & \Delta\varepsilon'_{1} \\
P_{i+2,j,n+1} - P_{i+2,j,n+\frac{1}{2}} & = & \Delta\varepsilon_{2} & -\Delta\varepsilon'_{2}
\end{array} \tag{80}$$

Upon completing the next iteration and bearing in mind that the old (n+1) matrix is now the (n+1/2) matrix, another comparison will show the $\Delta\epsilon$'s all have changed sign. The magnitude of the $\Delta\epsilon$'s are believed to be directly related to the time-increment size because of the second reason: All the higher-order spatial derivatives are included through approximations using the time derivative and the first and second partial spatial derivatives of the time derivative. Hence, all the truncation errors will be directly associated with the time step.

Evaluation for σ

In order to find what affect σ, defined in equations (23) and (24), had upon the resulting calculations, a simplified system was selected for calculations using a range of constant values for σ. This system had uniform horizontal and vertical permeability with one-seventh of the interval, centered about mid-formation, opened for production. There were no simulated fractures or other well stimulations. The criteria for selecting the optimum value for σ was three-fold: First, the value selected should give the maximum stable time-increment size. Second, the value should give the maximum total time for a given number of time-increment calculations. Finally, the value should result in the best performance of the material balance error.

The first choice was $\sigma = 1$. Calculations were made for 255 time steps for a total producing time of 16.48 days. The material balance error at 15.03 days was 0.00075% of the original gas in place (OGIP), or 0.61% of the gas produced (GPD). The maximum time increment was 0.1514 days. For the next run, $\sigma = 0.9$, calculations were made for 151 time increments totalling 9.22 days. The maximum time step was 0.166 days and the material balance error at 5.06 days was 0.0001% (OGIP), or 0.25% (GPD). Comparison of this run to the first 151 time increments of the run for $\sigma = 1.0$ showed a 10 per cent increase in total time and a better material balance. Next, a 158 time-increment case for $\sigma = 0.8$ was run. Total producing time was 10.32 days and the maximum time increment was 0.17 days. The material balance error at 10.07 days was 0.00056% (OGIP), or 0.68% (GPD). Comparing this to the first 151 increments for $\sigma = 0.9$ showed a 4 per cent increase in total producing time. A further reduction in σ to 0.7 was made for the next calculations. The maximum size of the 160 time increments was 0.1567 days. Total producing time was 10.52 days and the material balance error was 0.00048% (OGIP), or 0.57% (GPD). Comparison of these results to the run for $\sigma = 0.8$ revealed a smaller maximum time-step size; so, the next trial value was $\sigma = 0.75$. In 271 time increments, the maximum was 0.177 days and the total production time was 20 days. The material balance error at 20.0 days was 0.00098% (OGIP), or 0.60% (GPD). Since this was not radically different from the results using $\sigma = 0.8$, further interpolation was deemed unnecessary. From this limited analysis, it was concluded that $\sigma = 0.75$ should be used for the calculations.

Computer Programming

An IBM 7090 was available for use in solving the system of equations in this problem. The time-step limitations and the large number of equations required for describing this system made a large machine with immediate-access storage and rapid calculational speed mandatory. Since it was not possible to anticipate what computational techniques would be used to solve this system of equations, the ultimate computer program was developed in segmented or sub-program form to enable inexpensive interchanging of these sub-programs to form new programs. This system consists of a control program and a series of specialized programs. The control program calls upon each specialist to do a particular job and then return control to the main program upon completion. The first sub-program is for placing all necessary data in the machine in proper form. Another was necessary for calculating all invariant coefficients such as the derivative of the logarithm of the permeability at each pressure point, the cell radii, and cell volumes. Next, a sub-program was used to calculate the matrix $D_{i,j,n}$ as given in equation (57). Following this is a routine for calculating the coefficients of the boundary equation according to the type being used. The matrix $D_{i,j,n+1/2}$, obtained from evaluating equation (65), is calculated one row at a time as it is used in the solution of equation (66). Also included in this sub-program is the programming for utilizing the Thomas Method to get the pressure matrix, $P_{i,j,n+1}$. When appropriate, one sub-program is called upon for checking the convergence and another for specialized diagnostic routines utilized mainly during model development. The remaining sub-programs are for printing results and for putting the data in an acceptable form to be plotted by a mechanical x-y data plotter.

Each computer run required from 5 to 40 minutes IBM machine time, depending upon the complexity of the rate schedule, the model parameters, and the length of the time span for which the results were needed. A total of 60 to 80 runs was made utilizing the final model.

A representative sample is included in the presentation of this work.

The one-dimensional model results presented in connection with work shown in Chapters IV and V were obtained with an existing computer program. The mathematical basis of this model has been published previously. (36) Machine-time requirements for these cases ranged upward to 1/2 minute per case.

Model Justification

There are few criteria for certifying the validity of the calculational results obtained from using this model. The most obvious requirement is that the model duplicate the behavior obtained from a one-dimensional model when the properties and boundary conditions are such that all resulting equi-potential lines are vertical. Figure 3 shows the results of producing such a system using both models, whose properties are tabulated in Table I. From the equations, one would expect identical performance as shown. However, this comparison also shows that there are no round-off errors causing instabilities between rows in the two-dimensional solution. Other justifications must lie in the ability of the model to predict performance analogous to that one would expect of such a physical system. One phase of the justification work was accomplished through making computer runs to obtain comparative results for problem areas of recent interest, such as the effects of partial well penetration (21) on resulting wellbore pressure measurements. These results are presented in Chapter VI. Additional verification is presented in the next chapter wherein it is shown that the model performance violates no principles of fluid flow as currently understood.

Summary

A finite difference approximation to the two-dimensional partial-differential equation for unsteady-state gas flow that is capable of describing flow behavior through widely varying permeability configurations has been developed. Additionally, it is capable of describing flow through various types of boundary conditions such as open-hole completions, partially penetrating wells and single-plane fractures. Inclusion of the variable flow rate boundary equations makes it possible to study periods of pressure build-up as well as draw-down tests. While the treatment of the permeability functions is not entirely correct as verified by the increasing material balance error for permeability discontinuities at large distances away from the wellbore, it does provide a much greater detailed description of the possible permeability variations than heretofore presented.

An iterative scheme has been developed that will solve these equations. The maximum permissible time step for which the solution remains stable in multi-layered systems is generally too small to warrant use of the model as a long-term predictive tool. The size of the time step is dependent upon the formation thickness—areal drainage radius ratio; the number of model divisions in the vertical dimension compared to those in the radial dimension; the horizontal to vertical permeability ratio; the porosity and the absolute magnitude of the permeability. Therefore, the most beneficial use for the model in its present form is in the study of the short-term transient effects about the wellbore both in pressure draw-down and build-up analysis.

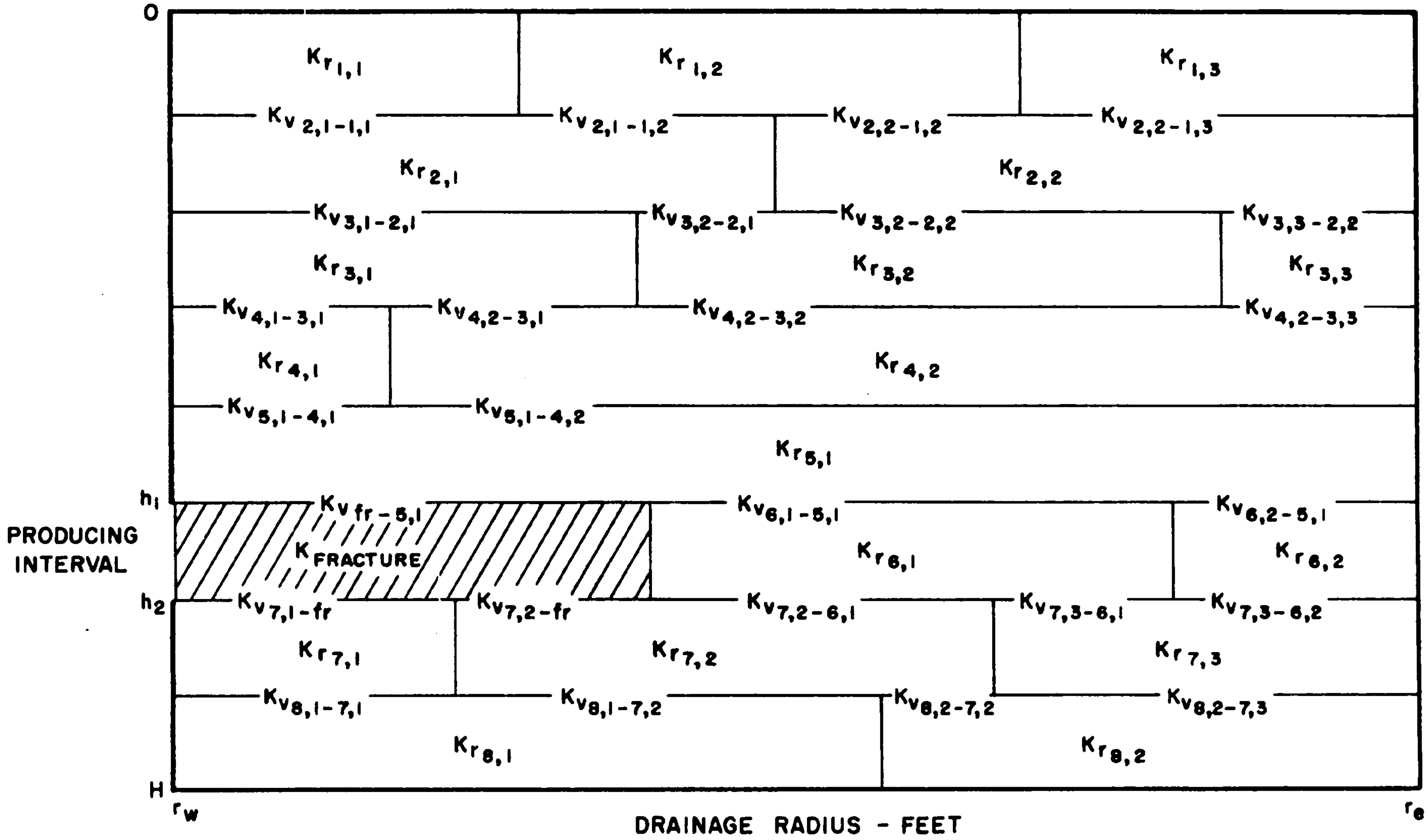

Figure I RADIAL CROSS-SECTION OF CYLINDRICAL, SINGLE-WELL MODEL SHOWING SAMPLE PERMEABILITY DISTRIBUTION AND WELL COMPLETION

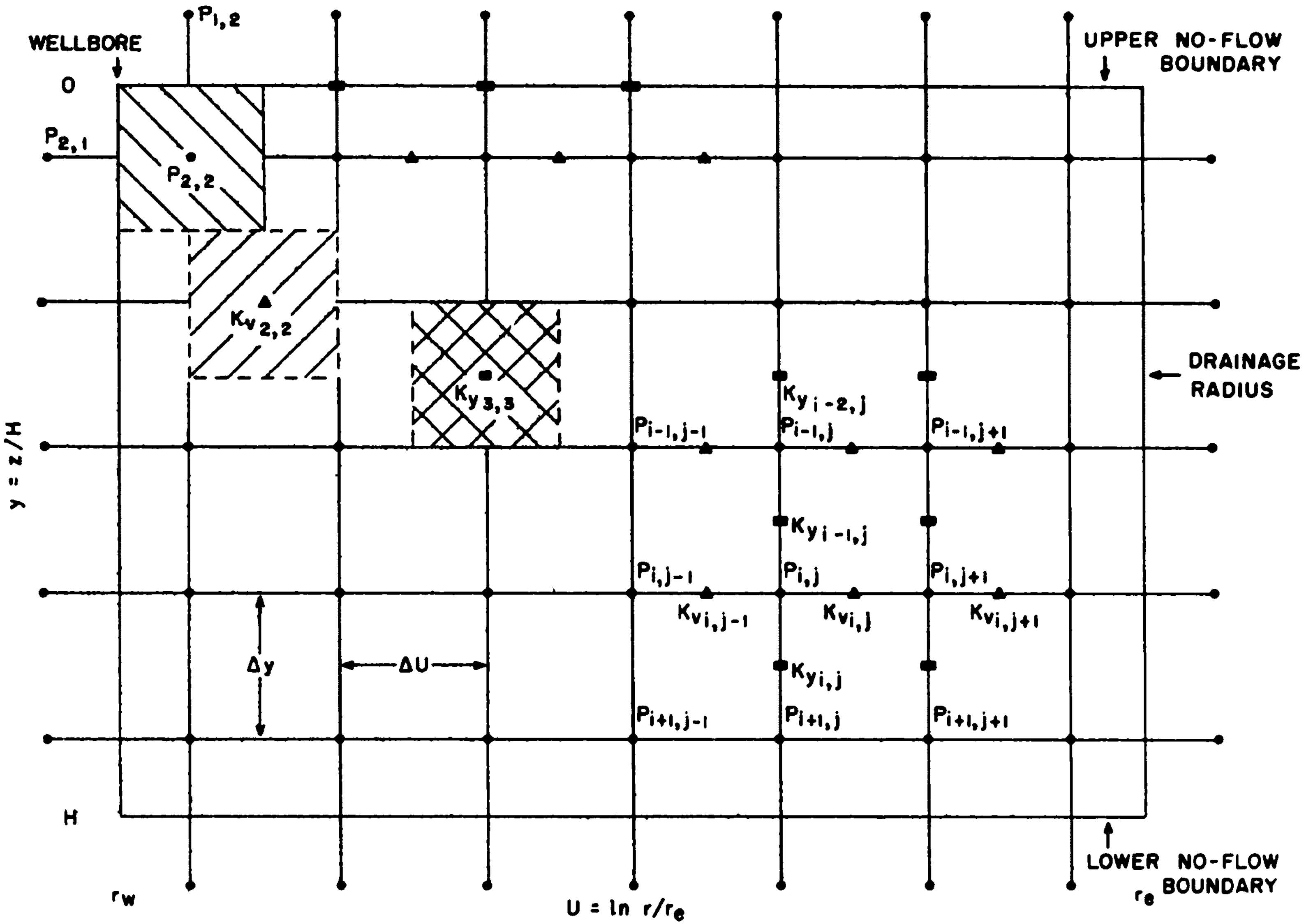

FIGURE 2 GRID NETWORK REPRESENTATION FOR MATHEMATICAL MODEL

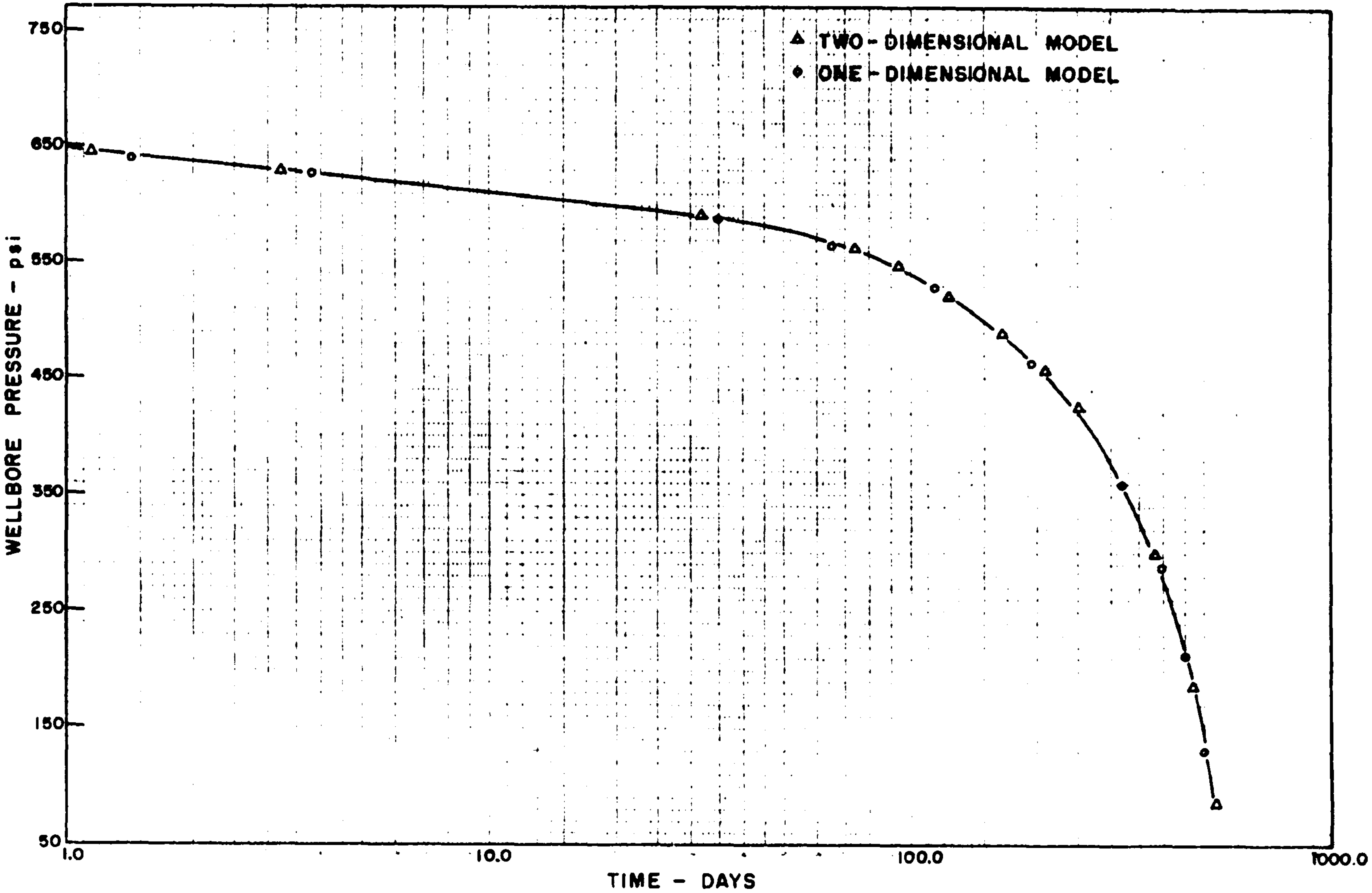

FIGURE 3 COMPARISON OF CALCULATED PRESSURES USING ONE- AND TWO-DIMENSIONAL UNSTEADY-STATE MODELS

TABLE I

CONTROL VARIABLES FOR PRESSURE COMPARISON BETWEEN ONE- AND TWO-DIMENSIONAL UNSTEADY STATE MODELS

Variable Name	One-Dimension	Two-Dimension
Formation Pressure, psi	800	800
Standard Pressure, psi	15.025	15.025
Drainage Area, acres	40	40
Formation Thickness, ft	100	100
Porosity, per cent	25	25
Formation Temperature, °F	90	90
Standard Temperature, °F	60	60
Number Cells, radial	51	51
Number Cells, vertical		3
Flow Rate, MCFD	1500	1500
Wellbore Radius, ft	0.25	0.25
Horizontal Permeability, md	4	4
Vertical Permeability, md		4
Gas Viscosity, cp	.012	.012

CHAPTER III

VARIABLE CAPACITY

A more complete description, than heretofore given, of the relatively short-term transient period and the geometrical parameters upon which its life span depends, will be presented. Supplementary to the verbal descriptions of the effects of parameters such as formation thickness and vertical permeability on the calculated pressure behavior, will be graphical presentations of numerical examples. These results were obtained from hypothetical data through use of the FORTRAN programs developed for the IBM 7090 computer. The purpose of this analysis is to provide a thorough understanding of the phenomena in order that proper recognition of actual producing geometries, wherein the transient effects may significantly affect the reliability of predicted performances, may be assured. Contrary to the conclusion reached by Pendergrass and Berry (29), it will be shown that in some completion geometries the "early-transient period" can last for a significant time and is a matter for practical concern. This "early-transient period" is analogous to what we choose to call the vertical component of variable flow capacity.

Perhaps the easiest way to define variable flow capacity is to define what is meant by constant capacity and designate all situations outside this category as being of variable capacity. Consider a producing formation having uniform horizontal and vertical permeability (not necessarily identical), uniform porosity, and uniform thickness. Then divide the formation into a number of imaginary layers. Assume that a well penetrating the entire interval is completed open-hole in this formation. From the moment of initial production, all the layers will contribute identical quantities of gas to make up the total production rate. The radius of drainage (1) will move uniformly in the radial direction. There will be no pressure gradient in the vertical direction. The apparent flow capacity, obtained from wellbore pressure movements, will stay the same and will be equal to the permeability—thickness product. This system is producing at constant capacity. A constant capacity system is defined as the state of a producing formation when each and every horizontal segment, regardless of its permeability, is contributing its proportionate share to the producing rate; and, when the apparent permeability-thickness product determined from wellbore pressure and flow-rate measurements remains unchanged. The fractional proportionate share for any layer is defined as the porosity-thickness product for the layer divided by the sum of this product for each layer.

The system described above is the only one that starts at constant capacity and remains constant throughout its producing life. Others produce for a period of time as a variable capacity system and then change to one having constant capacity. Still others remain in a state of variable capacity for a large percentage of their producing life.

As indicated by the name, variable capacity can occur only during a transient period. When confining our discussion to two dimensions, the transient period can be thought of as having two components; radial and vertical. At first, technology successfully ignored both components because of the rapid disappearance of their effects in high permeability formations. Then, as the formations became tighter, the radial component of the transient period was first recognized and attempts made to include it in the calculations by using the isochronal testing method. (8) The vertical component, partially defined in recent theoretical papers, (19,29,34) was ignored as far as the analysis of transient data was concerned; although it was generally recognized that early measurements reflected the presence of a "skin effect". (41) In previous work the assumption has been made that all such distortions would be dampened out within an insignificant amount of time. Also, it is necessarily assumed that the capacity within the drainage radius, determined by the length of the flow test, is representative of the entire area subjected to drainage by that well. This is because the capacity determined from the testing is only the effective value for the limited area through which the drainage radius has moved. Any changes in capacity outside this area would be reflected at the wellbore and hence indicate a system in a state of variable capacity. An example of a variable capacity system for a long period of time would be a very tight formation drilled on wide spacing with radically changing areal fluctuations in the formation thickness. Predictive equations using the capacity value determined from short-term test data can give erroneous answers. They will be optimistic or pessimistic depending upon a resulting increase or decrease in the effective capacity and the gas reserves. However, this limitation on the radial component of variable capacity is recognized and, consequently, allowances are made. Too, the probability for radical changes in total formation capacity, excluding faulted areas or reservoir limits, is low enough to make it generally more prudent to use this analysis with its inherent assumptions than to attempt to gather data until all transient periods are definitely known to have expired. Fulfillment of this unrealistic criteria quite probably would require extremely long test periods.

In order to further clarify the radial component of variable capacity, consider an open-hole completion in a layered reservoir having concentric zones of uniform, but different, permeabilities. Again, upon initiating production, there are no vertical components of the pressure gradient because of its uniform movement through each zone. Too, proportionate contributions of all the layers to the producing rate is evident. However, in this case the effective capacity, as determined by any properly applied conventional analysis, is continuously changing until the transient reaches the outer boundaries of the drainage area. Thus, no single capacity value could necessarily be expected to duplicate this behavior until after this transient period was expired. However, with proper duplication of the pressure behavior during the entire transient period the concentric zones of permeability will have been identified and future matching assured.

Non-Uniqueness of Steady-State Permeabilities

The permeability distribution required to match wellbore pressure behavior after this transient period expired is not unique.

In order to demonstrate this, an arbitrary permeability configuration tabulated as Curve A in Table II was selected for calculating wellbore pressure (at a specified flow rate) as a function of time, using the one-dimensional model. This is shown as Curve A in Figure 4. A uniform permeability of 8 md was then chosen and the appropriate 4-cell skin was determined by trial-and-error pressure matching calculations. The resulting pressure match is shown as Curve B in Figure 4. Observe the pressure match starts after the first 10 days and continues for a two-year period until the calculations are terminated near a cut-off pressure of 200 psi. Still another permeability configuration tabulated as Curve C in Table II was selected and adjusted to obtain a pressure match. The resulting pressure is shown as Curve C in Figure 4. In all three cases the pressure behaviors were identical, or could be made identical with a slight adjustment of the skin values, after the initial transient period of some seven to ten days. These calculations are not presented to indicate that any permeability distribution with some associated skin effect will match the pressure behavior at the well; but, it does show that once the material balance stage of depletion starts, there is more than one representation of permeability that provides duplicate pressure behavior at the wellbore. The early portions of the curves are all unique. For this pressure is the result of flowing through a continuously-changing effective permeability which is a composite of the flow resistances measured from the wellbore to the drainage radius. As the drainage radius approaches the outer boundary, the curves converge. Hence, there is less chance of picking up minor changes in the permeability-thickness product for more remote sections of the drainage area. However, the divergence of pressure values in early times shows there is possibility for definitive information having reasonable accuracy when limited to the immediate vicinity of the wellbore. Figure 5 shows a plot of formation pressure versus log radius after periods of 78 days and 2 years for each of the three permeability distributions. The wellbore pressure is the same in all cases but the radial pressure distribution is different. Significantly different pressure values are restricted to the first 100 feet around the wellbore even though large differences in permeability extend out for some 200 feet.

Effect of Restricted Producing Intervals

Next, consider the homogeneous formation with only a small fraction of the formation open to production at the wellbore. When production is first initiated, the gas produced comes from the immediate vicinity of the opened interval. Thus, the formation would be producing as if the capacity were approximately equal to the permeability-thickness product of the opened interval (3) and the reserves equal to the porosity-thickness product. As the pressure sink forms, the contiguous layers start contributing to the flow capacity at a rate depending upon the vertical permeability. With each additional layer contributing, the net effective capacity of the formation will be increased and the skin effect more pronounced. This continues at any radial distance until the upper and lower impermeable boundaries are reached. Figure 6 attempts to illustrate the passing of a pressure transient through a cylindrical shell located at a radial distance of 17.9-20.8

feet from the wellbore in the formation whose properties are tabulated in Table III. The plot of pressure versus the vertical distance from the upper boundary shows the pressure in each layer as a function of time. Note that 1.2 days were required for a measureable pressure drop to occur in the lower-most section while the completed interval containing the fracture experienced a pressure drop almost immediately. The curve at 10.47 days shows a steady-state condition exists at that time and continues for the duration of the run. This is one illustration of the vertical component of variable capacity.

Effect of Formation Thickness

While the system is dominated by the vertical component of variable capacity, standard one-dimensional analyses of well test data are subject to considerable error. In order to ascertain the duration of this effect, one must show on what it depends. Formation thickness is a factor in determining the time required for the vertical component to disappear. The transient must travel from the completion interval to both the upper and lower extremities and establish flow paths to effectively drain all the reserves. In order to show the effects of formation thickness, hypothetical formations having net pays of 24.5 feet, 49 feet, and 98 feet and properties tabulated in Table IV, Runs 1, 2, and 3, are divided into 7 layers of equal thickness. The middle layer will be opened to production in all three cases. For the 24.5-foot section, this interval would be 10.5-14 feet; the 49-foot section, 21-28 feet; and the 98-foot section, 43-56 feet. Figure 7 shows the per cent gas produced from each layer as a function of time for each of the three thicknesses. Time requirements for reaching constant vertical capacity in each of the three cases ranged from 0.4 day for the thin section to more than 10 days for the thick section.

Effects of Vertical Permeability

Vertical permeability plays a very important role in determining the time required for the transient effects to reach the upper and lower boundaries. Just as the radial movement of the transient effects depends upon the permeability-porosity quotient, one would expect the same to be true for the vertical. To illustrate this, we take the system tabulated in Table IV, Runs 1, 4, and 5, where the vertical permeability is varied from 4.0 md to 1.0 md and 0.3 md. Figure 8 shows the time required for each of the systems to reach constant vertical capacity. As expected, the time requirements increase with decreasing vertical permeability.

Effects of Completion Interval Location

The location of the completion interval can alter the time requirements for constant vertical capacity. As shown by comparing Figure 9 with Figure 10, less time is required when a formation having uniform permeability is completed at mid-formation rather than at the upper or lower boundary. When completing at mid-formation, Figure 9 shows that 0.4 day is required in a 98-foot thick uniform system having 3 md permeability. Figure 10 also shows that 1.4 days are required for the completion interval 85-98 feet. The benefits derived from locating the completion interval near the center of the formation can be overshadowed by the presence of low permeabilities in this area. Such a comparison is shown in Figure 11. On the lower left portion of

Figure 11 is plotted the per cent gas produced from the completion interval of seven separate computer runs. The system used is the layered reservoir whose properties are tabulated in Table III. The time at which each curve decreases to 14.3 per cent signifies the termination of the period in which the vertical component of variable capacity exists. Interval 4 located at mid-formation is the first to reach this value. When comparing the runs in which the two adjacent layers were completed, the 2-md Layer 5 required less time than 6-md Layer 3 for the vertical component to disappear. The next two layers required the same amount of time. Layer 2 had a permeability of 2 md and Layer 6 had 4 md. A final comparison between the upper-most and the lower-most layers reveals that Layer 1 with 4 md had reached 14.3 per cent, while Layer 7 with 6 md had not. In two of the three comparisons, the lower permeability layer completion resulted in a more rapid disappearance of the vertical component of variable capacity. However, this is not enough data for general statements about these effects to be made.

Effects of Well Stimulation

The type of well stimulation used will affect the time requirements for constant vertical capacity. If we picture transient movement in fractured systems as being more rapid in the high conductivity area, then we can visualize a very rapid establishment of an extremely large area susceptible to cross-flow. Then little or no outward radial movement is required to establish flow paths for effective drainage. Consequently, the time requirement would be largely that required for the gradient to travel in the vertical direction from the fracture to the more remote boundary (whether upper, lower or both). Thus, the increased fracture radius could only reduce the time requirements to this minimal time.

From Aronofsky and Jenkins' equation showing that drainage radius movement is dependent upon the permeability, we should expect that the higher the permeability of the fracture, the more rapid the gradient movement and hence the faster disappearance of variable capacity. However, the gradient moves so fast that in reality the reduction in time would generally not be measureable. Figure 12 shows the time requirements to be the same for 3 different fracture conductivities in a uniform system with a 20-foot fracture located at mid-formation.

Effects of Porosity

Formation porosity should affect the vertical movement of the pressure gradient in a manner analogous to that observed for the horizontal component. That is, for decreasing porosity there is an increasing transient velocity. While runs presented in this work are calculated using a high porosity of 40 per cent in order to dramatize the transient effects, time values presented may be scaled directly as shown in Figure 13. Although all the other values used are realistic, analogous statements concerning scaling of values are pertinent for the other variables found in the dimensionless time parameter of equation (13); namely, reservoir pressure, gas viscosity, and permeability.

Effect of Variable Rate

All the work thus far presented shows that for a constant producing rate the vertical component of the transient effects will eventually disappear, never to return. Since formations are seldom produced at constant rates, the question of the effect of rate changes arises. Shown in Figure 14 is the per cent gas produced for three rows in a system, whose properties are tabulated in Table V, wherein the rate was changed every five days. As can be seen, the system never became one of constant capacity. In such a case, we cannot expect to duplicate the behavior with a one-dimensional model. More work needs to be done in order to determine the percentage deviation such practices would have on the ultimate predictions. Since it is necessary that any system subjected to one-dimensional analysis reach the condition of having an insignificant vertical component of variable capacity, it is important to determine the time period so required and take data in excess of that amount of time. Otherwise, our interpretations may be subjected to considerable error.

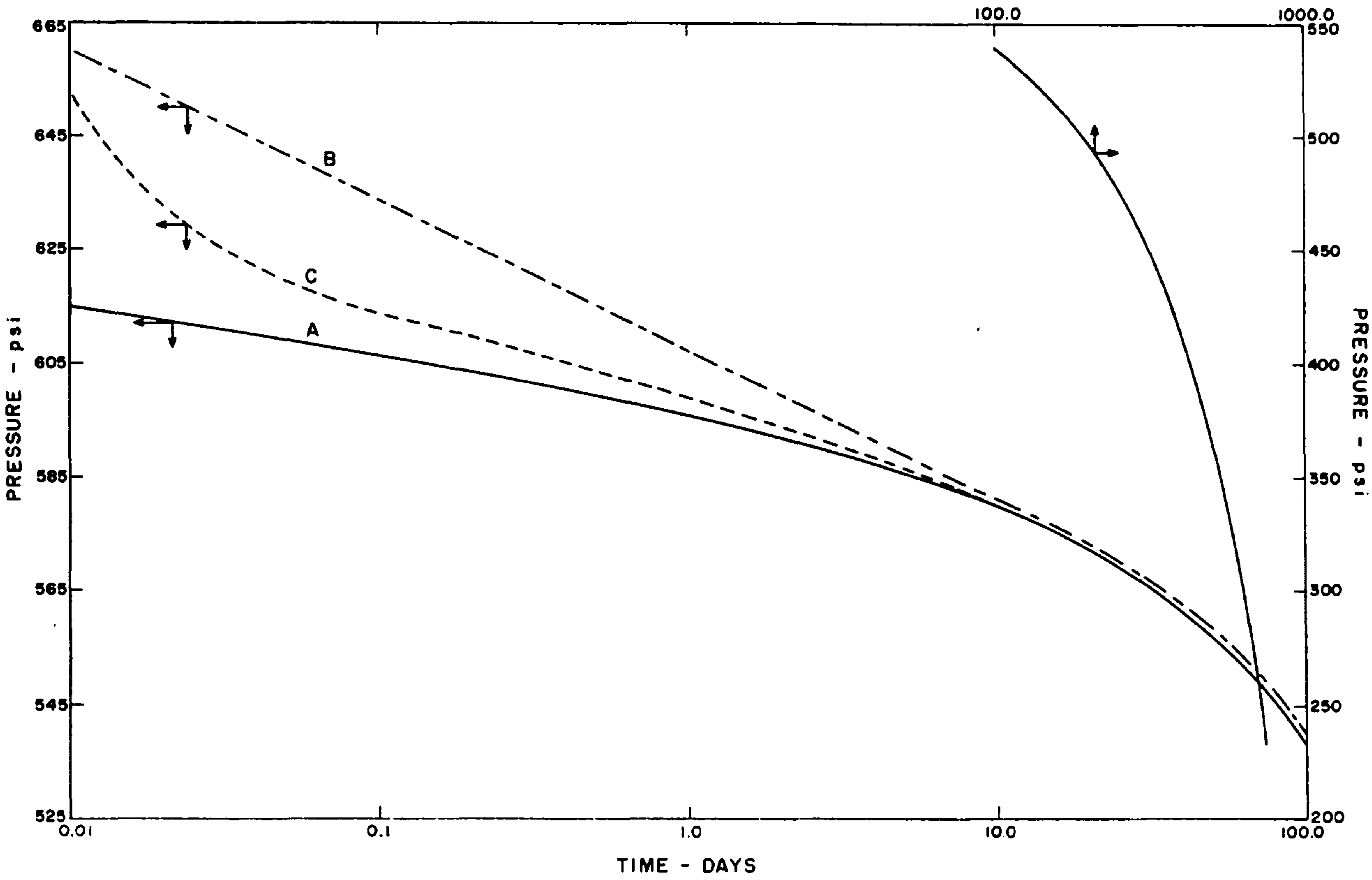

FIGURE 4 PRESSURE CALCULATIONS SHOWING NON-UNIQUENESS OF PERMEABILITY DISTRIBUTIONS FOR CONSTANT PRODUCING RATES EXCEPT FOR A SHORT INITIAL TIME PERIOD

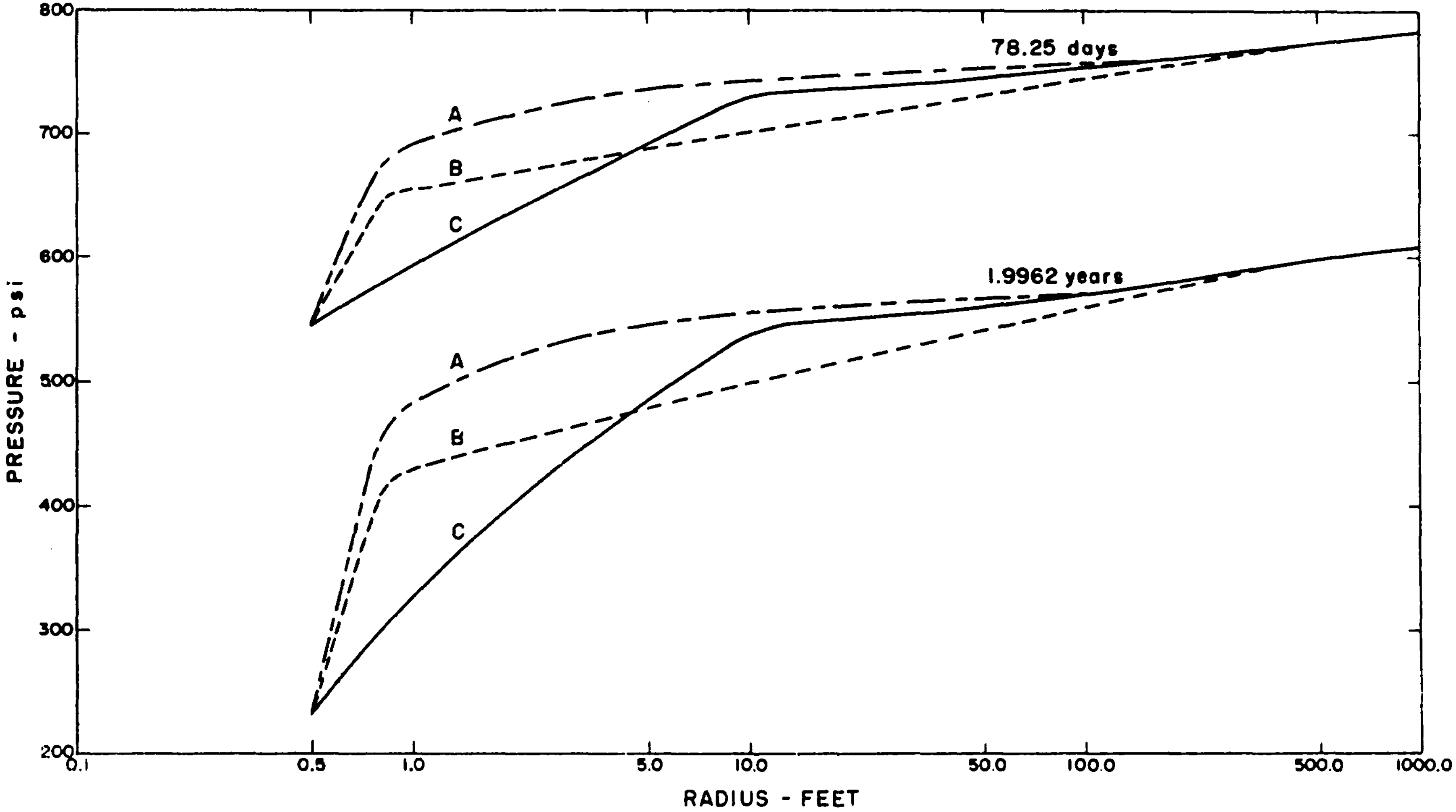

FIGURE 5 RADIAL PRESSURE DISTRIBUTIONS HAVING THE SAME WELLBORE PRESSURE FOR THREE PERMEABILITY CONFIGURATIONS GIVEN IN TABLE II

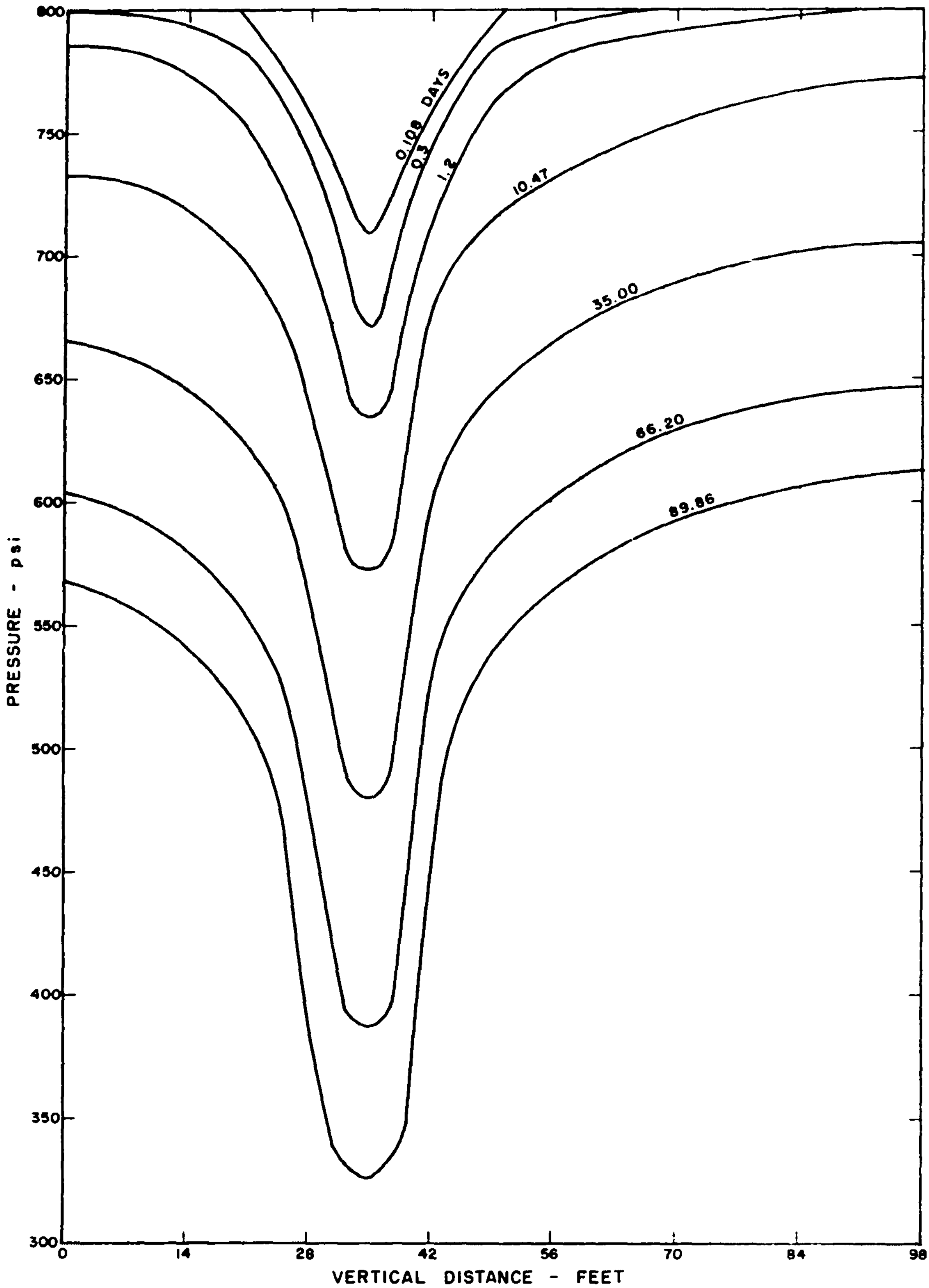

FIGURE 6 PRESSURE GRADIENT MOVEMENT IN A LAYERED FORMATION THROUGH A CYLINDRICAL SHELL HAVING AN INNER RADIUS OF 17.9 FEET

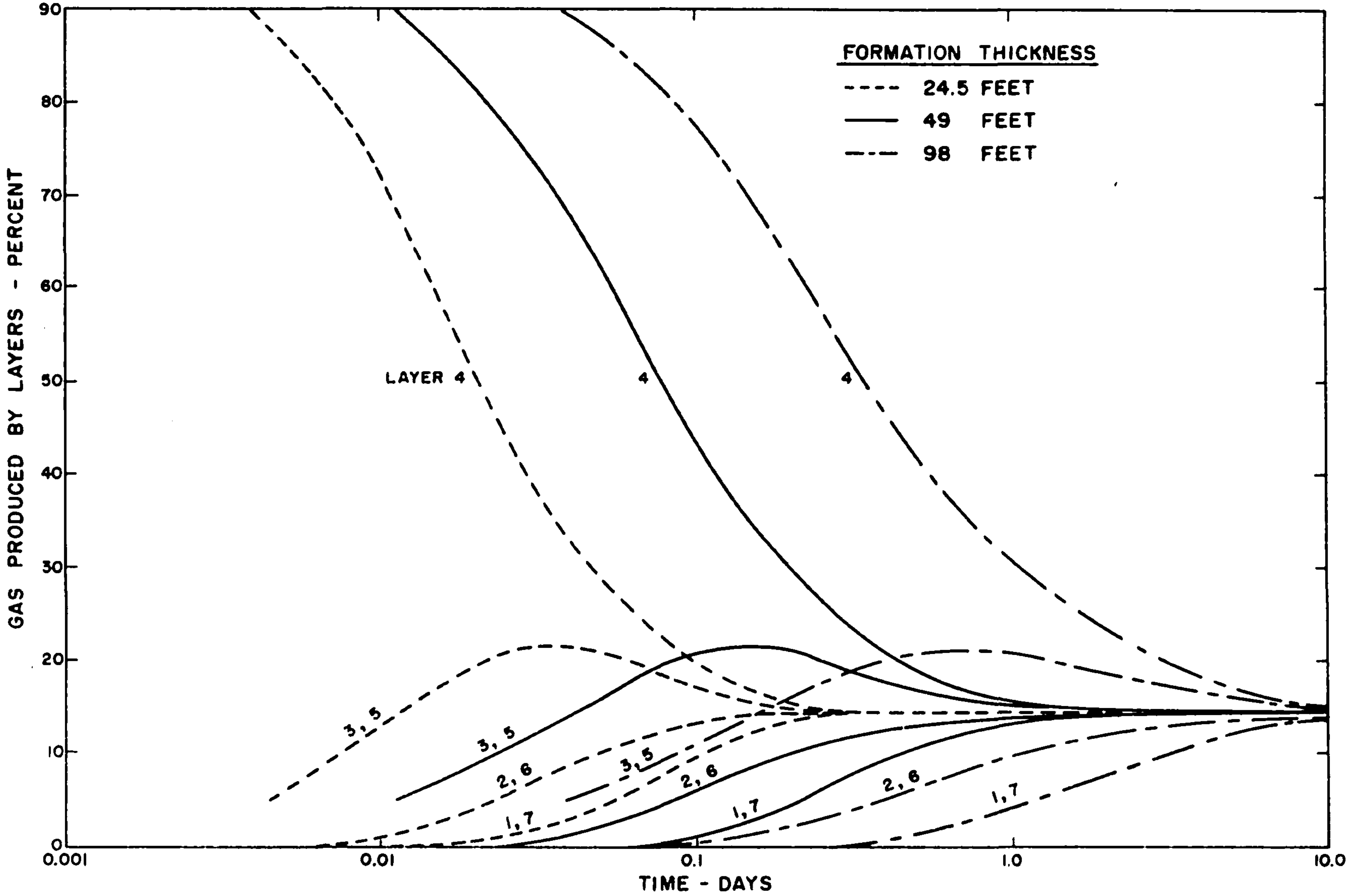

FIGURE 7 EFFECT OF FORMATION THICKNESS ON DURATION OF VERTICAL COMPONENT OF VARIABLE CAPACITY

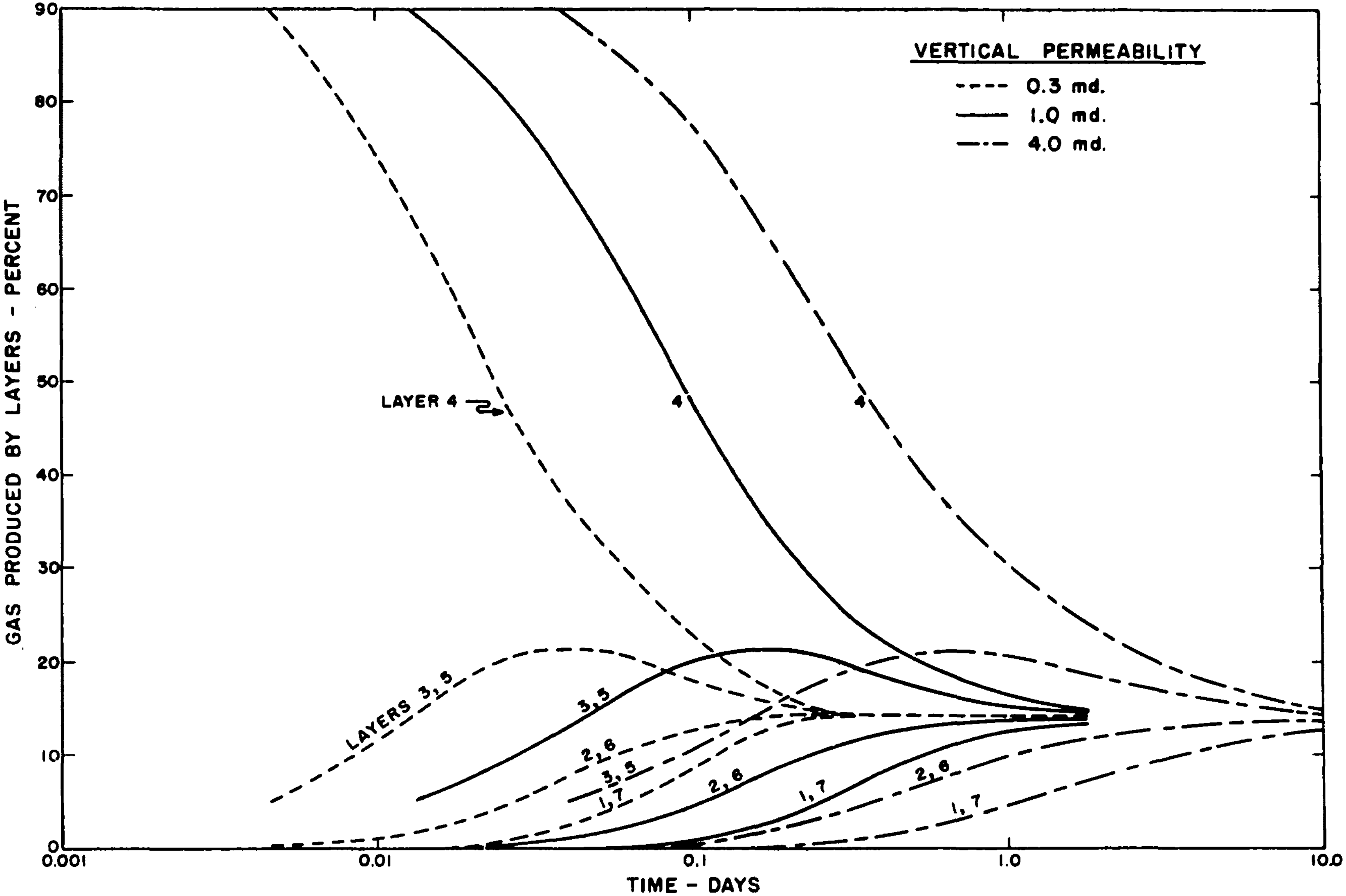

FIGURE 8 EFFECTS OF VERTICAL PERMEABILITY UPON THE DURATION OF THE VERTICAL COMPONENT OF VARIABLE CAPACITY

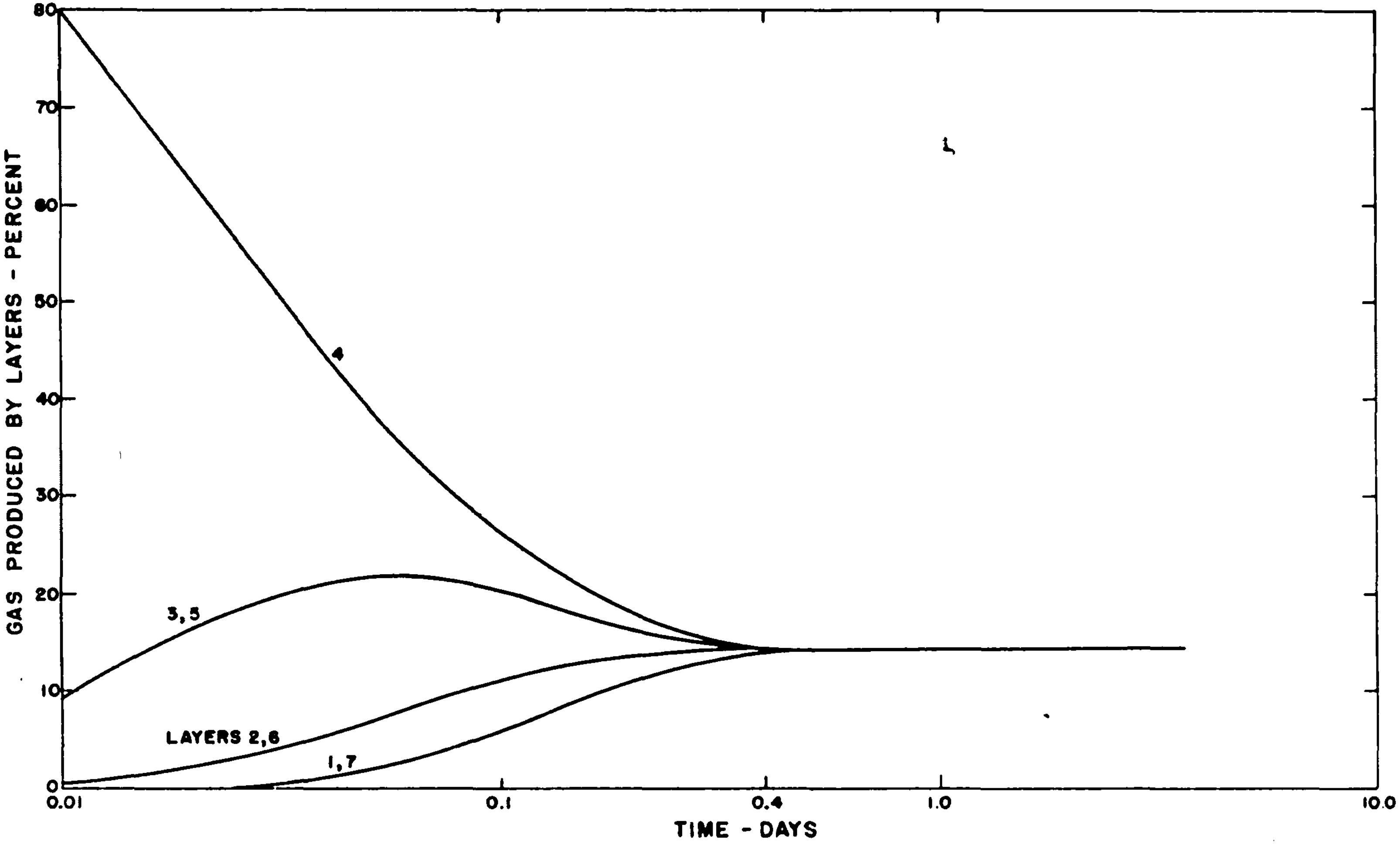

FIGURE 9 DURATION OF VERTICAL COMPONENT OF VARIABLE CAPACITY FOR UNIFORM SYSTEM WITH COMPLETION INTERVAL ABOUT MID-FORMATION

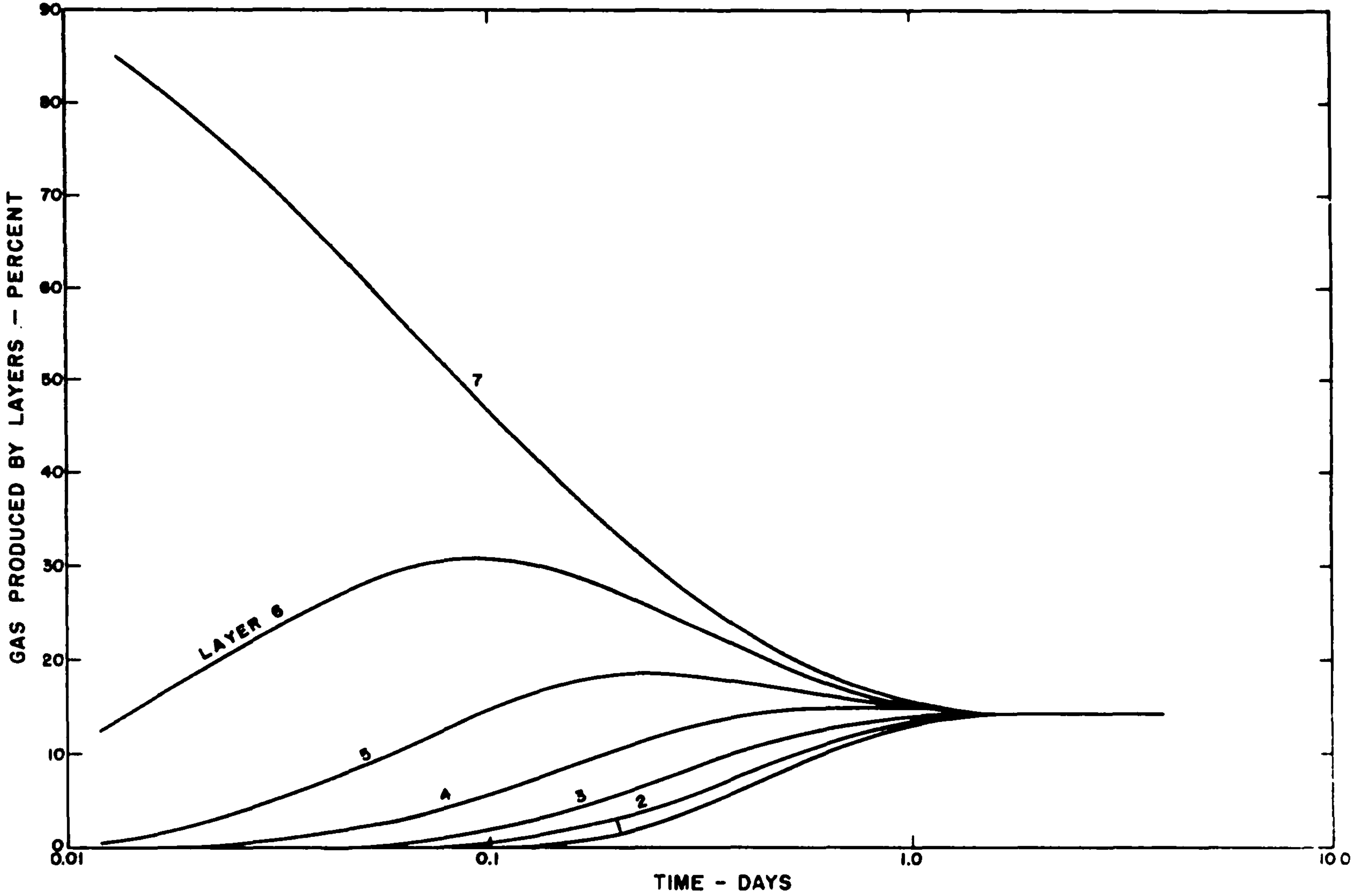

FIGURE 10 DURATION OF VERTICAL COMPONENT OF VARIABLE CAPACITY IN UNIFORM SYSTEM WITH COMPLETION INTERVAL AT 85-98 FT.

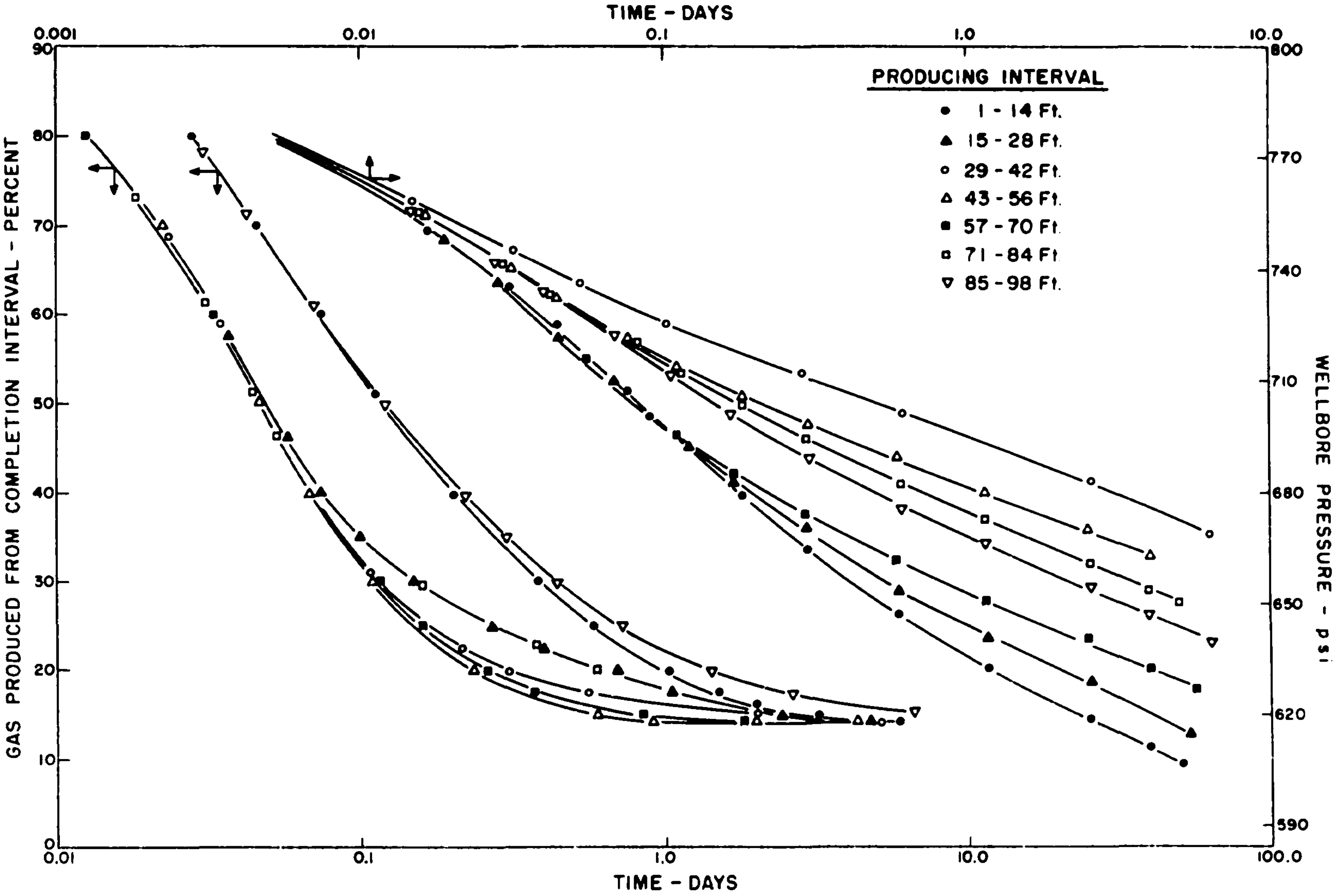

FIGURE 11 PRESSURE CALCULATIONS FOR EACH COMPLETION INTERVAL CONTAINING A SMALL FRACTURE AND THE CORRESPONDING CONTRIBUTION MADE TO THE PRODUCING RATE

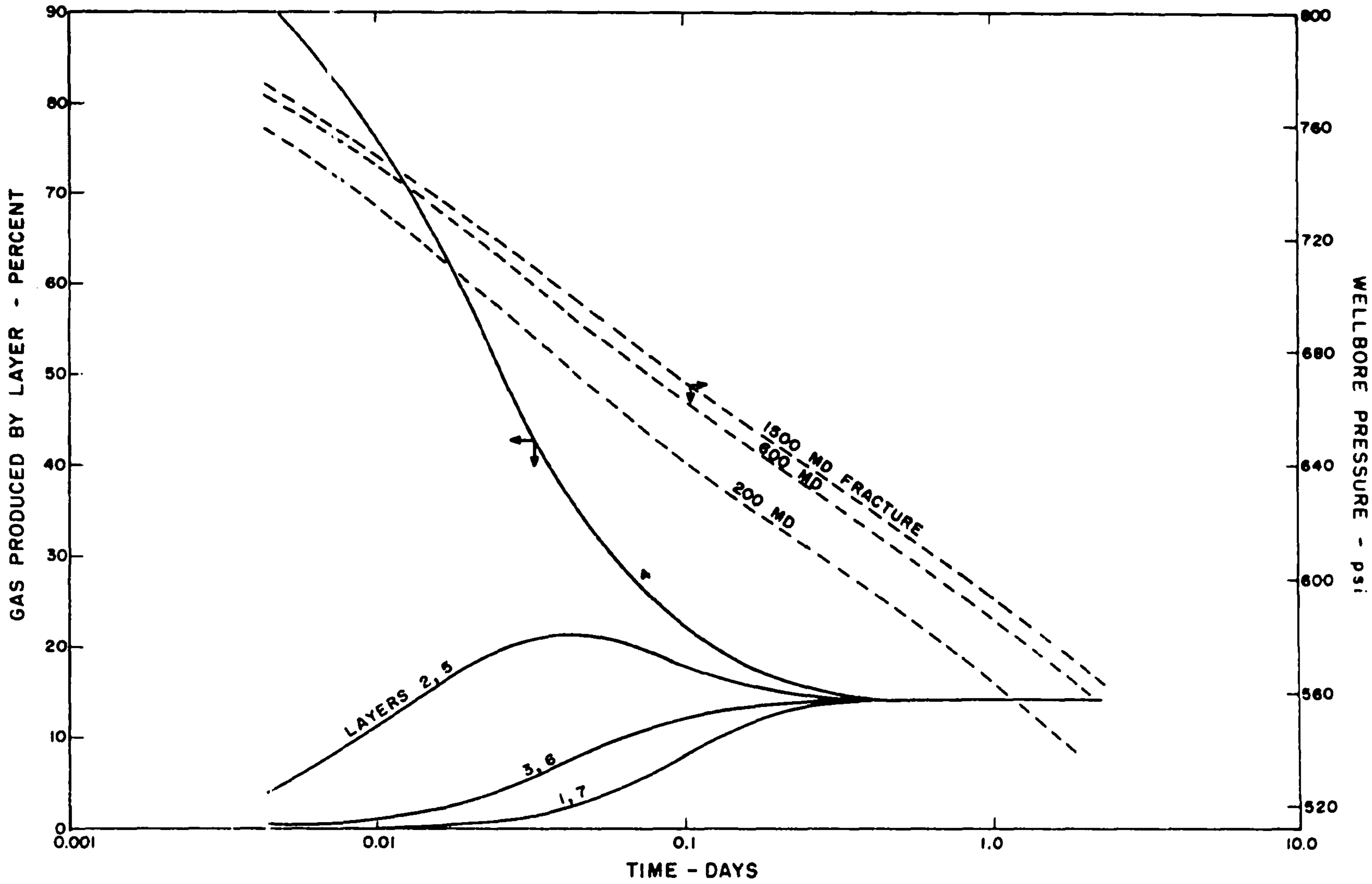

FIGURE 12 EFFECT OF FRACTURE CAPACITY ON THE VERTICAL COMPONENT OF VARIABLE CAPACITY AND THE WELLBORE PRESSURE BEHAVIOR

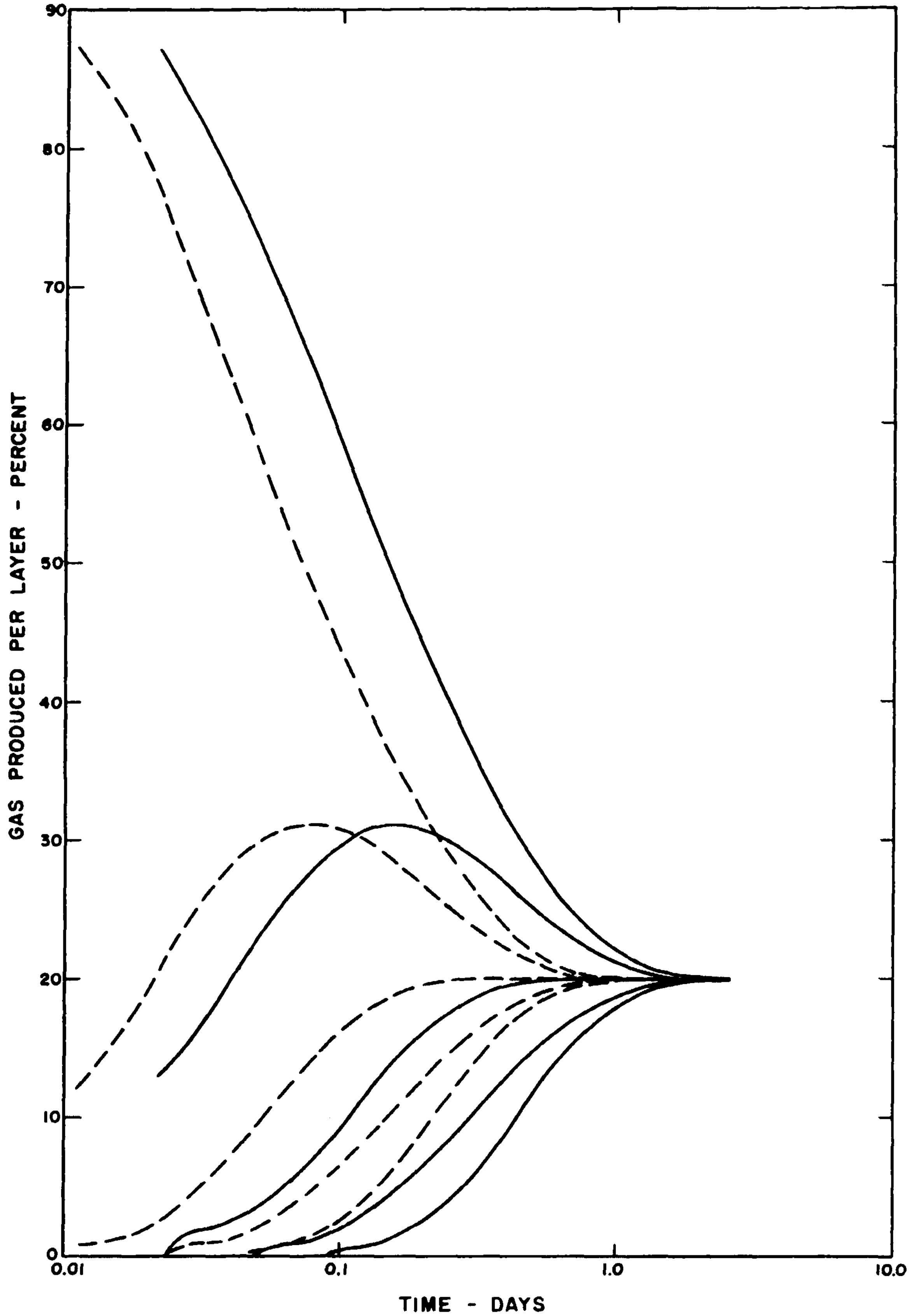

FIGURE 13 EFFECT OF POROSITY ON DURATION OF VERTICAL COMPONENT OF VARIABLE CAPACITY

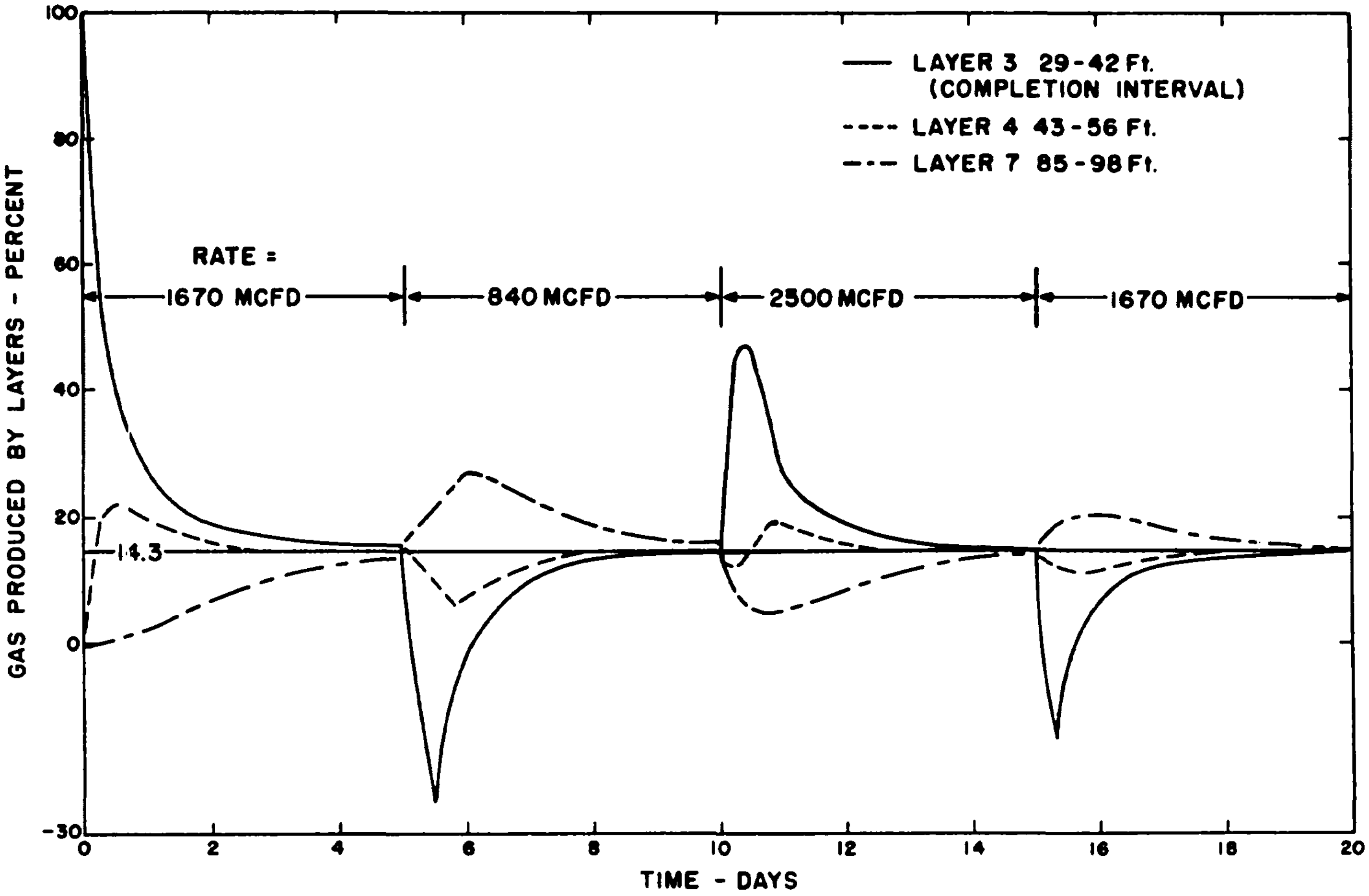

FIGURE 14 EFFECT OF RATE CHANGES ON VERTICAL COMPONENT OF VARIABLE CAPACITY

TABLE II

PERMEABILITY VALUES USED TO SHOW NON-UNIQUENESS
OF STEADY-STATE PERMEABILITIES

Cell Radius ft	Curve A Perm, md	Curve B Perm, md	Curve C Perm, md
0.5	0.732	0.99	2.9
0.585	0.732	0.99	2.9
0.683	0.732	0.99	2.9
0.799	0.732	0.99	2.9
0.934	4.0	8.0	2.9
1.092	4.0	8.0	2.9
1.276	4.0	8.0	2.9
1.492	4.0	8.0	2.9
1.744	4.0	8.0	2.9
2.039	4.0	8.0	2.9
2.384	8.0	8.0	2.9
2.787	8.0	8.0	2.9
3.258	8.0	8.0	2.9
3.808	8.0	8.0	2.9
4.452	16.0	8.0	2.9
5.205	16.0	8.0	2.9
6.084	16.0	8.0	2.9
7.113	16.0	8.0	2.9
8.315	16.0	8.0	2.9
9.721	24.0	8.0	2.9
11.364	24.0	8.0	15.0
13.285	24.0	8.0	15.0
15.530	24.0	8.0	15.0
18.155	24.0	8.0	15.0
21.224	24.0	8.0	15.0
24.812	32.0	8.0	15.0
29.006	32.0	8.0	15.0
33.909	32.0	8.0	15.0
39.640	32.0	8.0	15.0
46.341	32.0	8.0	15.0
54.174	30.0	8.0	15.0
63.332	26.0	8.0	15.0
74.037	26.0	8.0	15.0
86.552	24.0	8.0	15.0
101.182	22.0	8.0	15.0
118.285	20.0	8.0	15.0
138.280	18.0	8.0	15.0
161.654	16.0	8.0	15.0
188.979	14.0	8.0	15.0
220.923	14.0	8.0	15.0
258.266	12.0	8.0	8.0

TABLE II-Continued

Cell Radius ft	Curve A Perm, md	Curve B Perm, md	Curve C Perm, md
301.922	10.0	8.0	8.0
352.958	8.0	8.0	8.0
412.620	7.0	8.0	8.0
482.367	6.0	8.0	8.0
563.904	6.0	8.0	8.0
659.223	7.0	8.0	8.0
770.655	7.0	8.0	8.0
900.922	9.0	8.0	8.0
1053.209	9.0	8.0	8.0

TABLE III

CONTROL VARIABLES AND PERMEABILITY DISTRIBUTION FOR LAYERED RESERVOIR WITH REDUCED PERMEABILITY 180 FEET AWAY FROM WELLBORE

Variables	
Reservoir Pressure, psi	800
Standard Pressure, psia	15.025
Formation Thickness, ft	98
Area of Drainage, acres	40
Completion Interval, ft	29-42
Uniform Vertical Permeability, md	0.3
Gas Viscosity, cp	0.012
Formation Temperature, °F	90
Standard Temperature, °F	60
Fracture Radius, ft	20
Fracture Conductivity, md-ft	1,624
Porosity, per cent	40

Horizontal Permeability Distribution

Layer	Interval ft	Horizontal Perm-md (0.5-180 ft)	Model Cells Number	Horizontal Perm-md (180-745 ft)	Model Cells Number
1	1-14	4	40	0.3	10
2	15-28	2	40	0.3	10
3	29-42	6	40	0.3	10
3*	29-42	Fracture conductivity added to first 20 ft.			
4	43-56	4	40	0.3	10
5	57-70	2	40	0.3	10
6	71-84	4	40	0.3	10
7	85-98	6	40	0.3	10

TABLE IV

VARIABLES FOR MODEL RUNS USED IN THE STUDY OF THE EFFECTS OF FORMATION THICKNESS AND VERTICAL PERMEABILITY ON THE DURATION OF VARIABLE CAPACITY

Variables with Values Common to All Runs	
Reservoir Pressure, psi	800
Standard Pressure, psia	15.025
Formation Temperature, °F	90
Standard Temperature, °F	60
Porosity, per cent	40
Fracture Radius, ft	20
Drainage Area, acres	40
Horizontal Permeability, md	4

Variables with Different Values

	Run 1	Run 2
Formation Thickness, ft	98	49
Completion Interval, ft	43-56	22-28
Fracture Conductivity, md-ft	2,744	1,372
Flow Rate, MCFD	2,200	1,100
Vertical Permeability, md	0.3	0.3

	Run 3	Run 4	Run 5
Formation Thickness, ft	24.5	98	98
Completion Interval, ft	10.6-14	43-56	43-56
Fracture Conductivity, md-ft	686	2,744	2,744
Flow Rate, MCFD	550	2,200	2,200
Vertical Permeability, md	0.3	1.0	4.0

TABLE V

CONTROL VARIABLES AND PERMEABILITY DISTRIBUTION FOR LAYERED RESERVOIR WITH REDUCED PERMEABILITY 375 FEET AWAY FROM WELLBORE

Variables	
Reservoir Pressure, psi	800
Standard Pressure, psia	15.025
Formation Thickness, ft	98
Area of Drainage, acres	40
Completion Interval, ft	29-42
Uniform Vertical Permeability, md	0.3
Gas Viscosity, cp	0.012
Formation Temperature, °F	90
Standard Temperature, °F	60
Fracture Radius, ft	20
Fracture Conductivity, md-ft	1,624
Porosity, per cent	40

Horizontal Permeability Distribution

Layer	Interval ft	Horizontal Perm-md (0.5-375 ft)	Model Cells Number	Horizontal Perm-md (375-745 ft)	Model Cells Number
1	1-14	4	45	0.3	5
2	15-28	2	45	0.3	5
3	29-42	6	45	0.3	5
3*	29-42	Fracture conductivity added to first 20 ft.			
4	43-56	4	45	0.3	5
5	57-70	2	45	0.3	5
6	71-84	4	45	0.3	5
7	85-98	6	45	0.3	5

CHAPTER IV

DUPLICATION OF TWO-DIMENSIONAL LONG-TERM PRESSURE BEHAVIOR THROUGH PROPER USE OF ONE-DIMENSIONAL TECHNIQUES

Conclusive evidence is presented that divides the calculated pressure behavior obtained from using the two-dimensional model into two time periods. The first occurs during the time that the vertical component of variable capacity plays a significant role in the pressure behavior. The vertical component is caused by the in situ geometry represented by the permeability distribution, completion interval location, and well stimulation. This occurs immediately upon initiating production and lasts for a relatively short period of time depending upon the values of parameters previously discussed. Successive changes in rates, including no-flow periods for pressure build-up, will be followed by similar transient periods. Calculated pressures during these times cannot be duplicated using one-dimensional techniques. The second period occurs after expiration of the first and is usually of much longer duration. During these times, the pressure behavior can be duplicated through proper use of one-dimensional techniques. This includes the proper representation of formation capacity and skin effect. The correct formation capacity for the one-dimensional model will be shown to be the sum of the capacities of the individual layers. For cases where the conductivity within any layer changes radially, such as one containing a fracture, equivalent changes in the radial dimension must be represented in the one-dimensional model. One-dimensional representation of the skin effect will be limited to short zones of decreased (or increased) permeability contiguous to the wellbore. Equivalent skin-effect representations in the form of very small wellbore radii are not practical in the numerical techniques used. The ability to match the long-term pressure behavior for a schedule of producing rates makes it unnecessary to develop a multi-dimensional predictive tool. Economics dictate the preference for proper application of the one-dimensional technique.

The limitations imposed on the permissible size of the time step in order to maintain stable calculations using the numerical technique developed in Chapter II restrict the economical application of this method to phenomena that occur within a relatively short period of time. Applications where this analysis would provide useful information include optimization of well completions, draw-down test analysis, and pressure build-up analysis.

Several series of test cases were designed and run in order to determine model capabilities and to discover how the various parameters affected the calculated pressures. Examination of these plots of wellbore pressure and/or wellbore pressure squared versus log time revealed similar behavior to that obtained using a one-dimensional model after the initial period of variable capacity had passed. Therefore, it seemed reasonable that behavior during these periods of constant capacity could be duplicated by the simpler model.

The first attempt to match the calculated behavior of a two-dimensional run by use of the one-dimensional model was for a system having uniform horizontal and vertical permeability with the producing interval centered about mid-formation. Descriptive data for this run were outlined in the discussion on variable capacity and is tabulated in Table VI. The same number of model divisions, or cells, in the radial direction was used in both sets of calculations. This made each cell in the one-dimensional model equivalent in volume to the sum of the cells in the vertical direction of the two-dimensional model. All variables such as formation temperature, thickness, wellbore radius, porosity, and reservoir pressure were the same. The corresponding permeability descriptions remained to be determined. For an initial trial, the permeability in all but the first two cells of the one-dimensional model was made equal to the average value of the cells in the vertical direction at any radial point r; in this case, the uniform value. Other workers have found through use of more limited two-layered models that the pressure behavior could be duplicated after a short period of time by using a one-dimensional model with conductivity equal to the sum of the conductivities of the individual layers. (19) The permeability of the first two cells was designated as that necessary to describe the skin effect. For a 49-cell model, this amounts to having a reduced (or an increased) permeability over an approximate distance of two inches for the skin description. Several permeability values for the two cells were run until one was found that would yield an identical pressure behavior as shown in the upper set of curves labelled "Completion Interval 43-56 Ft." in Figure 15. Compare the time at which the pressure match starts with the time the system becomes one of constant capacity as shown in Figure 9. Each of the seven layers is within a few per cent of contributing its share to the producing rate. Certainly, the pressure behavior is duplicated from the end of the period of variable capacity to the end of the run.

Next, an attempt was made to match the behavior of the least efficient completion interval for this same formation; i.e., the bottom (or top) 14 feet. The permeability of the skin yielding a pressure match was somewhat lower than that in the previous case. Notice also that it required a longer period of time for this match to take place. Again, once the pressure behavior was duplicated, it continued for the duration of the runs as seen in the lower set of curves marked "85-98 Ft." in Figure 14. Comparing Figures 9 and 10, which give the times required for each system to reach constant capacity, shows the latter took considerably longer. This confirms the physical likelihood that the system must reach constant capacity conditions before a one-dimensional model will give a realistic measure of the system's performance. If the ability to duplicate the behavior depends upon the system being at constant capacity, then data must be taken, in the latter case, for a longer period of time to obtain the correct pressure match.

Since the 2-cell skin description was an arbitrary choice, another selection using 4-cells was chosen to substantiate the non-uniqueness of an appropriate skin description. This increased the interval of altered permeability to approximately six inches about the wellbore. Again, a match was obtained and is shown in Figure 15 as the same curve (A and C) as that obtained when using a 2-cell skin of different permeability. Examination of the pressure profile within the one- and two-dimensional models shows a difference for each case analogous to that shown in Figure 5; however, the behavior as measured in the wellbore is identical. Because the 4-cell skin results in a less steep pressure gradient in the immediate vicinity of the wellbore, it was selected for further matching runs.

In the presentation on variable capacity, it was shown that for each change in flow rate there followed a period of variable capacity. Also, it was postulated that the one-dimensional model would not duplicate the pressure behavior of the two-dimensional model during these periods. For successful use of this matching procedure, all prolonged periods of constant capacity must be duplicated. The next set of calculations was for a single change in rates to see if the pressure behavior could be matched for the two periods of constant capacity. As shown in Figure 16, such was the case. The upper set of curves represents the match for the initial 10-day production period at 350 MCFD and the lower for the latter 10-day period at 450 MCFD. Hence, it may be inferred that the one-dimensional model will duplicate the pressure behavior for all extended periods of constant capacity. Thus, the one-dimensional model may be used in reservoirs of this type for long-term, constant-rate predictive purposes once the appropriate skin value and formation conductivity have been determined.

In order to further substantiate this inference, calculations for other representative two-dimensional systems were made and their behavior matched. The next system chosen was a group of runs made from the basic data tabulated in Table III. The effects of layered horizontal permeability are combined with a very low vertical permeability, reduced permeability away from the wellbore, and a small fracture of fixed conductivity located at various intervals between the upper and lower boundaries. These runs were made as a part of a study to optimize the location of the completion interval. For permeability values to use in the one-dimensional model, we selected the average, 4 md, for the first 40 cells and 0.3 for the remaining 10 cells. In Figure 17, one can see that a 4-cell skin of 56.8 md-ft gives a pressure match for the completion interval 43-56 feet after the first three or four days. The time required for the vertical component of variable capacity to disappear in this system is some 5 or 6 days as seen in Figure 18. However, at the end of 4 days all the layers are contributing very nearly their proportionate share.

As a preliminary observation, one can see that the usual well test lasting approximately 4 hours (considerably less than one day) will give erroneous results in this instance if interpreted in a conventional manner. (36) Too, the successful matching of the pressure behavior indicates that the effects of the completion interval, the well stimulation, and the particular vertical permeability distribution can be incorporated into the skin value. For the next comparison, move the fracture and the completion interval to the bottom 14 feet of the formation in the 6-md layer. In Figure 19, one can see that a longer period of time was required for the coincidence of pressure behavior. However, the skin value of 55.2 md-ft was very little lower than the previous one. This can probably be explained by the fact that the pressure gradient moves more rapidly in the higher permeability streak, thereby opening larger areas for cross-flow; and, consequently, almost overcomes the handicap of reduced efficiency caused by its location next to the lower formation boundary. Two other comparisons were made for fractures in completion intervals located at 29-42 feet and 57-70 feet. In both cases a pressure match was obtained after expiration of the initial period of variable capacity as can be seen in Figures 20 and 21. All of these runs validate the conclusion that the wellbore effects can be described as a skin value which is the limit of a continuously changing skin until the variable capacity period has elapsed. Actually, this skin value might serve as a basis for comparison of the relative merits of each completion.

In order to indicate the effects of vertical permeability on the matching procedure, one example was chosen from the data tabulated in Table VII. The difference from the previous group is a vertical permeability of 2 md and a reduced permeability zone of 2 md. The completion interval is located at 43-56 feet. As seen in Figure 22, a pressure match using a 4-cell skin of 1960 md-ft was obtained after 0.4 day. Figure 23 shows that the time required for the vertical component of variable capacity in this system to disappear is 0.6 day; but it is insignificant after 0.4 day. The fracture conductivity was the same in both cases; however, the 4-cell skin value of 1960 md-ft is much higher in this case, indicating the importance of vertical permeability on fracture efficiency. Being able to match two systems with different vertical permeabilities by using different skin values further substantiates the probable description of the effects of vertical permeability in this manner.

From the discussion on variable capacity, it was shown that once the system reached constant capacity it remained that way as long as the producing rate remained unchanged. It is now necessary to verify that once this point is reached, the pressure can be matched from that time forward as long as no rate changes are introduced. To do this, we calculated the pressure behavior of the system tabulated in Table III with a producing interval at 29-42 feet for 90 days. Figure 20 shows that a match was obtained after 6 days and duplication continued to the conclusion of the run. Looking at Figure 24, we see that 15 days were required for the system to reach constant capacity but all layers were contributing very nearly their proportionate share of the production after 6 days.

Even though the calculations involving fractured systems thus far discussed have resulted in matches for both increased and reduced effectiveness, as shown by the skin values, large fractures that substantially increase the productive capacity over that of the native formation must be included to further extend the validity of this matching technique. The data for the first case is tabulated in Table VIII, Run 1. It contains a high-capacity fracture with a radius of 59 feet. First attempts at matching the pressure behavior were through use of a formation conductivity of 294 md-ft and a skin effect consisting of a varying number of cells of increased conductivity. The number of cells ranged upward to 27 (equivalent to a radial distance of 22 feet) and the conductivity, to 19,498 md-ft. The resulting pressure curve is plotted in Figure 25 and labelled "27-Cell Skin 19,498 md-ft". It shows a match for the latter portion of the second rate but no match during the first rate. A plot (not included) of the duration of variable capacity for this system is almost identical to that shown in Figure 9. It shows the vertical component of variable capacity disappeared after 0.4 days, or early in the first rate period. However, no match could be found using a multiple-cell skin that commenced upon the disappearance of this vertical component. The curve, labelled "27-Cell Skin 9,898 md-ft" in Figure 25 shows the one-dimensional pressure behavior that matches the two-dimensional value at the single point, 3 days. For the remainder of the first rate, the pressure is too high. It is too low for the entire second rate. This indicates that our established procedures will not successfully match the pressure in this case. The cause for the unsuccessful attempts was determined to be the omission of a proper description for the radial component of variable capacity. The next matching attempt was made by adding the fracture conductivity to the formation conductivity in order to obtain the average permeability value for the cells containing the fracture. Here a match was obtained by using a 4-cell skin effect of 529 md-ft as shown in Figure 25 and labelled "4-Cell Skin 529 md-ft". This is another verification of the procedure for using the average permeability at any radial distance r determined to be the total capacities of the individual layers divided by the total thickness.

Another case involving a much larger fracture, having a 115-foot radius, was selected to verify the method of getting an average permeability value in the fractured area. Data for this case are tabulated in Table VIII—Run 2. Figure 26 shows the pressure match obtained using a 4-cell skin of 696 md-ft. The skin value is much lower than the conductivity of the fractured area but higher than that of the native formation. An attempt was made to match the pressure behavior by expressing the skin effect as an effective wellbore radius. This also failed, as can be seen in Figure 26. This shows the plot of the "best" of the attempted pressure matches using an effective wellbore radius of 50 feet. Again, this is caused by not having a descriptive effect of the radial component of variable capacity.

Summarizing the information on matching two-dimensional runs with a one-dimensional model, we find that in all cases, except those containing large fractures, a pressure match was obtained after the period in which the vertical component of the variable capacity had become insignificant. In the cases where the resulting skin was less than the formation conductivity, a short interval of reduced permeability could account for the effects of the well completion interval, the vertical permeability, and the well stimulation on the calculated pressure. In the cases having large fractures, where the resulting skin was much larger than the formation conductivity, we found that such a matching procedure was not possible because of the failure to account for the radial component of variable capacity. Here it was necessary to add the fracture conductivity to that of the formation in order to obtain the average permeability to be used in the fractured area. Coupling this with a 4-cell skin value resulted in pressure matches after the initial vertical component of variable capacity became insignificant. The most probable explanation for this behavior lies in the effect the skin has on the resulting pressure. Effectively, the skin is an added, or reduced, resistance to flow which displaces the pressure downward, or upward, by a fixed amount from that normally predicted at any given time. Thus, in the case of the large fractures, there would have to be a short period of time in which the reservoir pressure must be greater than the original pressure and, consequently, this constitutes an invalid solution.

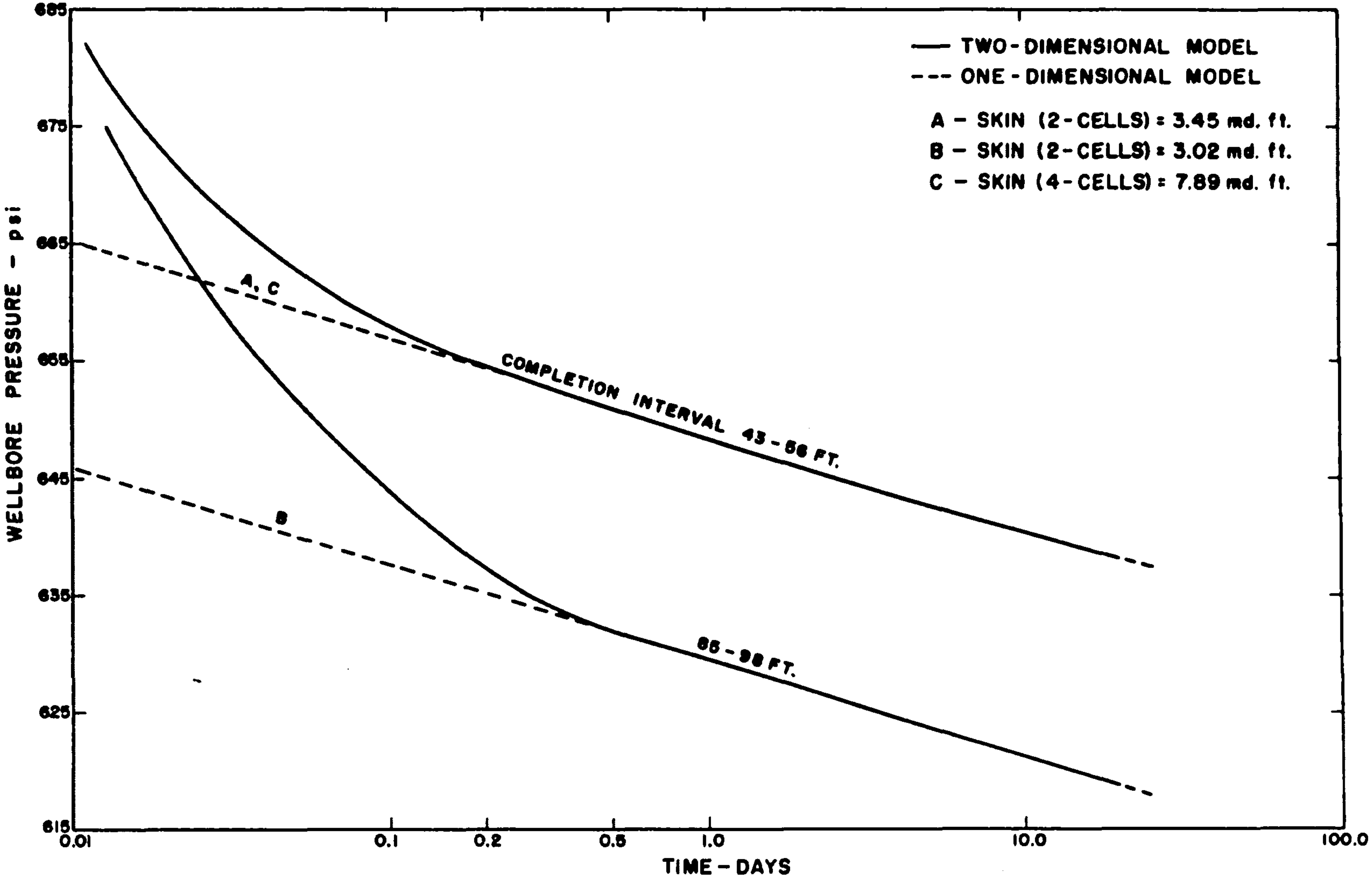

FIGURE 15 MATCHING TWO-DIMENSIONAL CALCULATIONS USING ONE-DIMENSIONAL MODEL WITH AVERAGE PERMEABILITY PLUS SKIN-EFFECT TERM

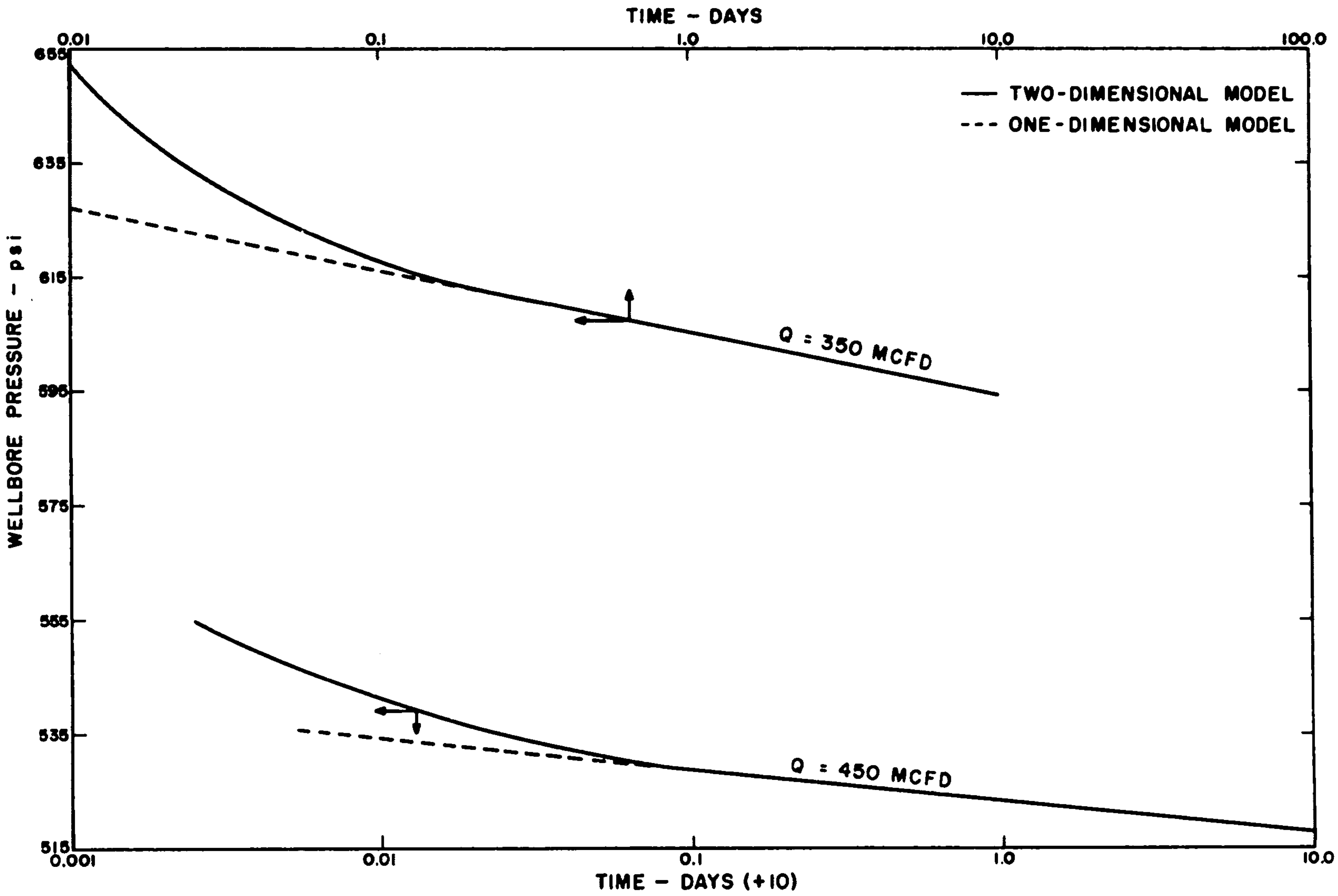

FIGURE 16 PRESSURE MATCHING FOR ONE RATE CHANGE IN FORMATION HAVING UNIFORM PERMEABILITY

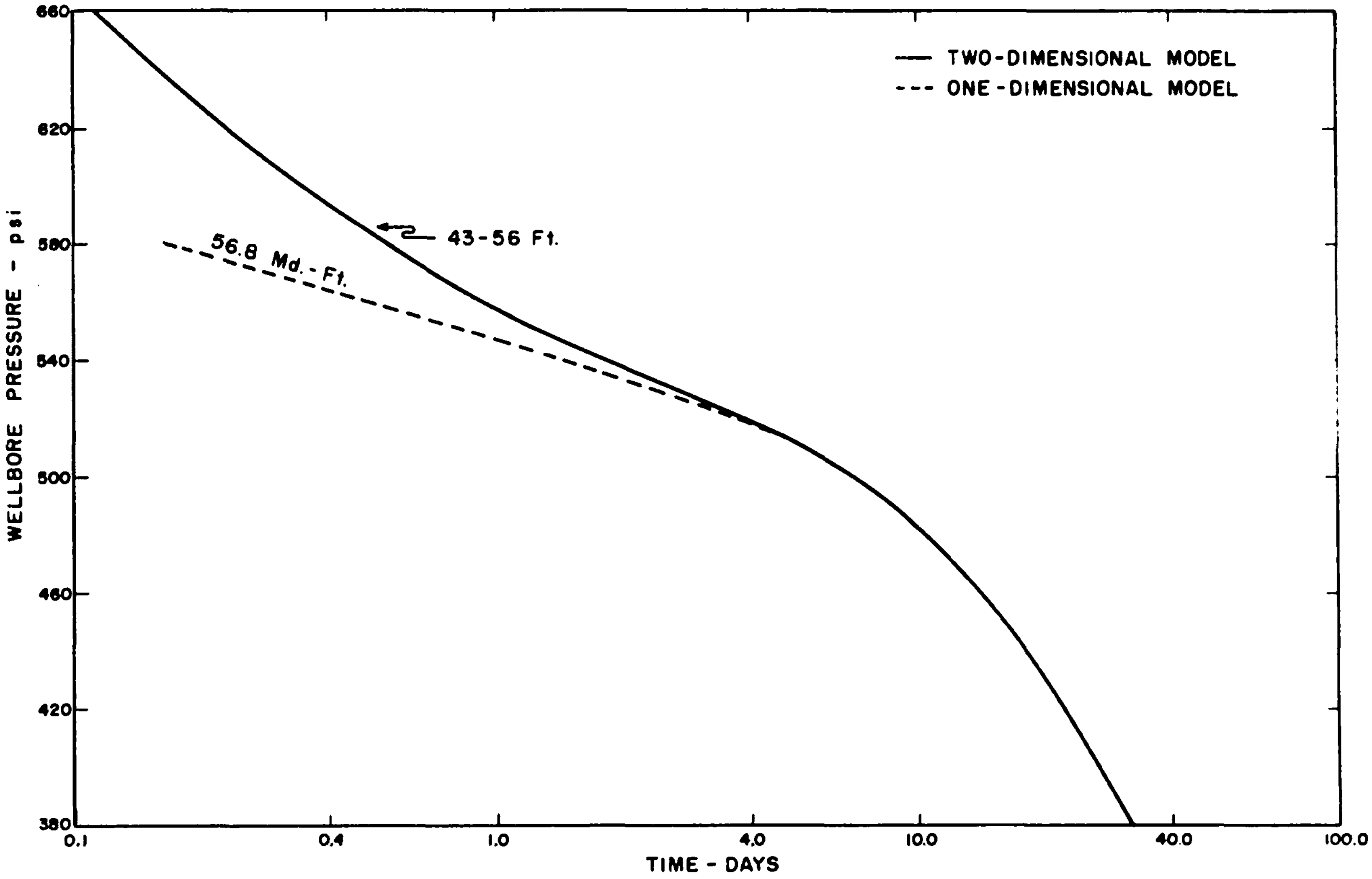

FIGURE 17 DUPLICATION OF PRESSURE BEHAVIOR USING ONE-DIMENSIONAL MODEL AFTER INITIAL PERIOD OF VARIABLE CAPACITY

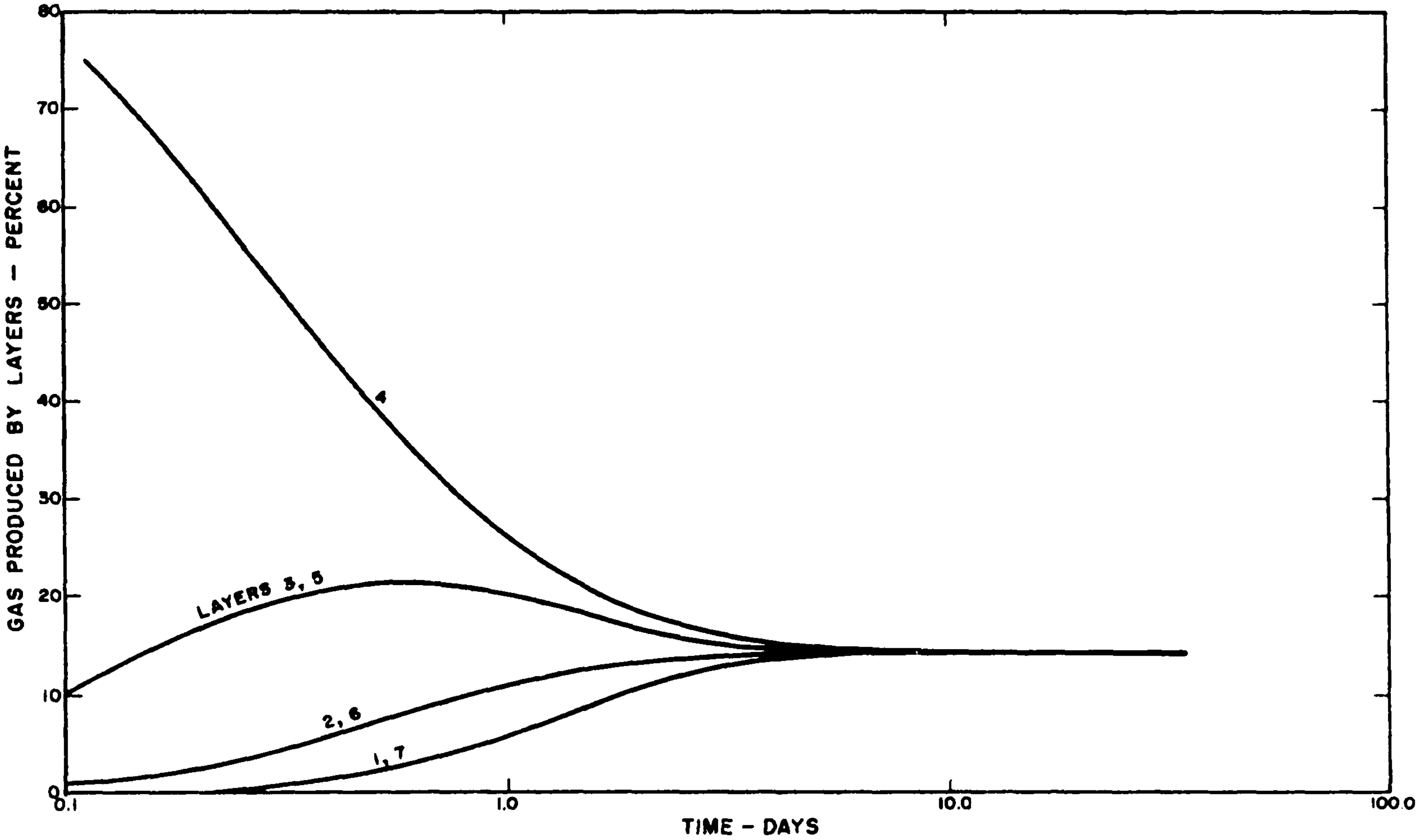

FIGURE 18 DURATION OF VERTICAL COMPONENT OF VARIABLE CAPACITY FOR LAYERED RESERVOIR WITH 0.3 md. VERTICAL PERMEABILITY

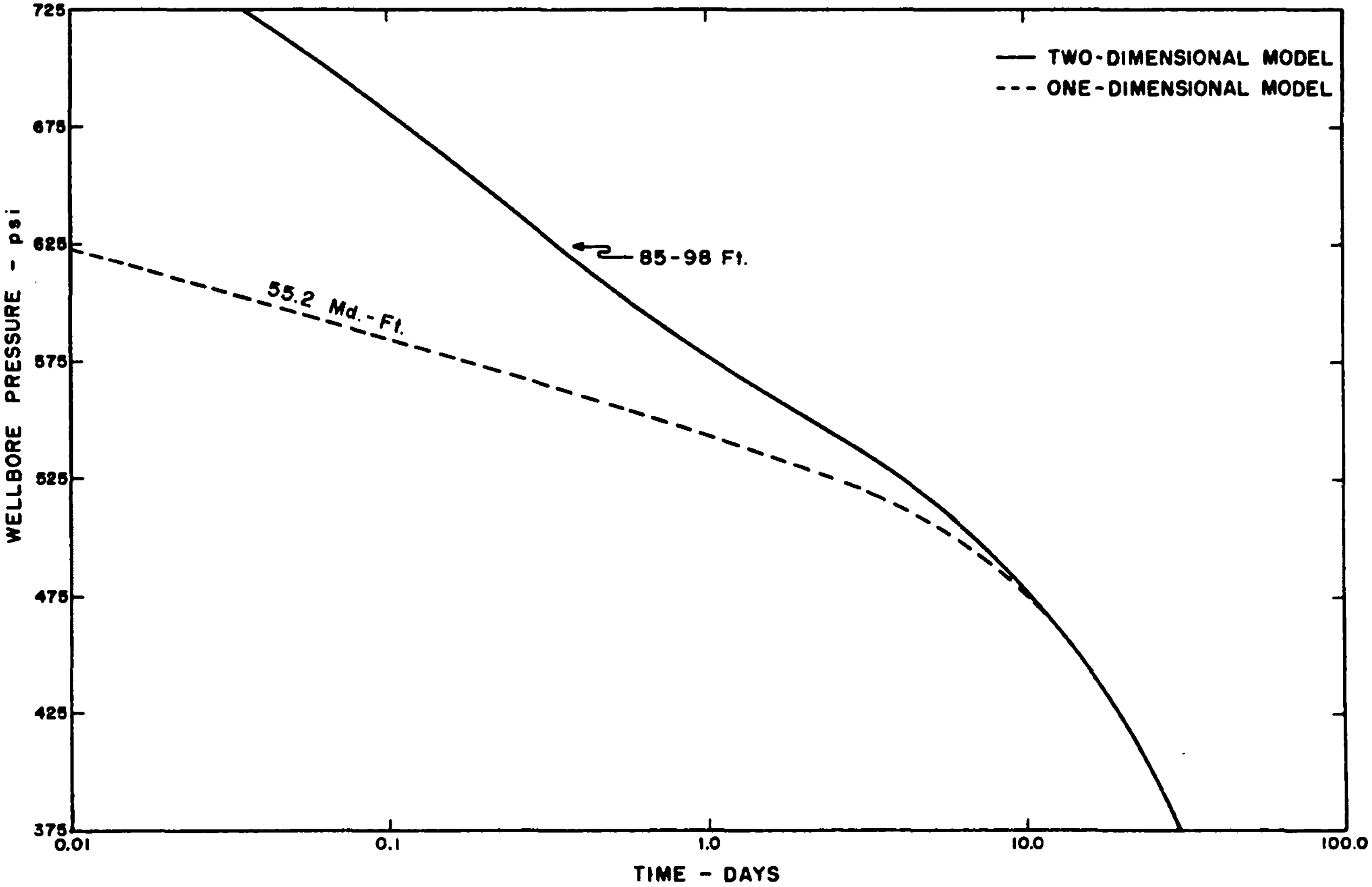

FIGURE 19 PRESSURE MATCH FOR LAYERED RESERVOIR WITH COMPLETION INTERVAL 85-98 FEET USING 4-CELL SKIN IN ONE-DIMENSIONAL MODEL

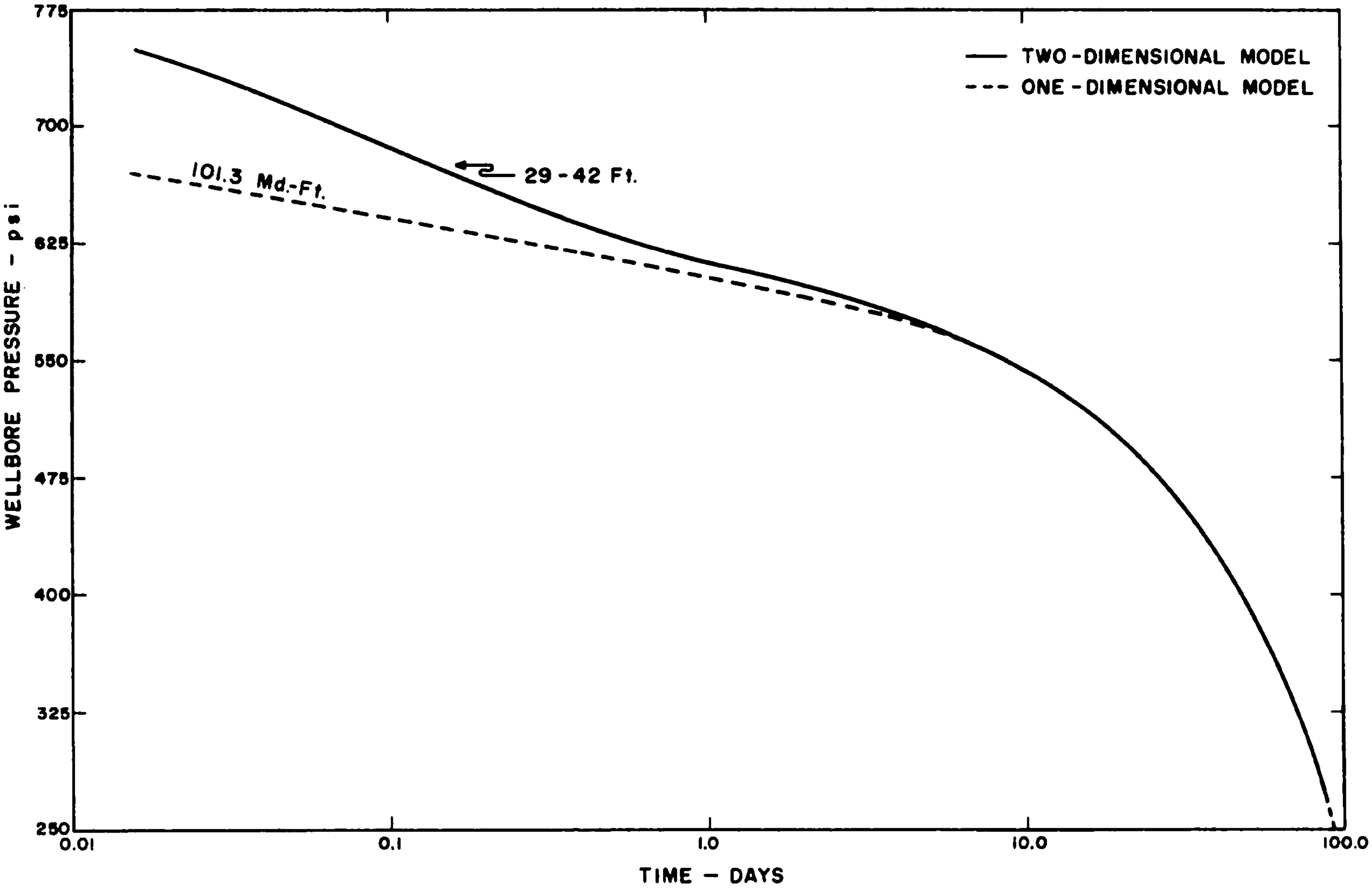

FIGURE 20 PRESSURE MATCH FOR LAYERED RESERVOIR WITH COMPLETION INTERVAL 29-42 FEET USING 4-CELL SKIN IN ONE-DIMENSIONAL MODEL

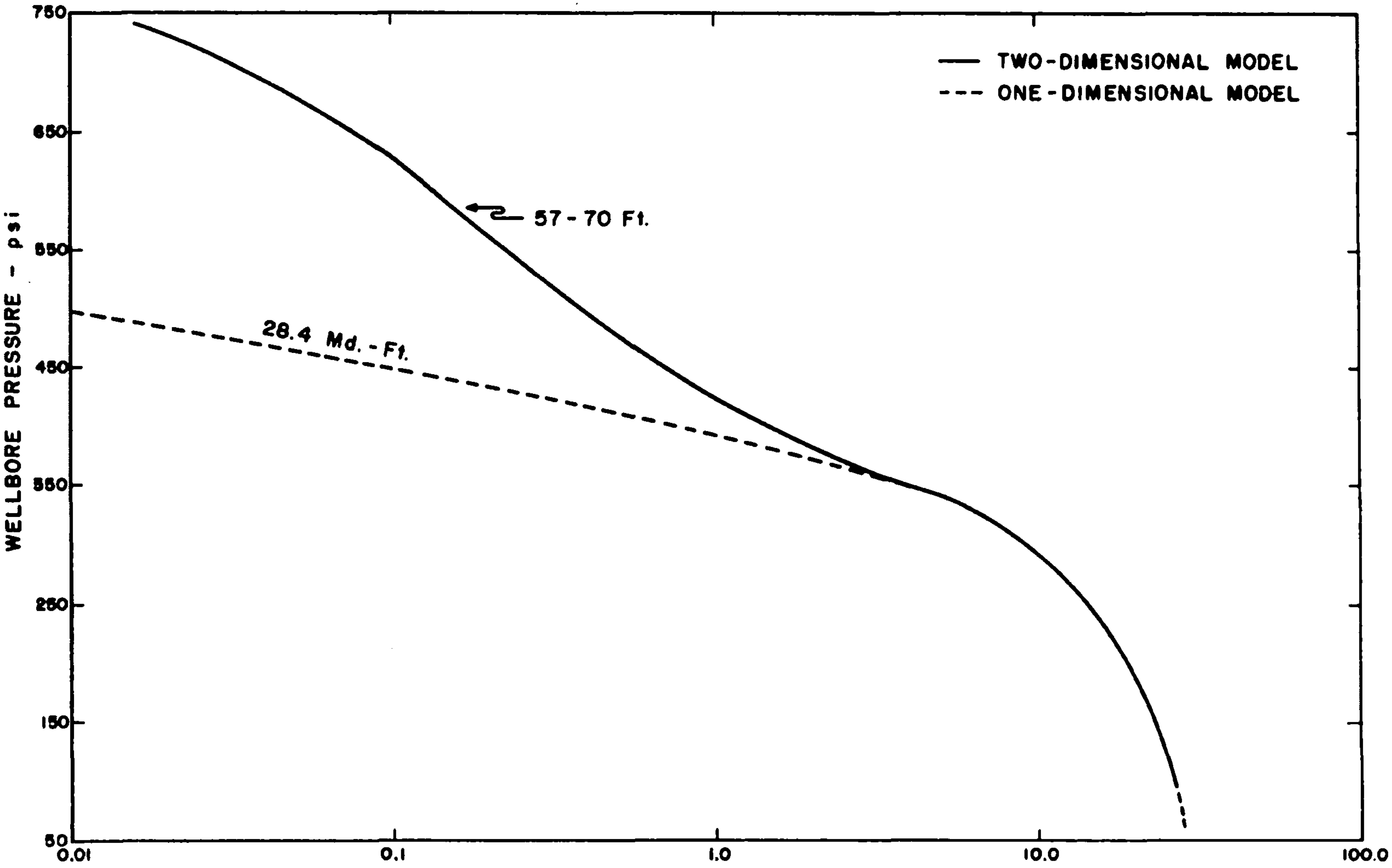

FIGURE 21 PRESSURE MATCH FOR LAYERED RESERVOIR WITH COMPLETION INTERVAL 57-70 FEET USING 4-CELL SKIN IN ONE-DIMENSIONAL MODEL

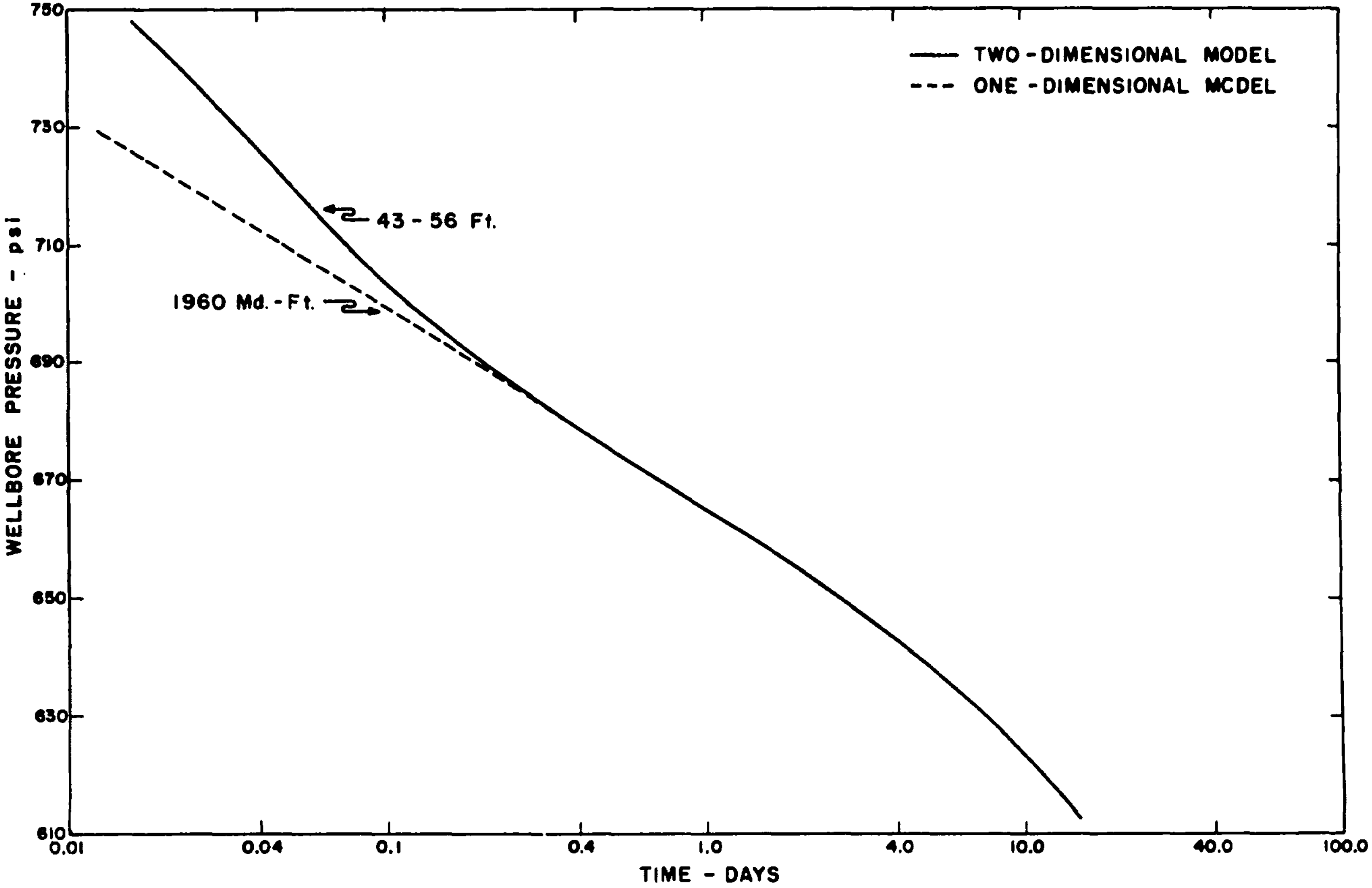

FIGURE 22 PRESSURE MATCHING FOR LAYERED RESERVOIR WITH 2 MD. VERTICAL PERMEABILITY

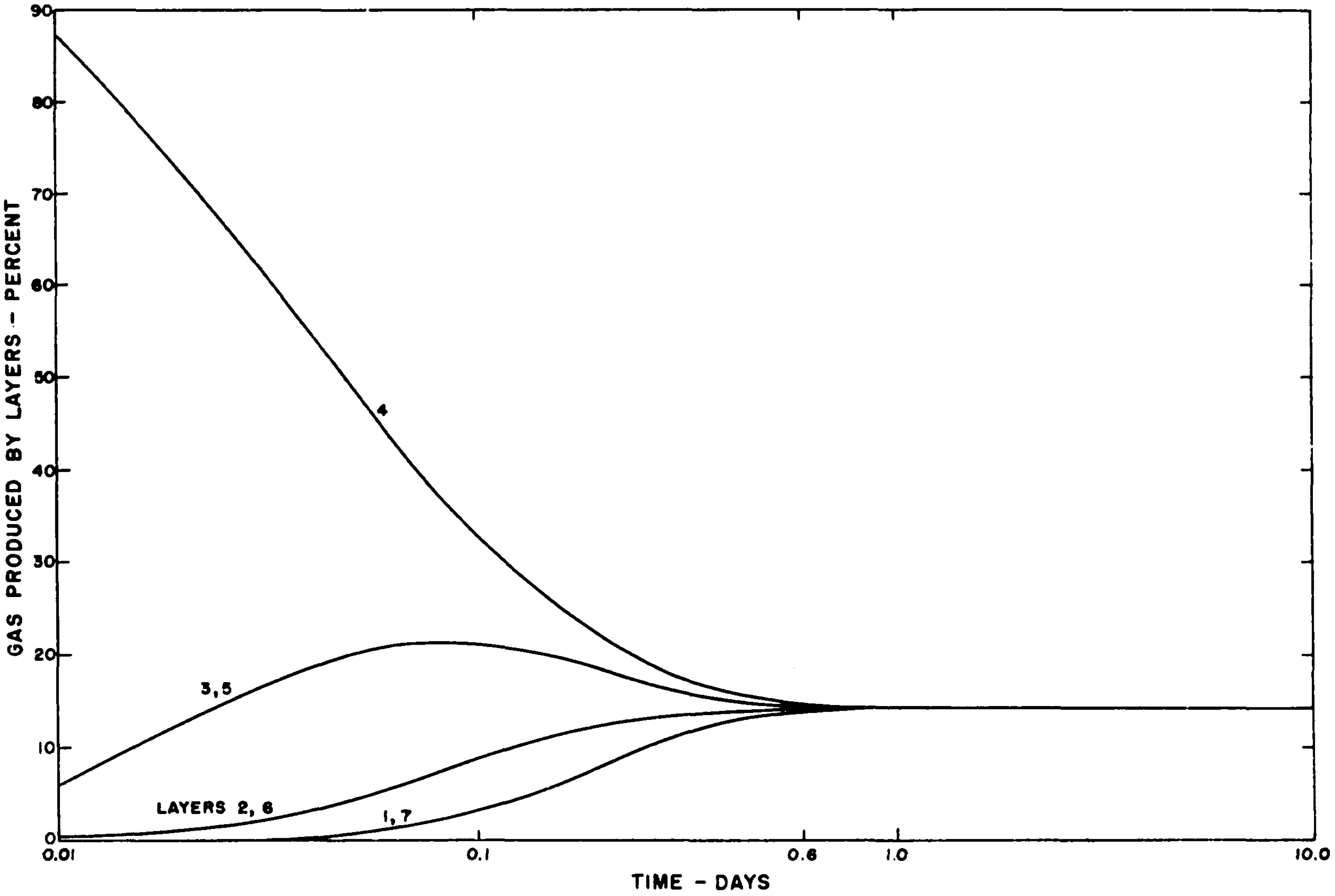

FIGURE 23 DURATION OF VERTICAL COMPONENT OF VARIABLE CAPACITY IN LAYERED RESERVOIR HAVING 2 Md. VERTICAL PERMEABILITY

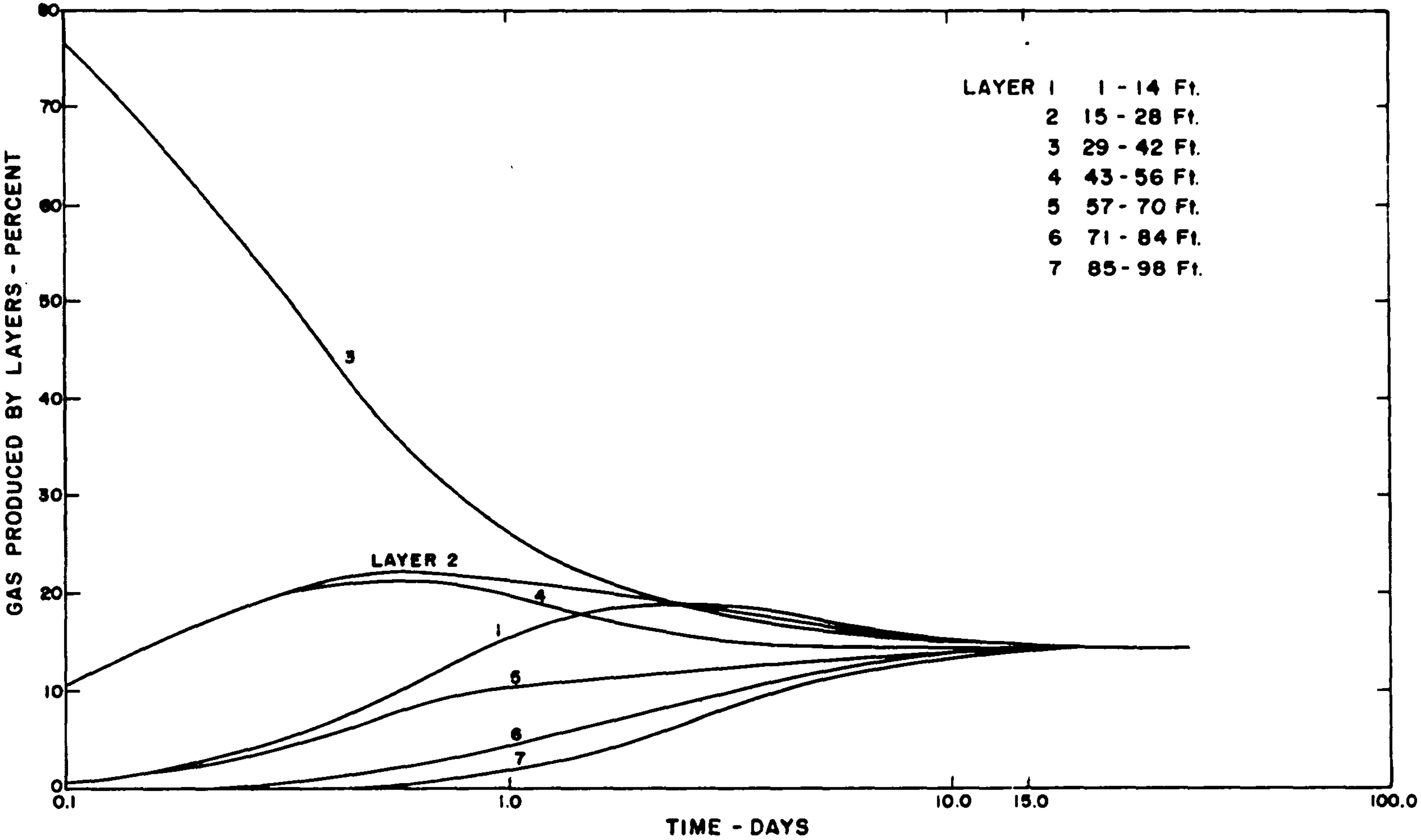

FIGURE 24 DURATION OF VERTICAL COMPONENT OF VARIABLE CAPACITY FOR LAYERED SYSTEM HAVING 0.3 Md. VERTICAL PERMEABILITY

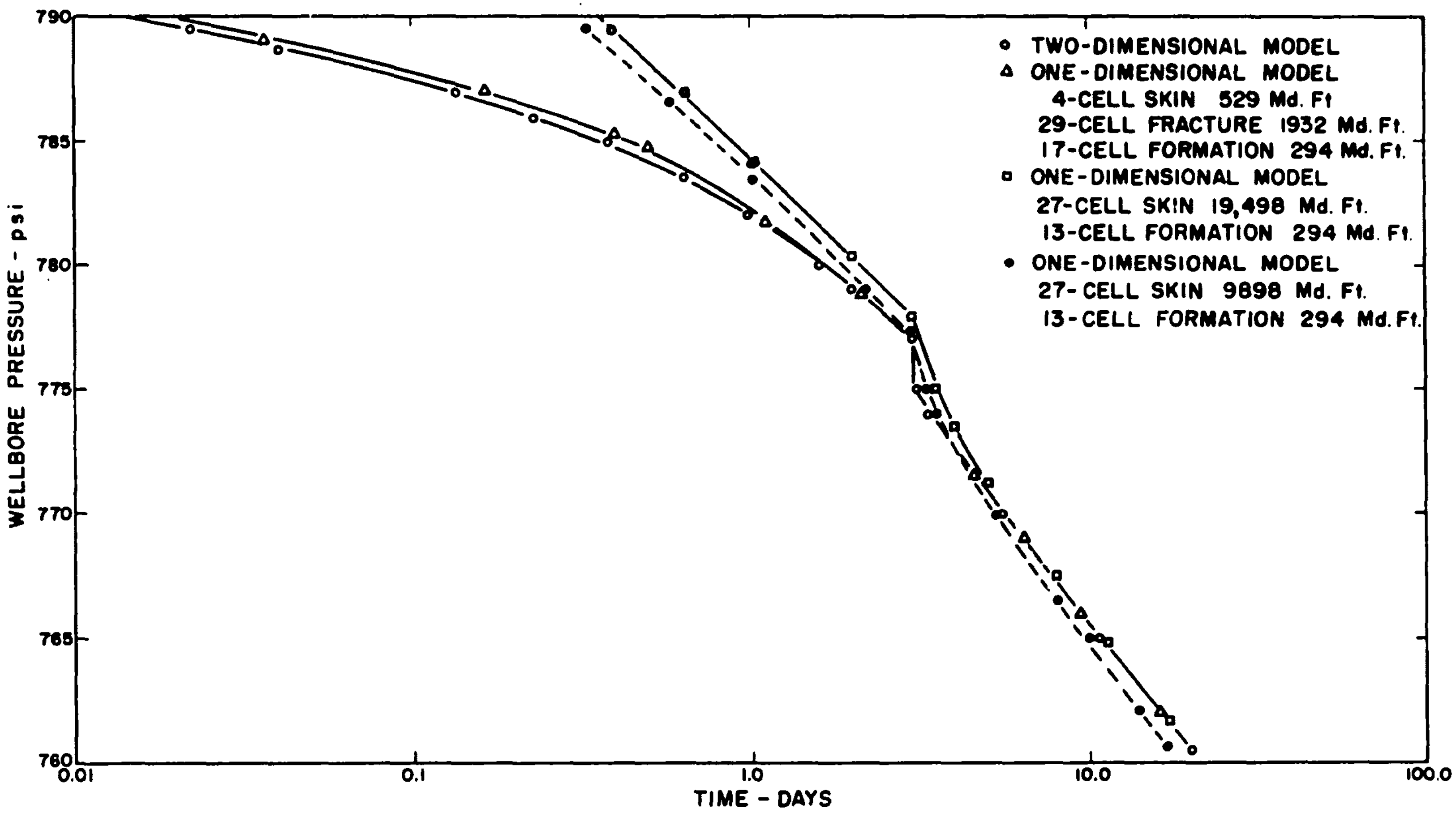

FIGURE 25 PRESSURE MATCHING FOR UNIFORM SYSTEM HAVING LARGE FRACTURE USING ONE-DIMENSIONAL MODEL

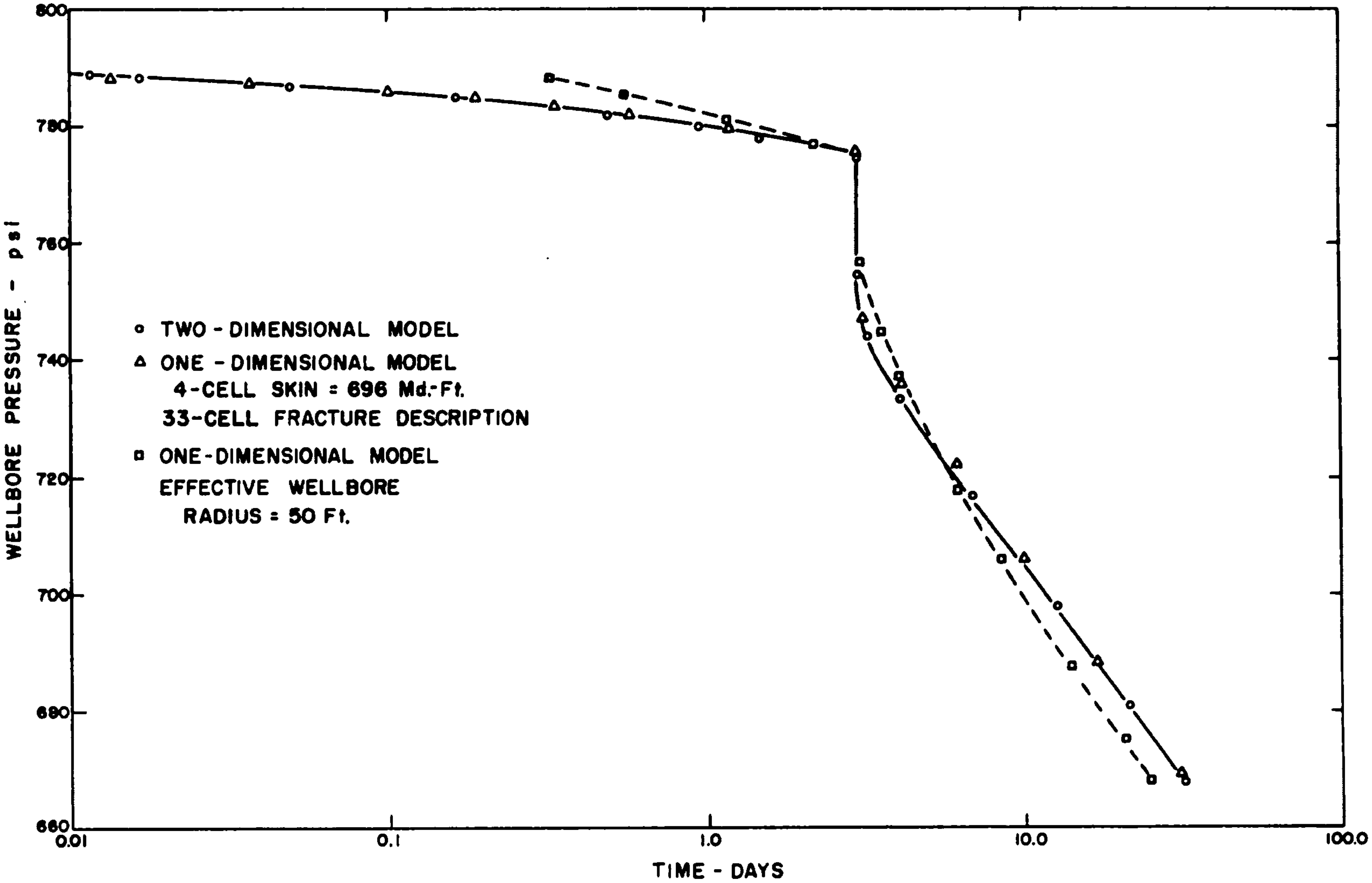

FIGURE 26 PRESSURE MATCH FOR UNIFORM SYSTEM WITH LARGE FRACTURE USING TOTAL CONDUCTIVITY AT ANY RADIUS FOR ONE-DIMENSIONAL MODEL

TABLE VI

MODEL PARAMETERS USED FOR MATCHING TWO-DIMENSIONAL MODEL BEHAVIOR WITH A ONE-DIMENSIONAL MODEL

System Description	2-D Model	1-D Model
Horizontal Permeability, md	3.0	3.0
Vertical Permeability, md	3.0	
Drainage Area, acres	40	40
Formation Thickness, ft	98	98
Porosity, per cent	40	40
Wellbore Radius, ft	0.5	0.5
Gas Viscosity, cp	0.012	0.012
Reservoir Pressure, psi	800	800
Standard Pressure, psi	15.025	15.025
No. Model Cells, radial	49	49
No. Model Cells, vertical	7	
Formation Temperature, °F	90	90
Standard Temperature, °F	60	60
Completion Interval, ft		
Run 1	43-56	
Run 2	85-98	
2-Cell "Skin-Effect", md-ft		
Run 1		3.45
Run 2		3.02
4-Cell "Skin-Effect", md-ft		
Run 1		7.89

TABLE VII

CONTROL VARIABLES AND PERMEABILITY DISTRIBUTION FOR LAYERED RESERVOIR WITH 2.0 MD PERMEABILITY 180 FEET AWAY FROM WELLBORE

Variables	
Reservoir Pressure, psi	800
Standard Pressure, psia	15.025
Formation Thickness, ft	98
Area of Drainage, acres	40
Completion Interval, ft	29-42
Uniform Vertical Permeability, md	2.0
Gas Viscosity, cp	0.012
Formation Temperature, °F	90
Standard Temperature, °F	60
Fracture Radius, ft	20
Fracture Conductivity, md-ft	1,624
Porosity, per cent	40

Horizontal Permeability Distribution

Layer	Interval ft	Horizontal Perm-md (0.5-180 ft)	Model Cells Number	Horizontal Perm-md (180-745 ft)	Model Cells Number
1	1-14	4	40	2.0	10
2	15-28	2	40	2.0	10
3	29-42	6	40	2.0	10
4*	43-56	Fracture conductivity added to first 20 ft.			
4	43-56	4	40	2.0	10
5	57-70	2	40	2.0	10
6	71-84	4	40	2.0	10
7	85-98	6	40	2.0	10

TABLE VIII

MODEL PARAMETERS FOR UNIFORM SYSTEM HAVING HIGH-CAPACITY FRACTURE AND LARGE RADIUS

	Run 1	Run 2
Horizontal Permeability, md	3.0	3.0
Vertical Permeability, md	3.0	3.0
Formation Thickness, ft	98	98
Area of Drainage, acres	40	40
Porosity, per cent	40	40
Fracture Conductivity, md-ft	1,638	2,478
Fracture Radius, ft	59	115
Completion Interval, ft	43-56	1-14
Producing Rate, MCFD		
0-3 days	600	999
3-20 days	700	2800
20-21.6 days	0	
Wellbore Radius, ft	0.5	0.5
Gas Viscosity, cp	0.012	0.012
Reservoir Pressure, psi	800	800
Standard Pressure, psia	15.025	15.025
No. Model Cells, radial	49	49
No. Model Cells, vertical	7	7
Formation Temperature, °F	90	90
Standard Temperature, °F	60	60

CHAPTER V

THE EFFECTS OF VARIABLE CAPACITY ON WELL-TEST ANALYSIS

In the preceding two chapters we have established that parameters such as completion interval location, permeability stratification, etc., affect the time duration that a system has a vertical component of variable capacity. Further, it was shown that this component must be missing, or at least insignificant, before the one-dimensional unsteady-state gas model would duplicate the performance of the two-dimensional system. As a consequence of the ability to duplicate the behavior after this initial period of time, one can postulate that established techniques (8,31,36) for predicting long-term performance should continue to be valid when utilizing data that properly reflect constant capacity reservoir characteristics. We shall establish this as fact; show how erroneous results of large magnitudes can result from neglecting the vertical component of variable capacity; and, recommend a test procedure that will minimize the error.

It will be assumed that a rather complete and logical presentation for testing wells by flowing them at constant rates (36) has established the desirability of having test data for at least three different rates separated by periods of complete pressure build-up. Further, the predictive equations obtained by the succession of steady-states solution will be assumed to be proven sound and reliable. In this work (36), it was shown that for Darcy flow the plot $(P_d^2-P_w^2)/Q$ versus log time is the same straight line for every flow rate, Q. From the slope of this curve, the formation capacity could be calculated; and hence, the effective permeability. Using the numerical value obtained for the slope, the effective wellbore radius, which includes the skin effect, can be calculated. Then, by using the succession of steady-states predictive equation, one can obtain long-term deliverability predictions. This was verified through duplication of results obtained by using the finite-difference approximation to the one-dimensional differential equation as given in Appendix A of the subject paper. (36)

Using an analogous approach to interpret the two-dimensional model runs which initially have a vertical component of variable capacity, we will first show that the plot $(P_d^2-P_w^2)/Q$ versus log t for a given system is the same for all rates. Figure 27 shows the plot for three runs at rates of 280, 350, and 550 MCFD for the system whose description is tabulated under the column labelled "2-D Model" in Table VI. The completion interval used in these cases was 43-56 feet. Notice that the plots are all identical but are no longer a straight line for the entire run. A fracture having a radius of 115 feet and a conductivity of 2,478 md-ft was added to this system. Three runs at producing rates of 999, 3500, and 9900 MCFD through the completion interval located at 1-14 feet were calculated and the results shown in Figure 28. Again, the curves are identical but not a straight line. Finally, two runs were made on the system whose description is tabulated in Table III. Rates of 1470 and 1670 MCFD were calculated for the completion interval 85-98 feet through a layered system having a small fracture, very low vertical permeability, and reduced permeability away from the wellbore. These results, presented in Figure 29, show the same superpositioning of curves. Since the curves presented are representative examples of all the completion geometries and permeability distributions studied, we can conclude that the plot $(P_d^2-P_w^2)/Q$ versus log t will be single-valued for all Q in the two-dimensional calculations for Darcy flow, as it was in the one-dimensional case.

In each of the three examples cited, the plots were not straight lines. This indicates the presence of a changing effective permeability with time. As a further check, we need to establish that once the vertical component of variable capacity is gone, this plot will be a straight line provided there is no radial variation in permeability. Comparing the time required for the plot in Figure 27 to become a straight line with the time required for the disappearance of variable capacity, as shown in Figure 9, we see the interdependence as previously cited. Figure 30 shows the plot $(P_d^2-P_w^2)/Q$ versus log time for the completion interval 1-49 feet in the system tabulated in Table IX. Here it is shown that the plot is a straight line for the duration of the run excepting the initial period of variable capacity. This run extends beyond the stabilization time of 20 days into the material balance depletion stage. Figure 31 shows the plot for four completion intervals of the system tabulated in Table III. A straight line segment was not attained during the entire length of time the calculations were made. This was caused by the continuously changing formation permeability as measured at the wellbore and by the zone of reduced permeability encountered some 200 feet away from the well. Hence, one would not expect the slope to become constant until the external boundary was reached and the system passed into the material balance depletion stage.

Since the slope, and thus the effective permeability, was shown to vary during this initial period, it was apparent that different deliverability predictions would be forthcoming, depending upon the length of the flow test. In order to demonstrate the magnitude of the probable errors through improper data analysis, we will present sample calculations for two systems. The first will be for the formation whose properties are tabulated in Table IX with completion interval 1-24.5 feet. Figure 32 shows the calculated wellbore pressure as a function of time using the two-dimensional model producing at 400 MCFD. If the data were taken for a short time period—for example, 4 hours—and the results analyzed according to current practice (36), we would first calculate the plot $(P_d^2-P_w^2)/Q$ versus log time. For deliverability predictions, we would follow the calculational procedure outlined in Appendix B. Figure 33 shows this data for the duration of the run, but presently we shall limit ourselves to that acquired during this initial 4-hour period. Upon performing the specified calculations, we obtain deliverability predictions to a pre-determined cut-off pressure. The match obtained with the 4-hour test data is shown in Figure 32. The wellbore pressure plotted as a function of time up to an arbitrarily selected cut-off pressure of 200 psi is shown in Figure 34. This would be our prediction for the system based on the limited 4-hour test data. As the span of time over which this data is taken grows longer, the effective permeability approaches the known value used in the two-dimensional calculations. The next set of calculations shown is for a test period of 4 days. Only the data taken in the interval 2-4 days, shown in Figure 33, was used to determine the slope. The resulting match with the test data is shown in Figure 32. The large difference between "observed" and calculated pressure behavior is caused by the changing capacity until the entire skin is developed. This difference diminishes until convergence occurs after a period of one day. Figure 34 also shows the succession of steady-states prediction for this effective permeability and wellbore radius. Comparison with the prediction obtained from the 4-hour test shows that the number of 400 MCFD producing days for the short-term test was 22 per cent below the actual behavior. Figure 34 also shows the one-dimensional model prediction obtained through the trial-and-error matching procedure. Both this answer and that obtained from interpreting the 4-day test data are the same, within calculational accuracy. As would be expected, Figure 32 shows the match holds for early times. In this case, standard interpretation of the short-term testing procedure would have resulted in too conservative an estimate for the long-term deliverability.

The second case is for the system whose properties are tabulated in Table VI. It contains a fracture in the interval 1-14 feet having a 115-foot radius and a conductivity of 7,518 md-ft. Curve A of Figure 35 shows the plot of $(P_d^2-P_w^2)/Q$ for a rate of 5000 MCFD. Again, following the outlined procedure in determining the effective permeabilities and the effective wellbore radii for different lengths of flow tests, we get the information shown in Figure 36. The most rapid changes in permeability and skin effect occur in early times. However, it can be seen that a small change is still taking place at the end of 15 days. Figure 37 shows the comparison between the two-dimensional calculation, the one-dimensional matching run, and the 4-hour and 15-day pressure predictions obtained from the succession of steady-states solution. As expected, the pressure behaviors are duplicated, within calculational accuracy, during the respective time periods. Figure 38 shows the number of producing days predicted for the 4-hour test data, the 15-day test data, and the one-dimensional matching run. While the 4-hour prediction is overly optimistic, the 15-day predictions are suitable. Intermediate-length test periods would result in predictions lying between these two limiting cases. The difference in the number of producing days for the 4-hour test and the 15-day test is 125 days, or a 52 per cent error. This time the short-term prediction would have proved too optimistic.

Carter, et al. (6) presented field test data on a fractured well (their Figure 10) that exhibits the same characteristic plot of Δp^2 versus log t as shown in Figure 35. Similarly, data presented in their Figures 7 and 8 quite probably are from fractured wells. The dangers of selecting the best straight line through this short-term data for determining formation capacity have been discussed. Carter properly recognized that longer test periods should be used and data during the latter part be analyzed, to provide more accurate results.

We have shown, in the case of the fractured system having low permeability, that short-term test data can result in optimistic predictions which can be highly erroneous. Similarly, a formation with a partially penetrating well or fractional interval completion, that is tested for short time periods, can yield predictions much-too conservative. Hence, we cannot take this type data, blindly interpret the results, and necessarily expect to get the right answer. In order to overcome the possibility of not taking data for sufficient time to allow the vertical component of variable capacity to become insignificant, the first test period should be at a low flow rate for a long period of time—at least 24 hours and preferably 48 hours. (A method for more nearly predicting the time is yet to be developed.) Then, by plotting $(P_d^2 - P_w^2)/Q$ versus log t, one could determine the time at which the rate of change of the slope becomes insignificant. This time should be added to the usual 4-hour test for determining the test duration of each succeeding flow rate. Using conventional analysis (36) on data beyond this point should give an engineering approximation, providing there are no significant changes in formation capacity beyond the location of the radius of drainage at the end of the tests. Under all circumstances, this testing should provide an answer as good or better than the short-term test.

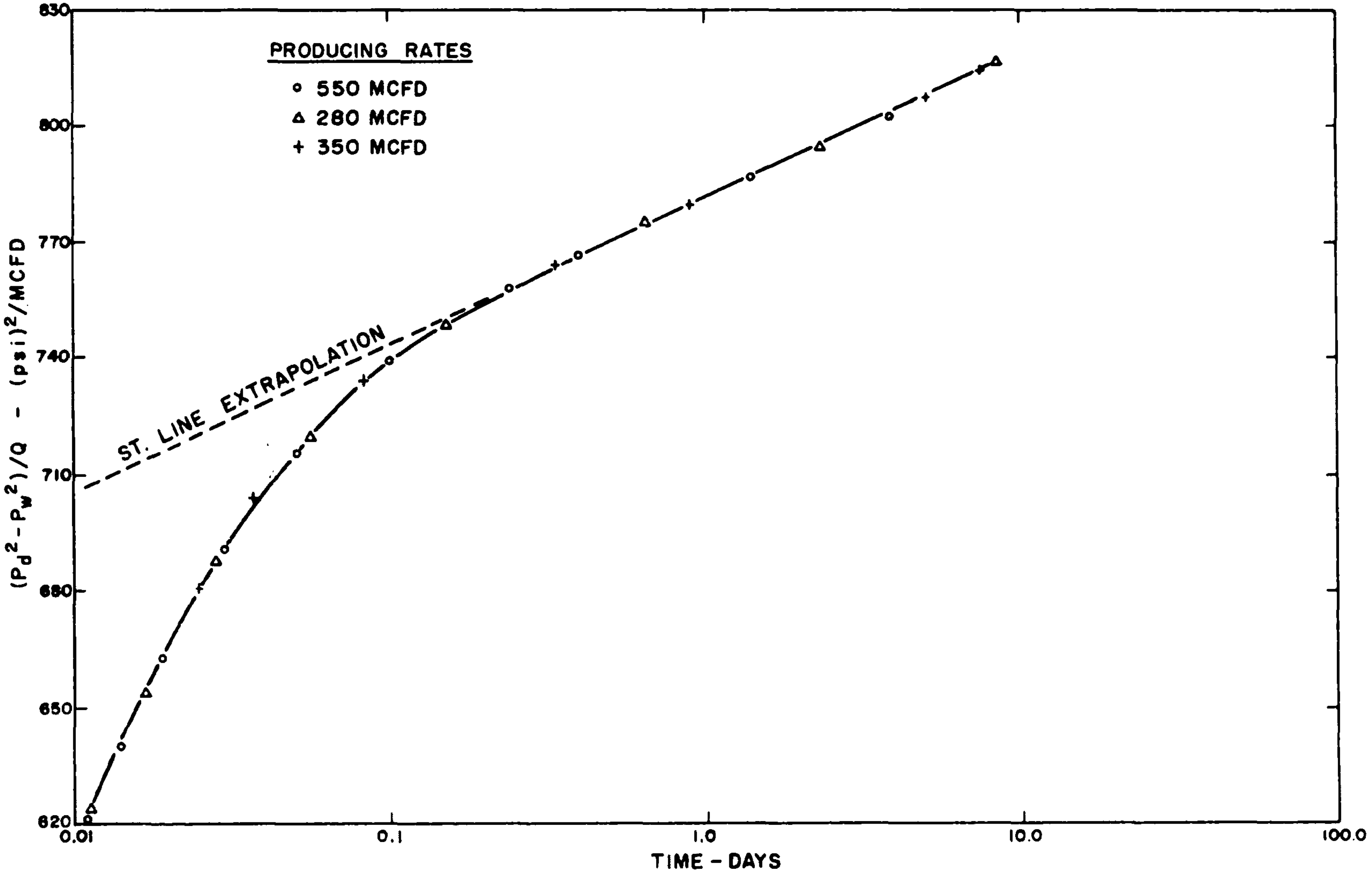

FIGURE 27 SIMULATED WELL-TEST DATA FOR UNIFORM SYSTEM WITH COMPLETION INTERVAL ABOUT MID-FORMATION

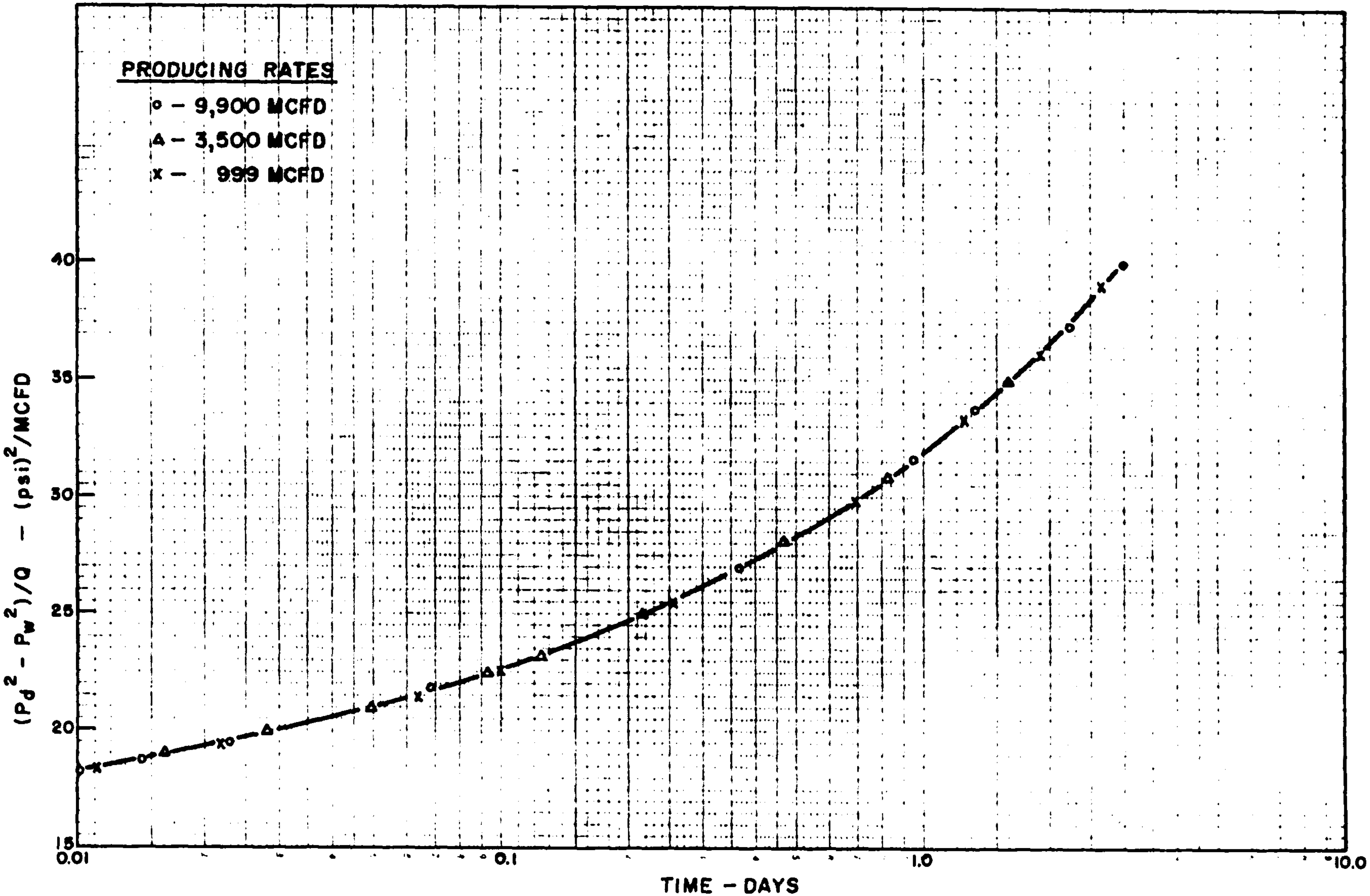

FIGURE 28 SIMULATED WELL-TEST DATA FOR UNIFORM SYSTEM CONTAINING A LARGE FRACTURE

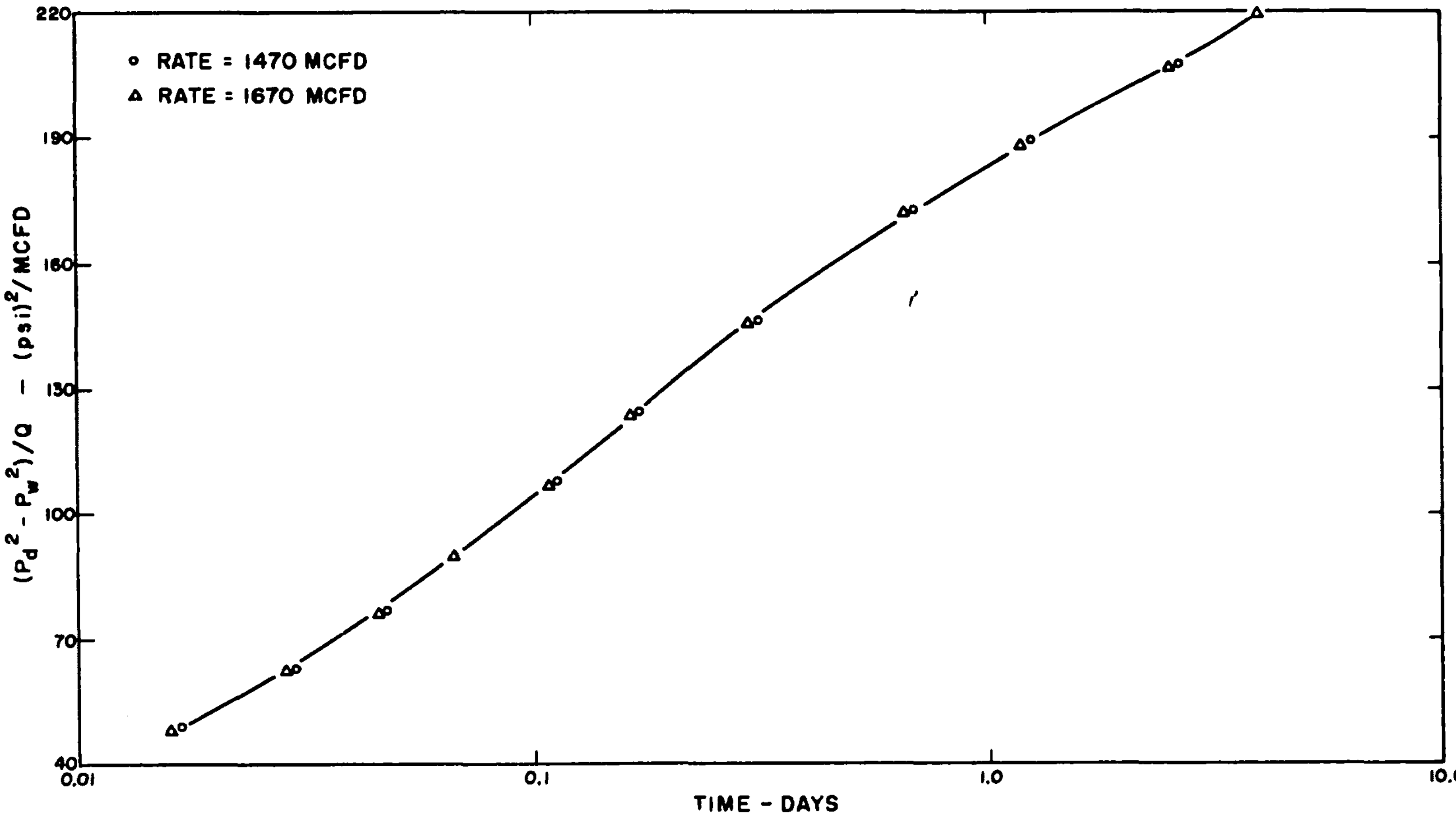

FIGURE 29 SIMULATED WELL-TEST DATA FOR LAYERED RESERVOIR WITH LOW VERTICAL PERMEABILITY

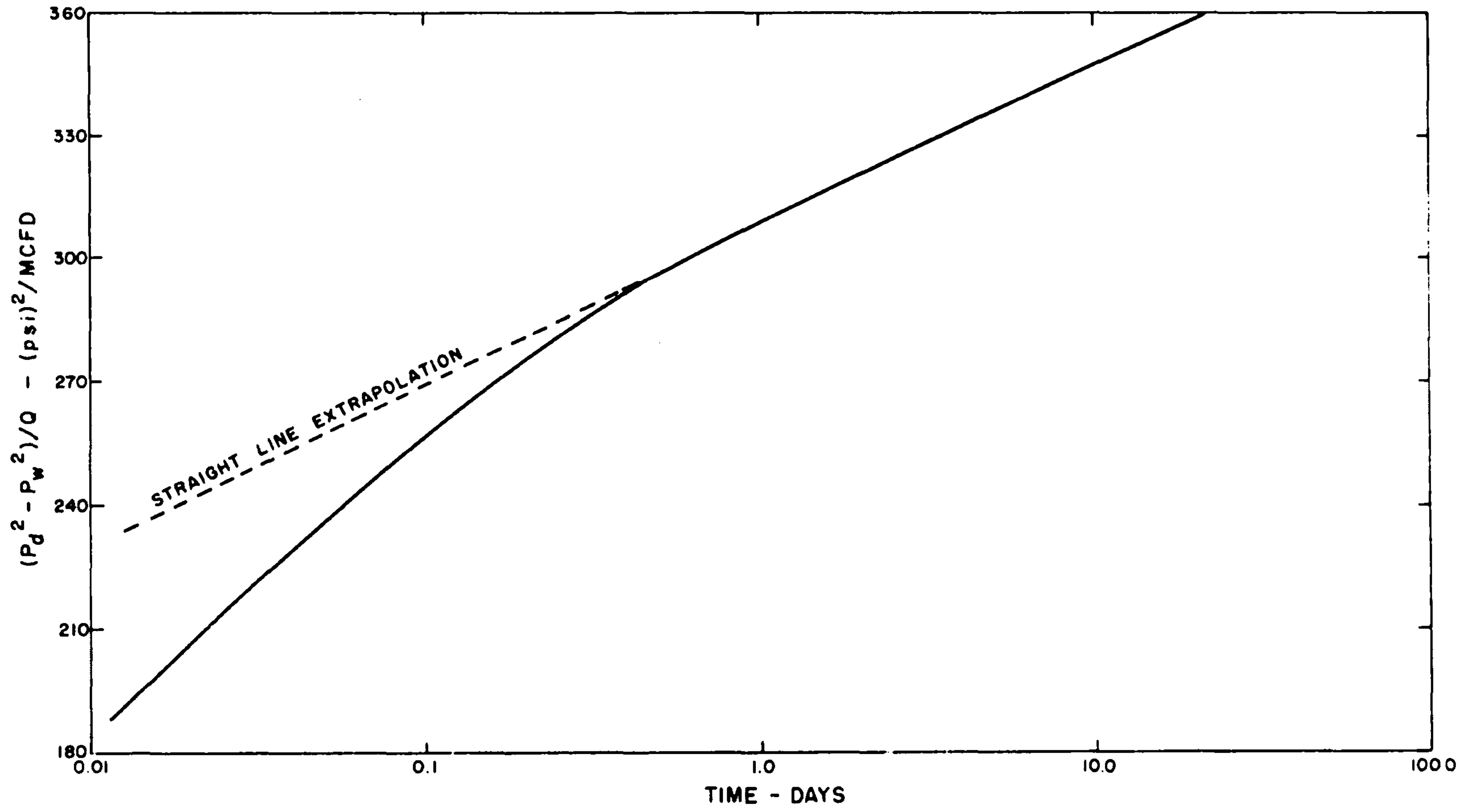

FIGURE 30 SIMULATED WELL-TEST DATA FOR UNIFORM SYSTEM HAVING THE TOP 49 FEET OPENED FOR PRODUCTION

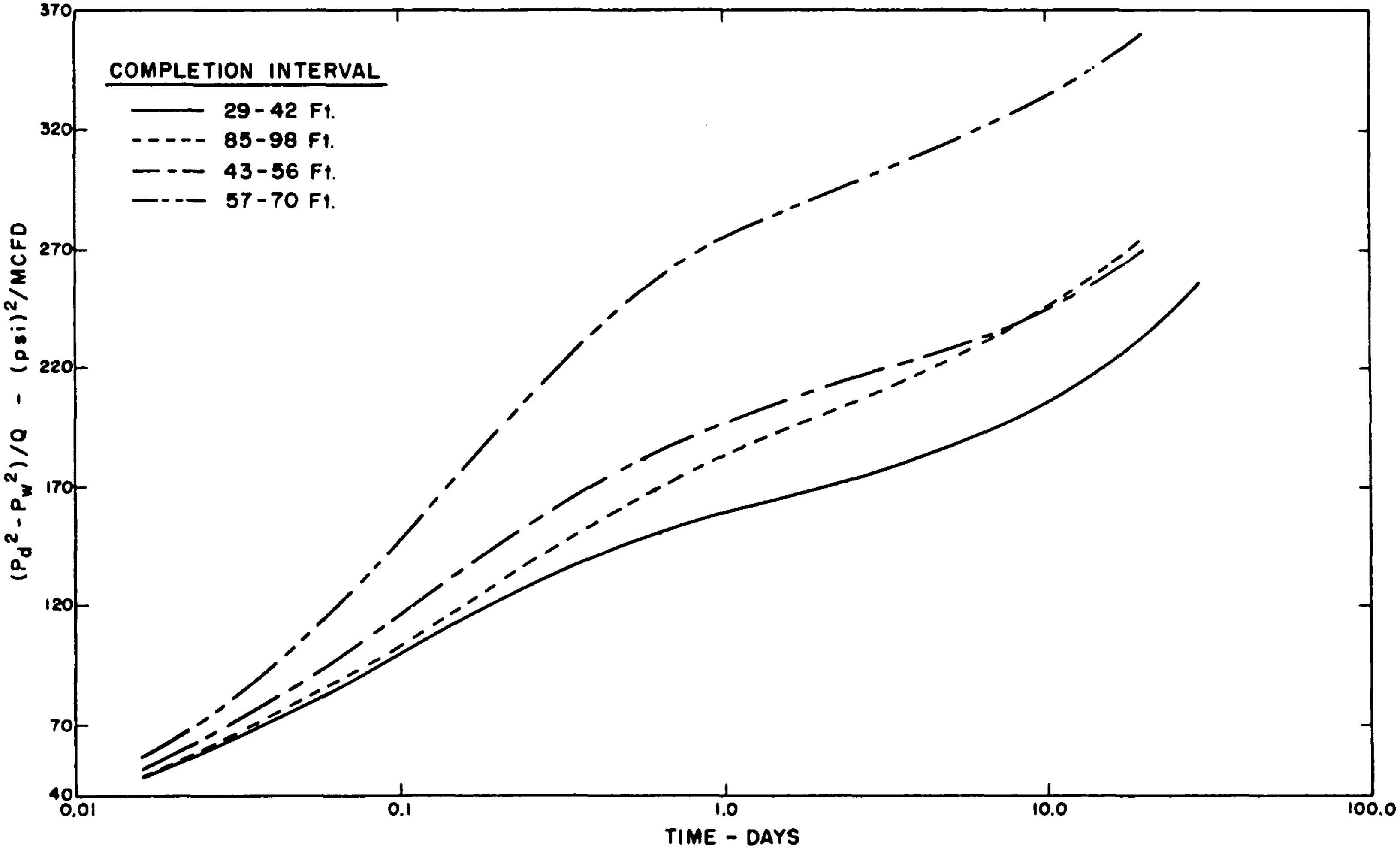

FIGURE 31 SIMULATED WELL-TEST DATA FOR SEVERAL COMPLETION INTERVALS IN A LAYERED RESERVOIR WITH LOW VERTICAL PERMEABILITY

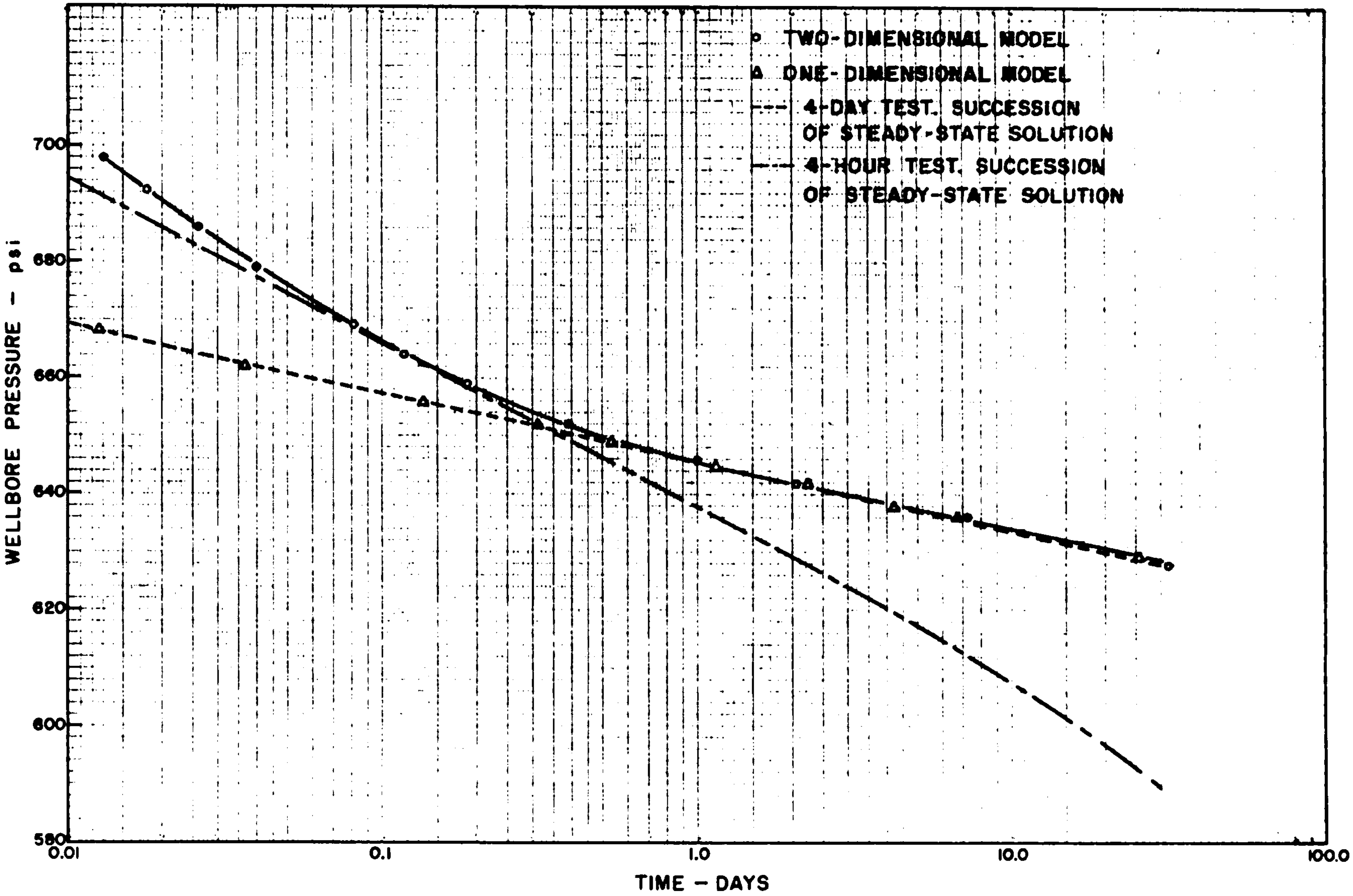

FIGURE 32 EFFECTS OF TWO FLOW-TEST TIME PERIODS ON THE EARLY PRESSURE MATCHING USING ONE-DIMENSIONAL TECHNIQUES

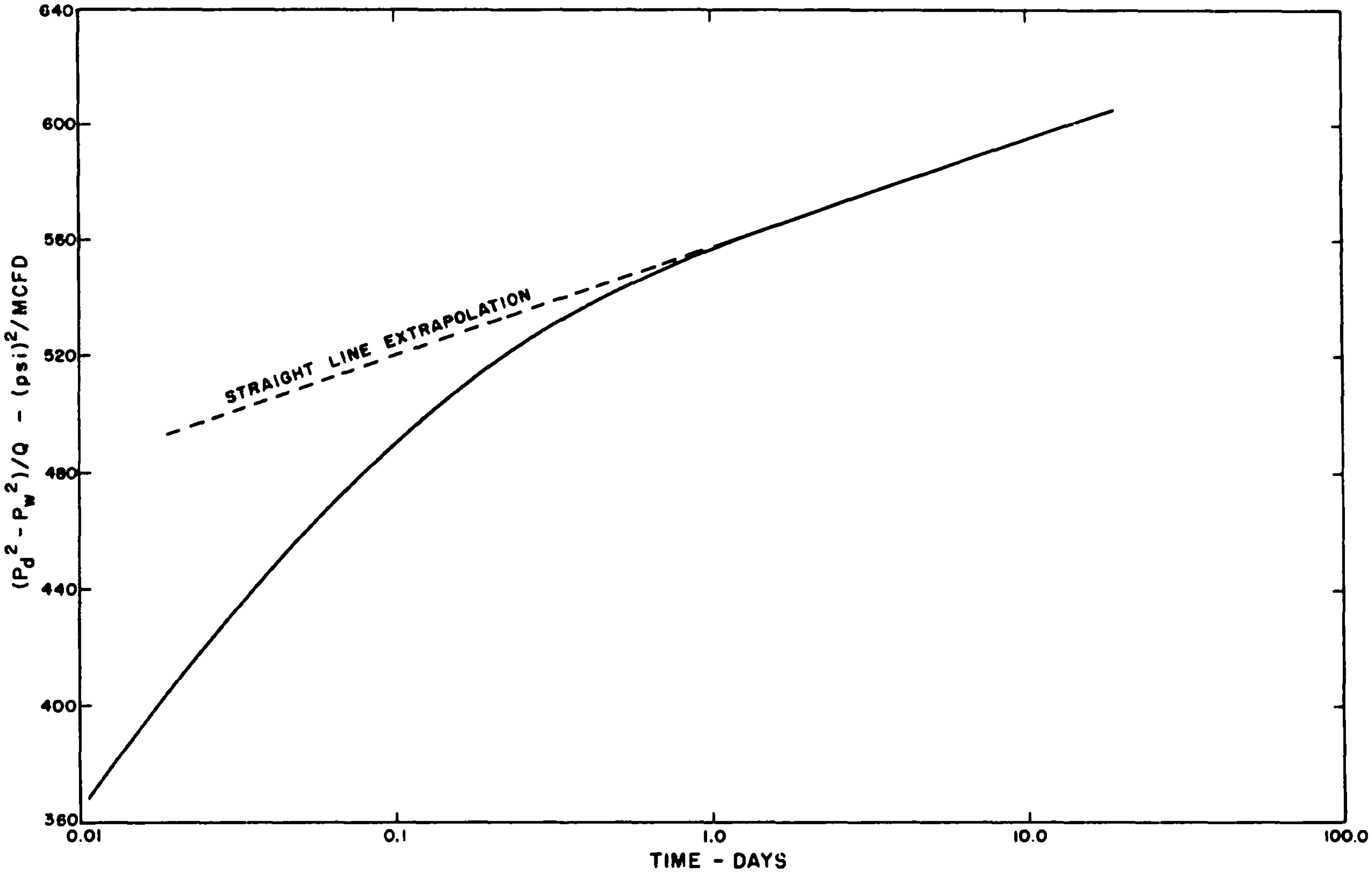

FIGURE 33 SIMULATED FLOW-TEST DATA TO SHOW EFFECT OF THE LENGTH OF TEST PERIODS ON DELIVERABILITY PREDICTIONS

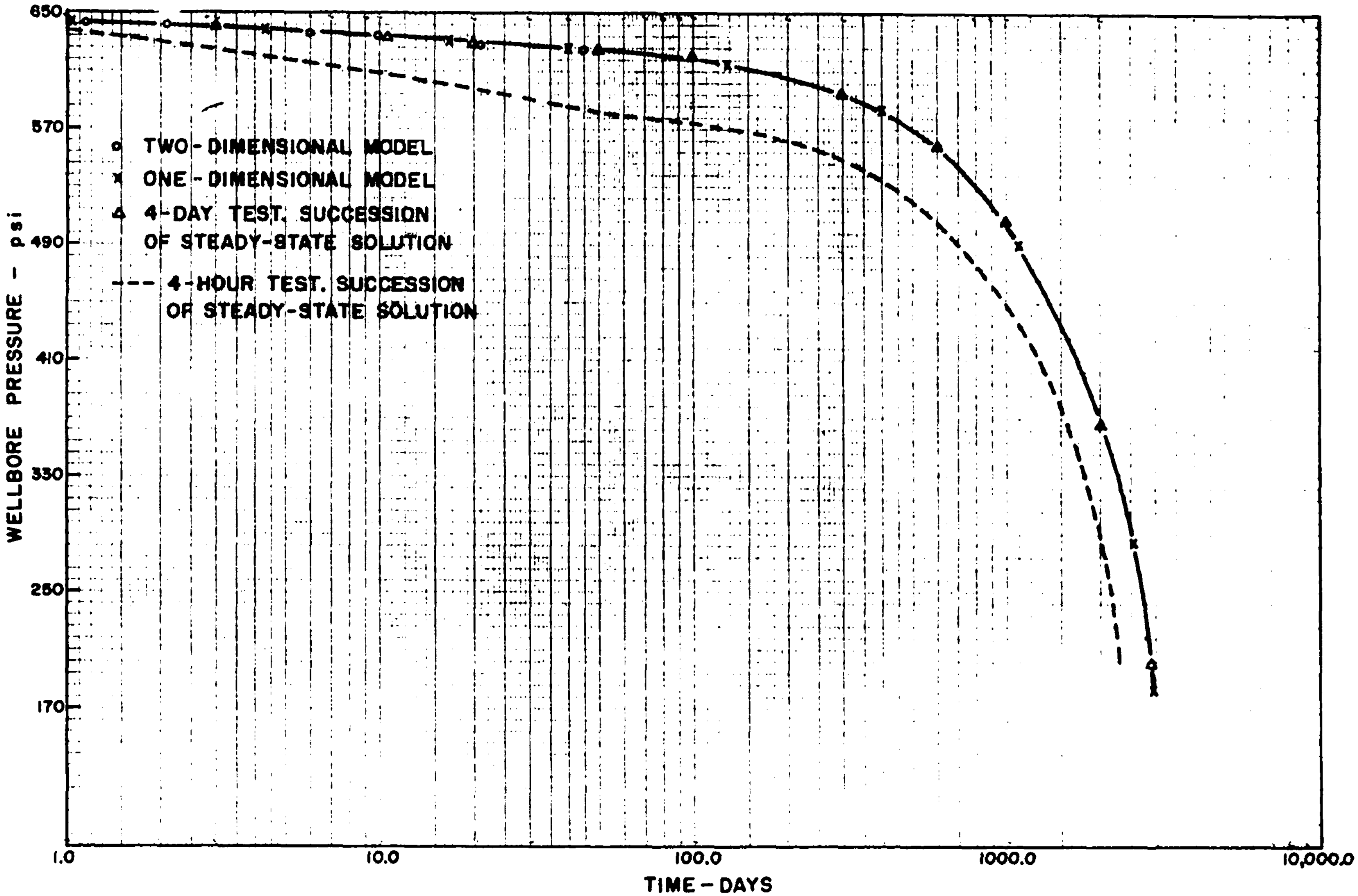

FIGURE 34 PREDICTED LONG-TERM WELLBORE PRESSURE PERFORMANCE FOR TWO FLOW-TEST PERIODS USING ONE-DIMENSIONAL TECHNIQUES

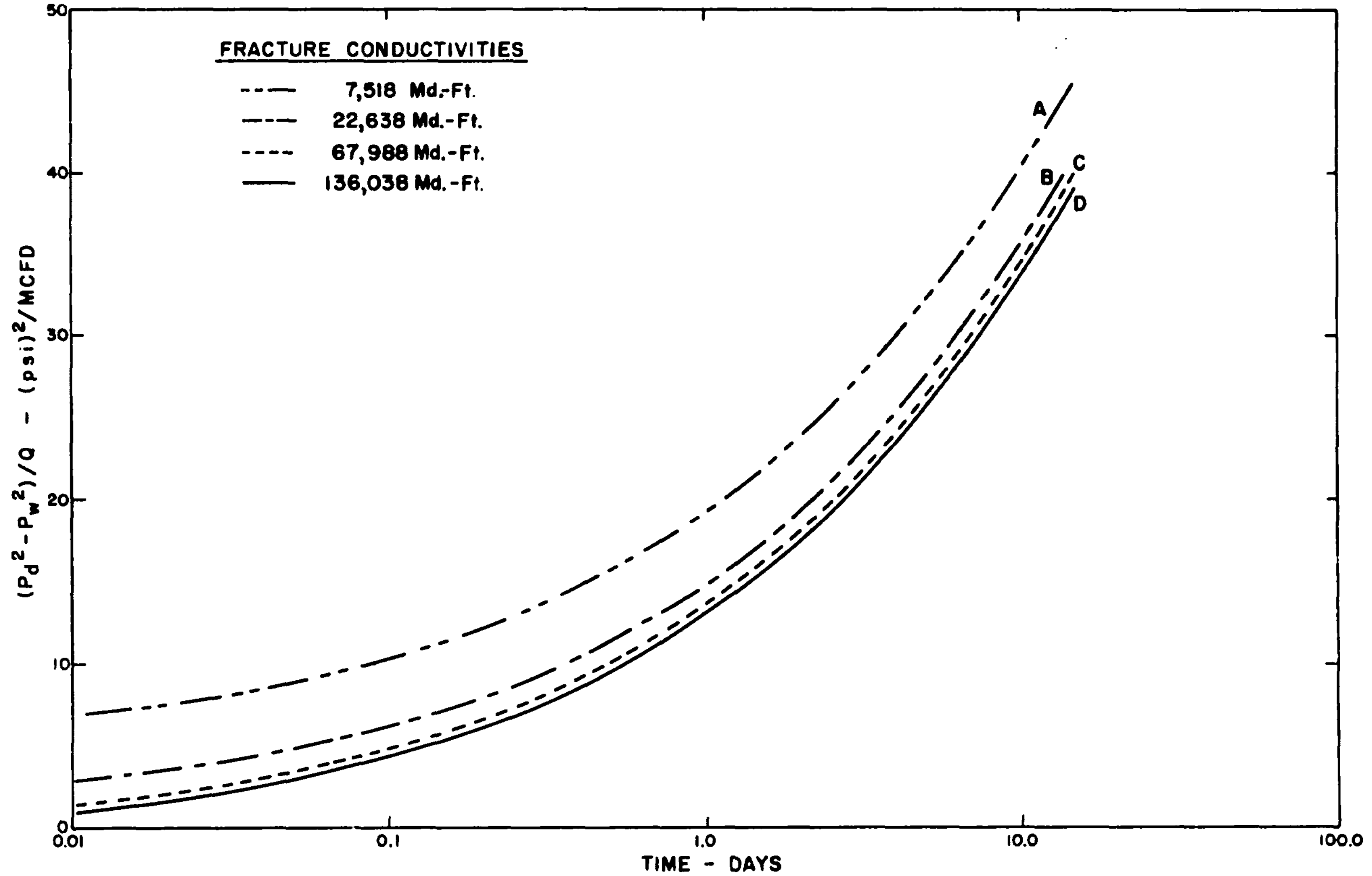

FIGURE 35 SIMULATED WELL-TEST DATA SHOWING THE EFFECTS OF INCREASING FRACTURE CONDUCTIVITY

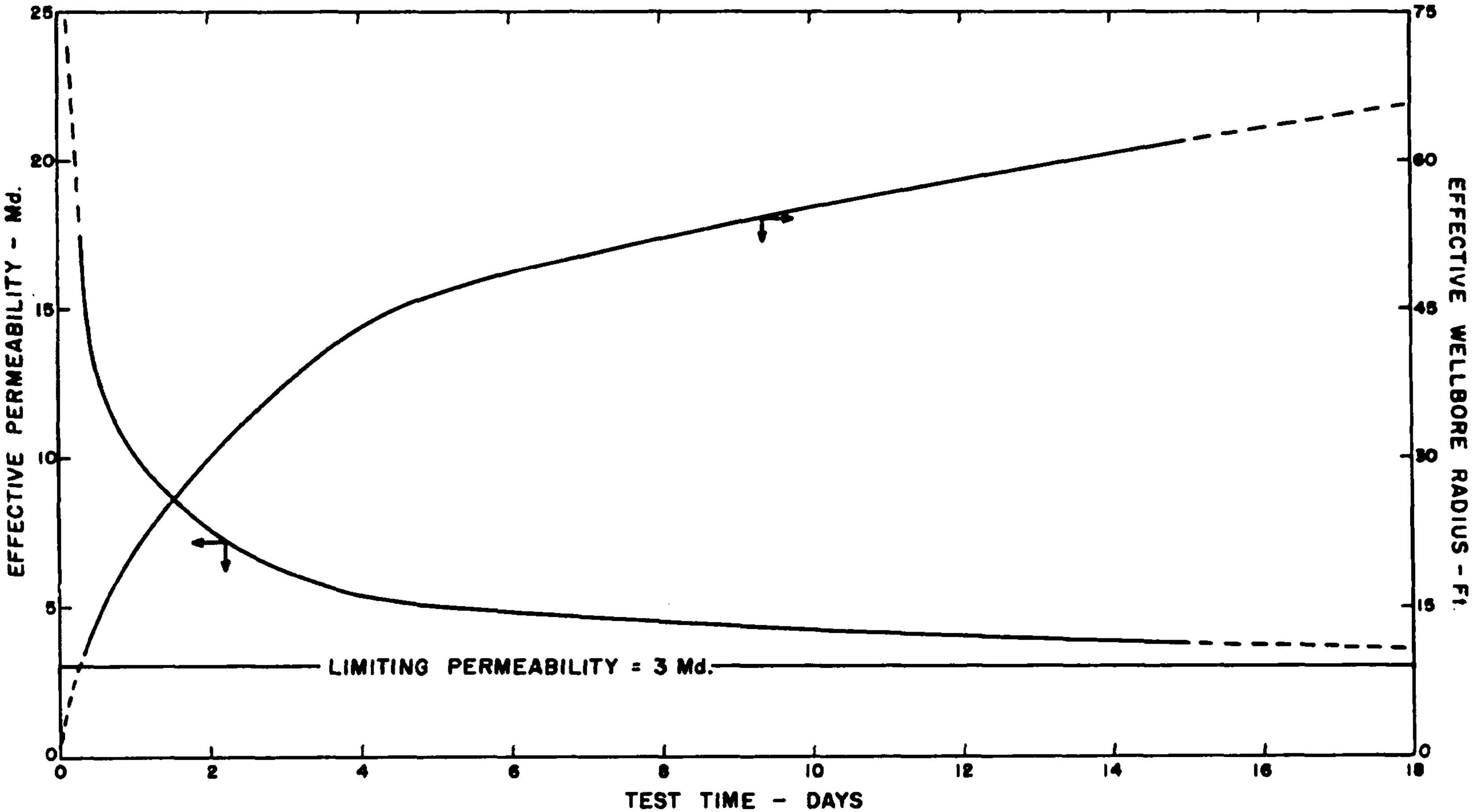

FIGURE 36 CALCULATED EFFECTIVE PERMEABILITIES AND WELLBORE RADII FOR DIFFERENT LENGTHS OF FLOW-TESTS IN A FRACTURED SYSTEM

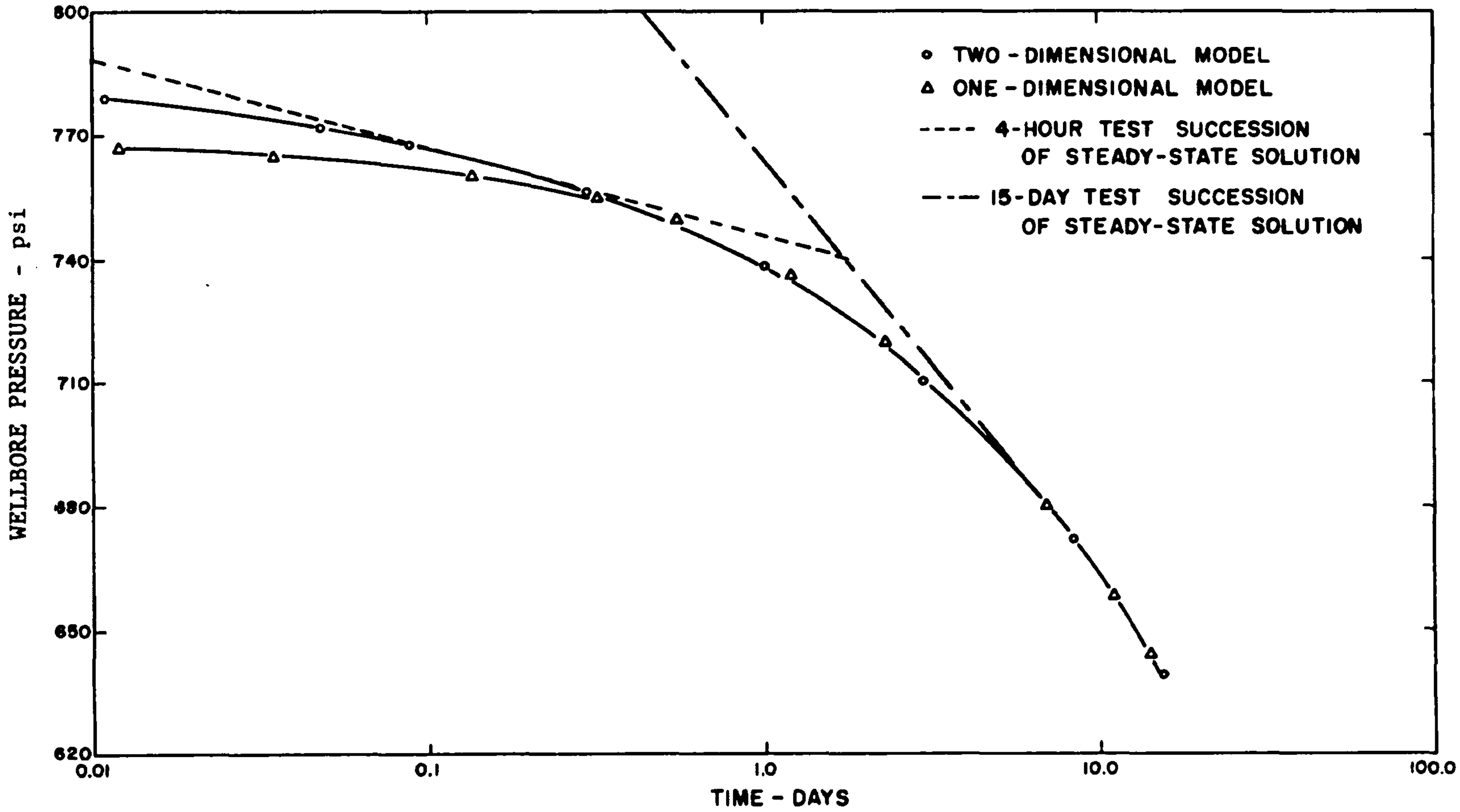

FIGURE 37 SIMULATED WELL-TEST DATA FOR A FRACTURED SYSTEM COMPARED WITH ONE-DIMENSIONAL RUNS USING SELECTED DATA

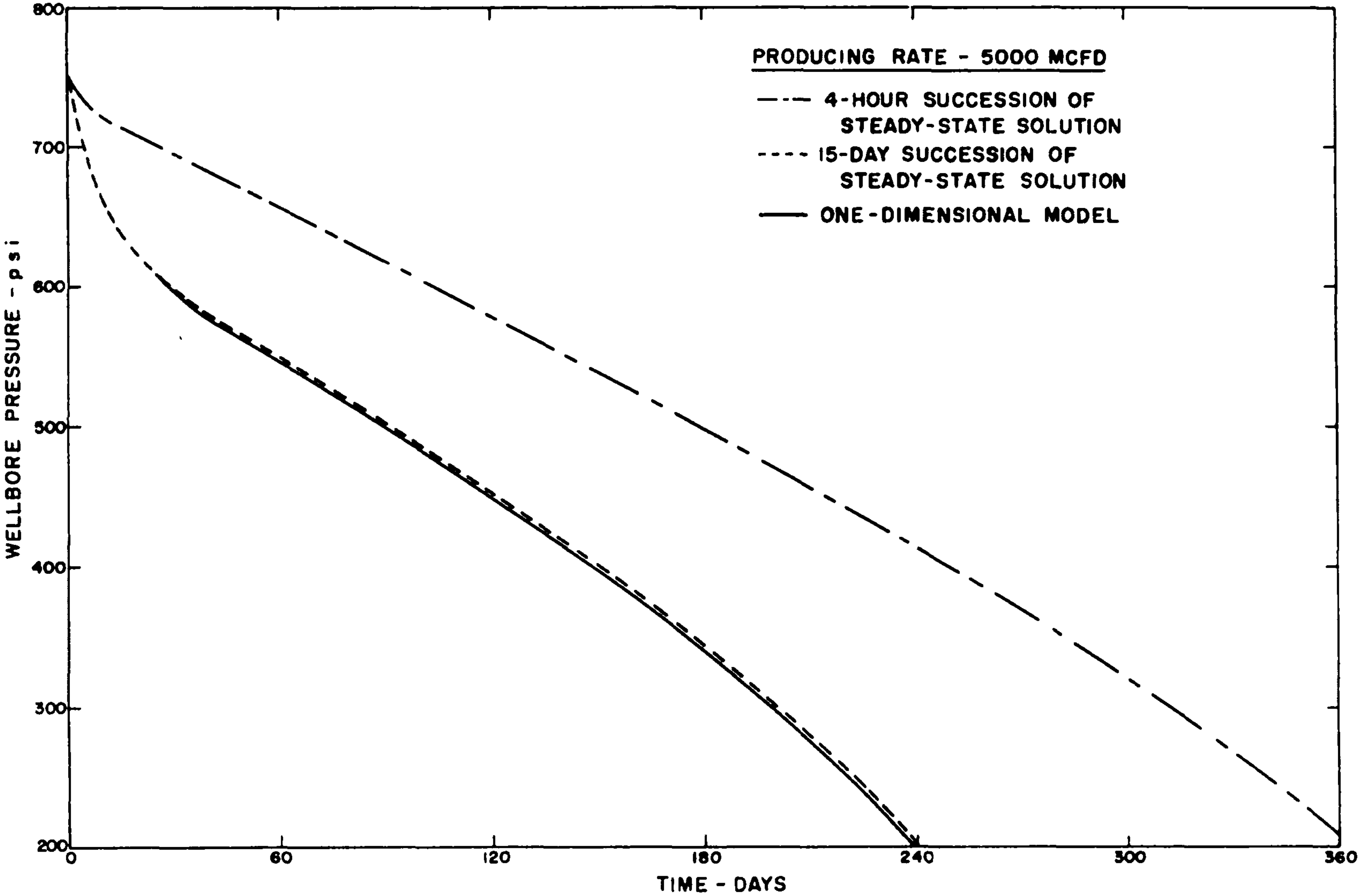

FIGURE 38 PREDICTED LONG-TERM WELLBORE PRESSURE PERFORMANCE IN A FRACTURED SYSTEM USING ONE-DIMENSIONAL TECHNIQUES

TABLE IX

LIMITING VALUES OF EFFECTIVE RADII FOR FRACTIONAL PRODUCING INTERVAL AT THE TOP OF THE FORMATION

System Description	Assigned Numerical Value
Horizontal Permeability, uniform-md	3.0
Vertical Permeability, uniform-md	3.0
Drainage Area, acres	40
Formation Thickness, ft	98
Porosity, per cent	40
Wellbore Radius, ft	0.5
Gas Viscosity, cp	0.012
Reservoir Pressure, psi	800
Standard Pressure, psia	15.025
Formation Temperature, °F	90
Standard Temperature, °F	60

Limiting Wellbore Radius-Ft	Fraction of Formation Opened to Flow
$5.(10^{-1})$	1
$9.8(10^{-3})$	1/2
$1.2(10^{-4})$	1/3
$2.4(10^{-6})$	1/4
$9.7(10^{-8})$	1/5
$3.7(10^{-9})$	1/6

CHAPTER VI

OTHER APPLICATIONS

There are numerous transient problems for which the use of this two-dimensional model should prove valuable. One of the shortest test periods used today is found in the oridnary drill-stem test. From calculations presented in this work, we can state that such tests may often be so limited they never get beyond this initial variable capacity period. This model should be most beneficial in establishing criteria for better designed testing. Similarly, the model may be used to check the equations and conclusions derived from a simplified model in a recent theoretical analysis of pressure phenomena associated with wireline formation testing. (24) Pressure build-up analysis is another problem concerned with short-term transient phenomena. Much attention has been given to this problem in the literature. (22,27,39) With this model, we can determine the effects fractures, completion interval location, stratification, and vertical permeability have on the pressure measurements. Additional problems, for which the model has demonstrated utility, are in the design of optimum completions and effects of fracture design on the resulting producing efficiency in systems having complex geometry.

Optimum Well Completions

An application for this model would be in the evaluation of parameters that determine what constitutes an optimum well completion within naturally occurring permeability distributions. Here, an optimum completion will be defined as the completion necessary to provide the anticipated production requirements for the longest period of time through the least expenditure of capital. If the answer is fracturing, then it is necessary to determine at what location between the upper and lower productive limits the fracture should be initiated. Also needed is an estimate of the areal extent required and the conductivity necessary to do the job. If the answer is selected zones for perforations, then be able to wisely choose them for the minimum interval size that will result in the least reduction in producing efficiency. From the work already presented, we know that the completion geometry can be described in terms of a variable skin effect for the period of time that the vertical component of variable capacity is insignificant. Then, completion optimization is the proper engineering of this geometry so that the limiting value of the variable skin effect will be at a maximum, when expressed either as an effective wellbore radius or a zone of altered permeability, once the transient has expired.

In order to illustrate this concept, we optimized the location of a small fracture in a stratified system having low vertical permeability and a zone of reduced permeability away from the wellbore. The properties of this formation are tabulated in Table III. A fracture having a radius of approximately 20 feet and a conductivity of 1,624 md-ft was located within one of the seven layers. Figure 11 showed the results of calculating the pressure behavior for each of the seven possible fracture locations. The most efficient completion was in the highest permeability streak near mid-formation while the least efficient was the top 4 md-layer isolated by a zone of 2 md-permeability. The percentage of gas produced for each completion interval was also shown in Figure 11. All the runs except those with completions in the upper (1-14 ft) and lower (85-98 ft) layers have reached the point where the vertical component of variable capacity was insignificant. Therefore, we could determine the limiting skin values expressed as effective wellbore radii through use of the succession of steady-states approximate solution or as a zone of reduced permeability when matching performance with the one-dimensional model. Another interesting observation obtained from the calculations was the completions in the two lower zones (85-98 ft and 71-84 ft) were more efficient than completing in the interval (57-70 ft) separating these zones from the remainder of the formation. The most probable explanation for this occurrence is that gradients move faster in the higher permeability zones and thus establish larger areas subjected to crossflow much quicker. This overcomes the relatively inefficient location with respect to mid-formation; therefore, the limiting skin effect is more favorable.

Effect of Completion Interval Location on Pressure Build-up Curves

The location of the completion interval affects the time requirements for the disappearance of the skin effect in pressure build-up measurements as well as in draw-down tests. Consequently, it behooves us to know how long this skin is expected to affect measurements in order that we do not misinterpret premature build-up data in an analogous manner to that shown possible in well-test analyses. Shown in

Figure 39 are the resulting build-up curves for three runs with completion intervals 29-42 ft, 43-56 ft, and 85-98 ft. The properties of this formation are tabulated in Table X. A constant producing rate of 1670 MCFD for a period of 35 days was calculated for each run before reducing the flow rate to zero. Notice that at least 10 days of pressure measurements are required before all three curves converge. The intervals 29-42 ft and 43-56 ft record essentially the same pressure after 5 days. Figure 40 shows that the time required for the vertical component of variable capacity to disappear in the system, with completion interval 85-98 ft, is 10-15 days. This closely approximates that required in build-up measurements as more clearly show in the plot of pressure versus log $\frac{T + \Delta t}{\Delta t}$ in Figure 41. Figure 41 shows in all three cases there are line segments that can be construed as straight lines. Employment of standard build-up analysis on short-term data will give erroneous values for formation capacity and static reservoir pressure even if the zone of reduced permeability, that starts showing up after 15 days, were not present. The long time period required for the disappearance of the skin effect may be clearly understood from Figure 42. This shows the pressure distribution from the wellbore to the drainage radius for each of the seven layers. Considering that the vertical permeability is 0.3 md and the formation is 98 ft thick, it is understandable that a long period of time is required for these vertical gradients to disappear.

Effects of Fracture Conductivity and Radius on Producing Efficiency

The effects of fracture conductivity and fracture radius upon well productivity may be more clearly shown through the improved description of a fracture. First, determine the effects of increasing the conductivity of a fracture having a fixed radius. As one comparative method to evaluate this, let us determine the increase in the number of constant-rate producing days resulting from each subsequent increase in conductivity. (This is equivalent to per cent of reserves recovered before going on declining rate production.) In the section on well testing, it has already been shown that the permeability of a fractured system approached the average formation permeability; and, the limiting value for the skin effect, a large effective wellbore radius. Extending the calculations for that example to the cases where the fracture conductivity has been increased to 22,638 md-ft, 66,998 md-ft, and 136,038 md-ft, we first plot $(P_d^2-P_w^2)/Q$ versus log t as shown in Figure 35, curves B, C, and D respectively. Then, following the procedure outlined in Appendix B, we obtain the parameters necessary to use the succession of steady-states solution as the predictive equation. Figure 43 shows the two-dimensional calculations for the first 15 days for each of the four conductivities. Figure 44 shows the number of producing days versus fracture conductivity. From this plot, it is apparent that for the viewpoint of producing this formation it is not worthwhile to try to increase the fracture capacity above the 67,000 md value. Here, we are excluding all considerations on the practicality or economic feasibility of obtaining such a fracture.

Similarly, the effect of increasing the fracture radius on the well productivity may be calculated. If the test is run long enough for the slope of $(P_d^2-P_w^2)/Q$ versus log to to become constant, then the succession of steady-states solution can be used. Alternatively, the fracture conductivity can be added to that of the formation out to the fracture extremity and the one-dimensional model used. Using either method, we can compare the extra benefits expected over the additional cost for creating the larger fracture.

Effects of Fracture Radius on Pressure Build-up Analysis

After 20-day production periods, the build-up curves were calculated to show the effect of the different fracture sizes on the time required for the pressure in the two systems to converge. We know they will converge, given enough time, to the static pressure determined by material balance depletion calculations. Figure 45 shows the plot of wellbore pressure versus log $\frac{\Delta t}{T + \Delta t}$ for both cases. The curves converge after 4 days indicating that this period of time is required before the distortions caused by the different sized fractures are gone. These are long-term skin effects and require longer periods of build-up before measuring the formation properties. The third curve shown is for an open-hole completion where the average permeability is used in place of the layered permeabilities. Here the pressure measurements closely follow those of the system with the larger fracture after 13 hours. Notice that the permeability barrier located 375 feet away from the wellbore did not show in the pressure build-up measurements. This is due to an insignificant drawdown in this area after a production period of 20 days.

High Permeability Layers Produce Gas Obtained from Crossflow

A series of one- and two-dimensional model calculations have been designed to show that high-permeability layers serve as carriers or transporters of gas from contiguous lower-permeability areas. The two-dimensional model used is equivalent to 5 layers, each 15 ft thick, having permeabilities of 9 md, 3 md, 6 md, and 3 md respectively, ordered from the top of the formation to the bottom. The layers are connected via a uniform 4 md vertical permeability. From each layer a production rate of 300 MCFD is maintained through a manifold arrangement where the wellbore pressures for each layer are not uniform in value. This model was produced for a period of time known to exceed that required for the vertical component of variable capacity to disappear. Then, three one-dimensional model runs were made for equivalent periods of time. These permeabilities also were 3 md, 6 md, and 9 md. All other variables were the same in both cases. Figure 46 shows the pressure versus log radius for the three one-dimensional model runs and for the five layers of the two-dimensional model at the end of 1.7425 days. Starting with the 9 md layers, we note in comparing these with the one-dimensional model run that the pressures are lower near the wellbore and are higher beyond a 230-ft radius. Beyond a radius of 500 ft, the two gradients converge. This shows that a larger-than-expected pressure drop is required to produce these reserves. Hence, they must be carrying gas from contiguous layers over some fraction of the flow path. Next, compare the 6 md layer with the one-dimensional model run having the same permeability. Both gradients are within 4 or 5 psi of each other. However, the one-dimensional model run is higher, indicating the 6 md acts as a carrier in a very small way. Finally, consider the 3 md layers. Here, gradients in both layers are considerably higher than would be expected from the one-dimensional run. This shows that the gas was not transported within the layers. Further, compare Layer 2 to Layer 5. The gradient in Layer 2 is less steep because there are two contiguous higher-permeability layers to serve as carriers while there is only one for Layer 5. This is the reverse behavior observed in the high-permeability streaks where the layer contiguous to only one low-permeability layer had a smaller gradient. Of course, this is not an unknown phenomena, for it is upon this concept of high-conductivity layers serving as carriers that fracturing has gained prominence.

Partial Well Penetration

The effect of a partially penetrating wellbore on the resulting productivity has received considerable attention. (3,15,25,26) Muskat (25) studied the problem for both isotropic and anisotropic media. However, for the anisotropic case, he limited the analysis to uniform horizontal-vertical permeability ratios greater than or equal to one. Dupuy (15) showed that, after an initial time period, the straight line portions of the plot of pressure versus log time were displaced by a constant pressure increment dependent on the per cent penetration of the well. Brons and Marting (3) limited their work to isotropic formations. However, they extended the analysis to include opened intervals other than partial-penetrating wells.

The model developed here is capable of duplicating the geometries and the anisotropies thus far studied for single-well reservoirs as well as generalizing their findings.

Figure 47 shows the results of calculating the wellbore pressure behavior to maintain a given flow rate for partial penetrations of 50 per cent, 33 per cent, 25 per cent, 20 per cent, and 17 per cent in an isotropic formation. These calculations confirm the findings of Dupuy. (15) An additional verification that the lower percentage partial penetration requires an equivalent added pressure drop is shown in Table IX. The effective wellbore radii are calculated for each percentage penetration using the succession of steady-states approximation solution. These extremely small values for the wellbore radius illustrate the lack of physical analogy. The effective wellbore radius serves as a means for describing an added pressure drop.

Initial Study of Other Geometries

In addition to the flow geometries presented, there were others studied that are not found in the literature. Sample problems have been run, but not included, where radical reductions in formation thickness (simulating pinch outs) have been represented by inserting zero values for appropriate horizontal and vertical permeability matrix points. The problem was further complicated by using a horizontal-vertical permeability ratio of 10. Shale streaks have been simulated by inserting continuous strings of zero vertical permeabilities in that matrix. Gas from the area above this barrier had to flow radially outward from the wellbore, around the barrier and to the producing interval. In both cases, the calculations gave results that could be qualitatively predicted from the work presented.

All the applications outlined show this model is very flexible. Detailed studies should greatly improve our understanding of the role of formation heterogeneities on transient phenomena. Such studies are beyond the scope of this work.

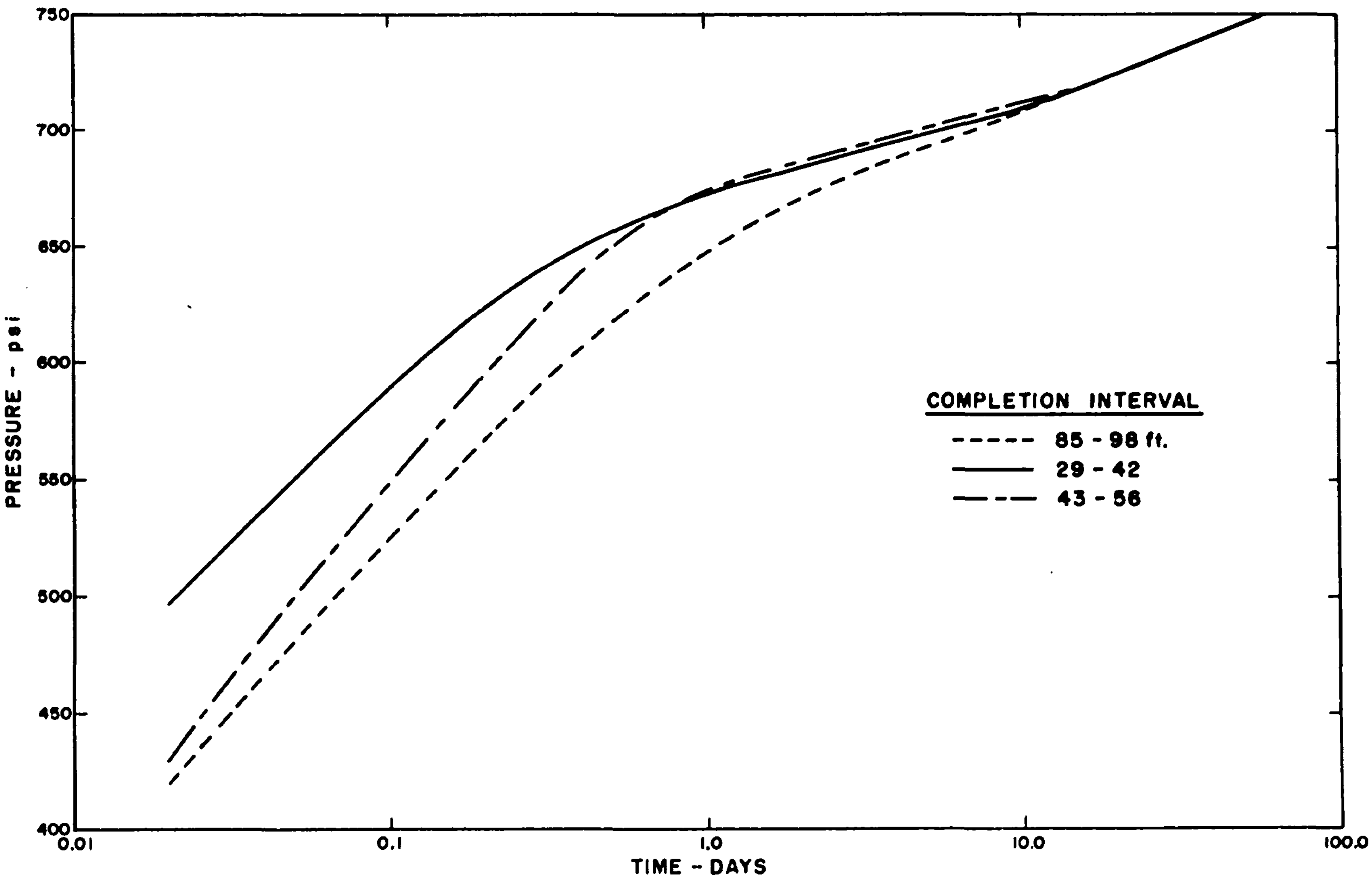

FIGURE 39 EFFECTS OF COMPLETION-INTERVAL LOCATION ON PRESSURE BUILD-UP MEASUREMENTS FOR A STRATIFIED MODEL

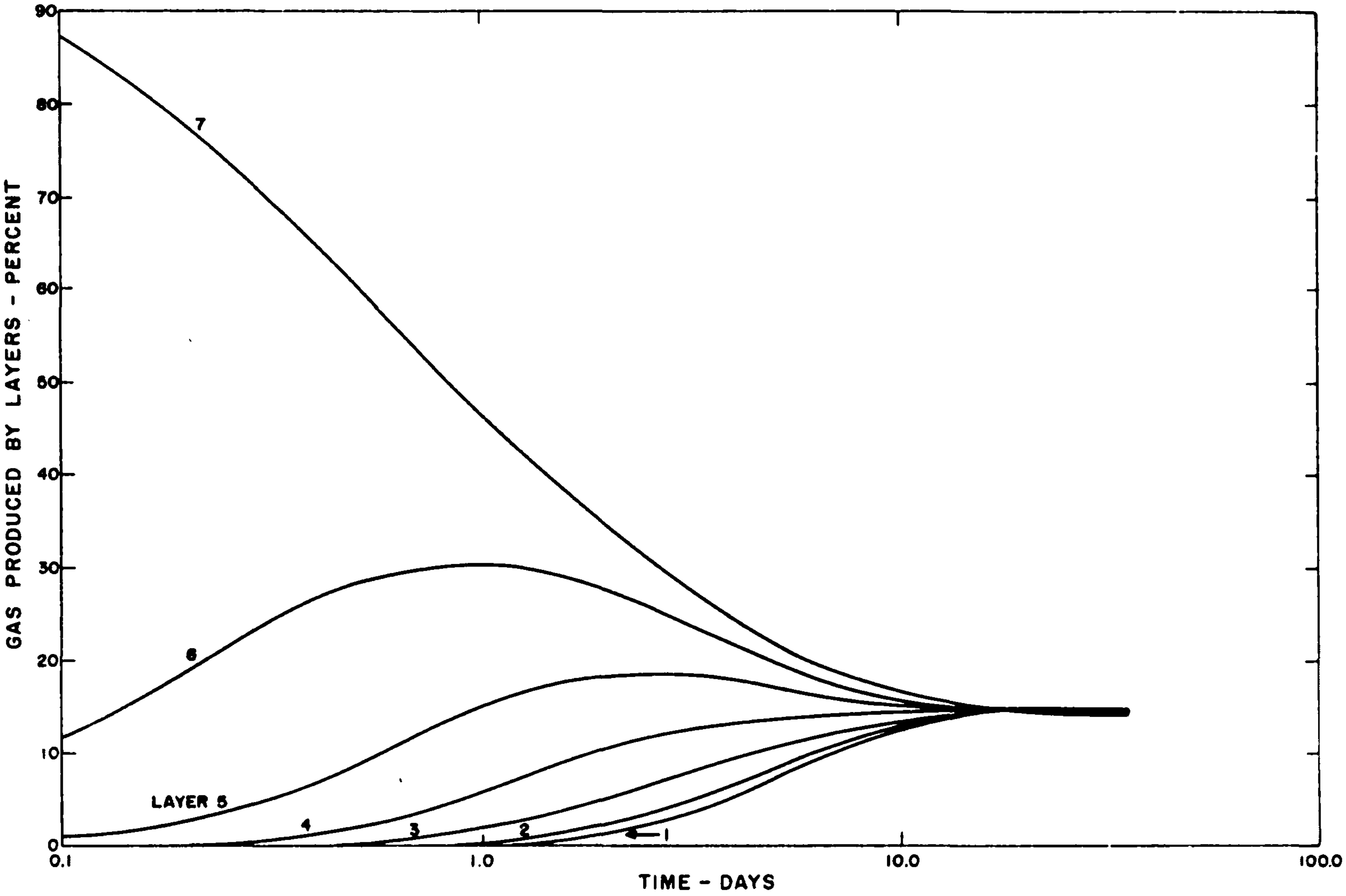

FIGURE 40 DURATION OF VERTICAL COMPONENT OF VARIABLE CAPACITY FOR LAYERED RESERVOIR WITH 0.3 Md. VERTICAL PERMEABILITY

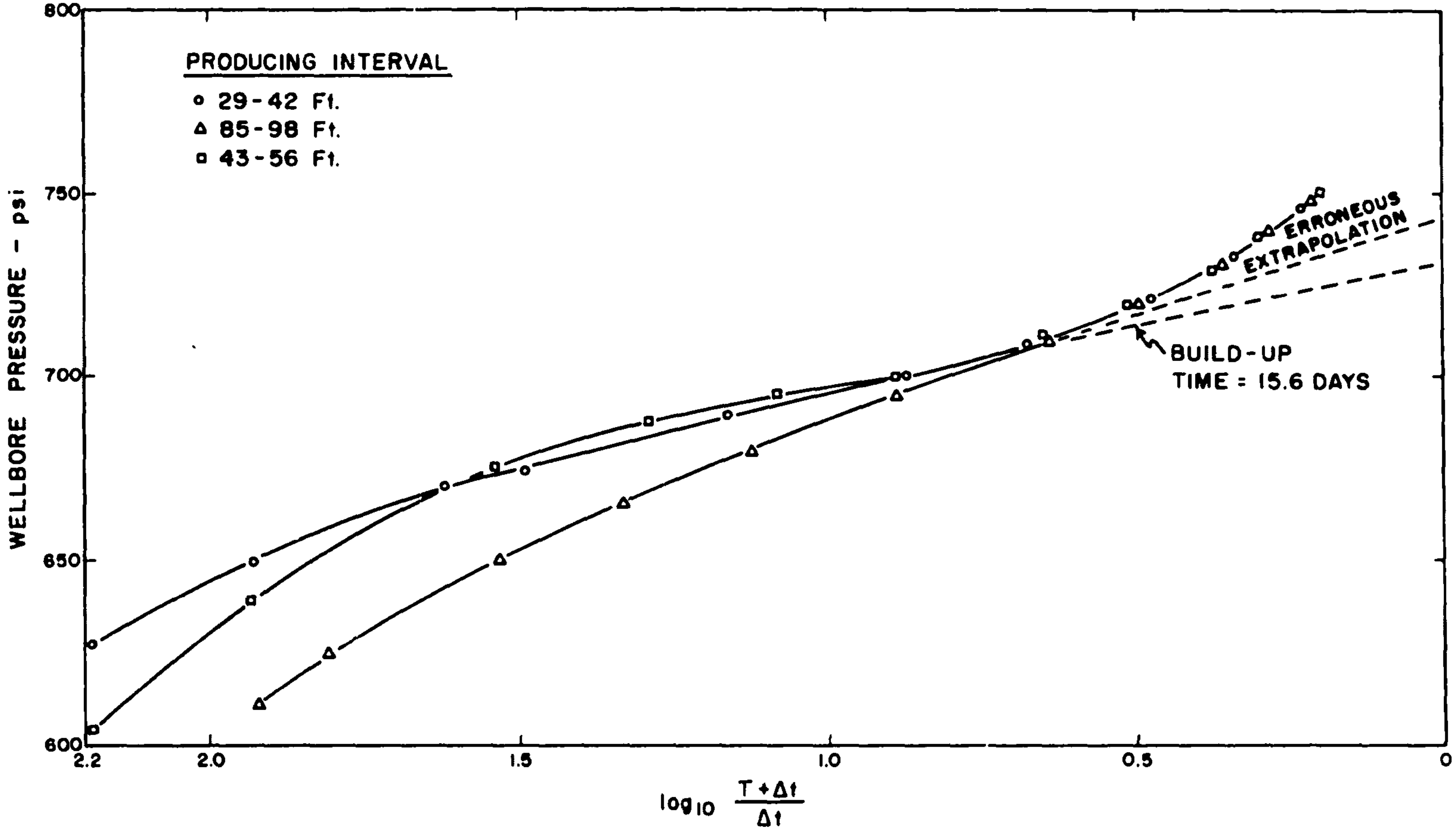

FIGURE 41 EFFECT OF COMPLETION INTERVAL LOCATION ON PRESSURE BUILD-UP MEASUREMENTS FOR A 35-DAY PRODUCTION TEST

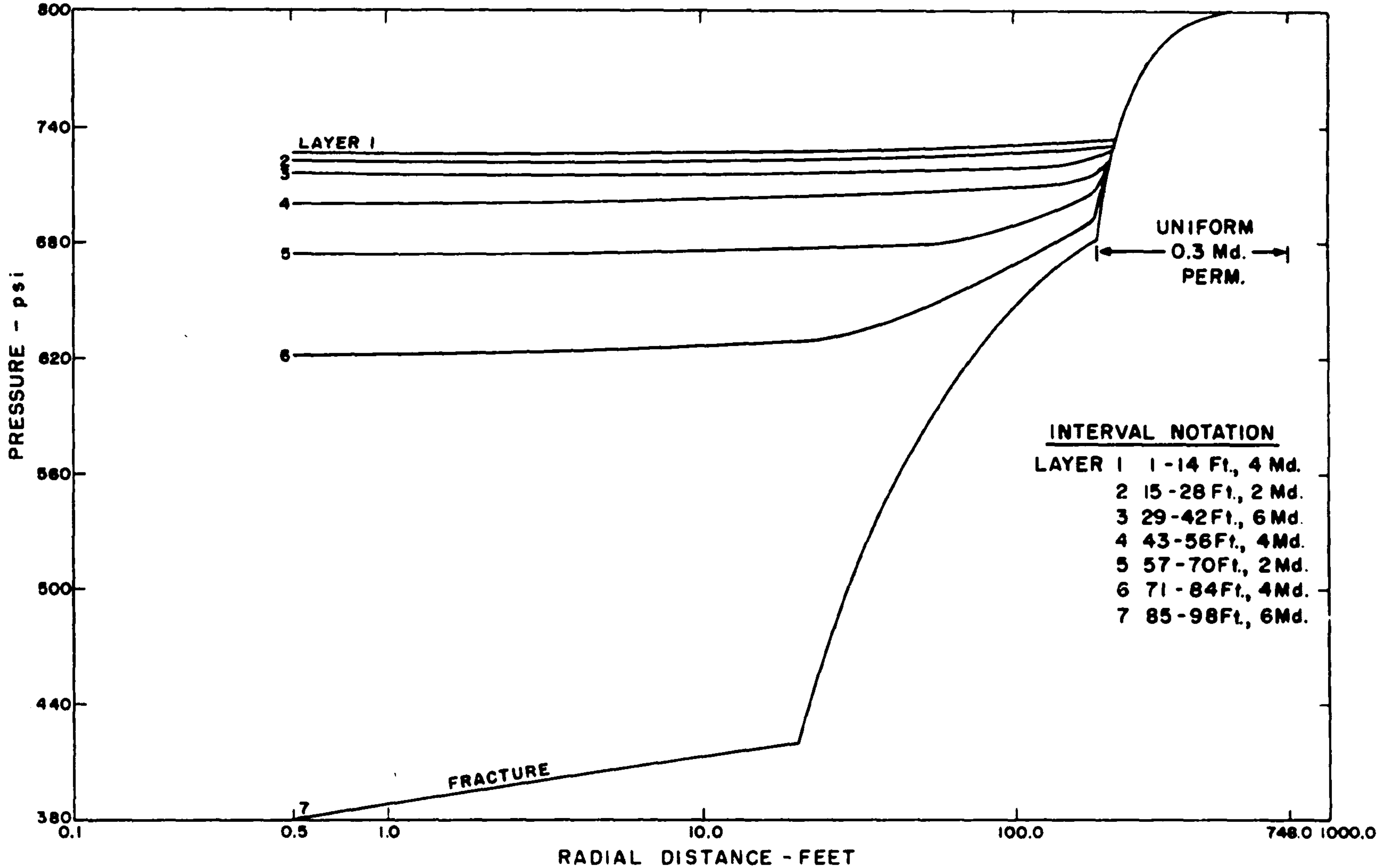

FIGURE 42 RADIAL PRESSURE DISTRIBUTION FOR EACH LAYER IN SYSTEM TABULATED IN TABLE III AFTER 30 DAYS PRODUCTION AT 1670 MCFD

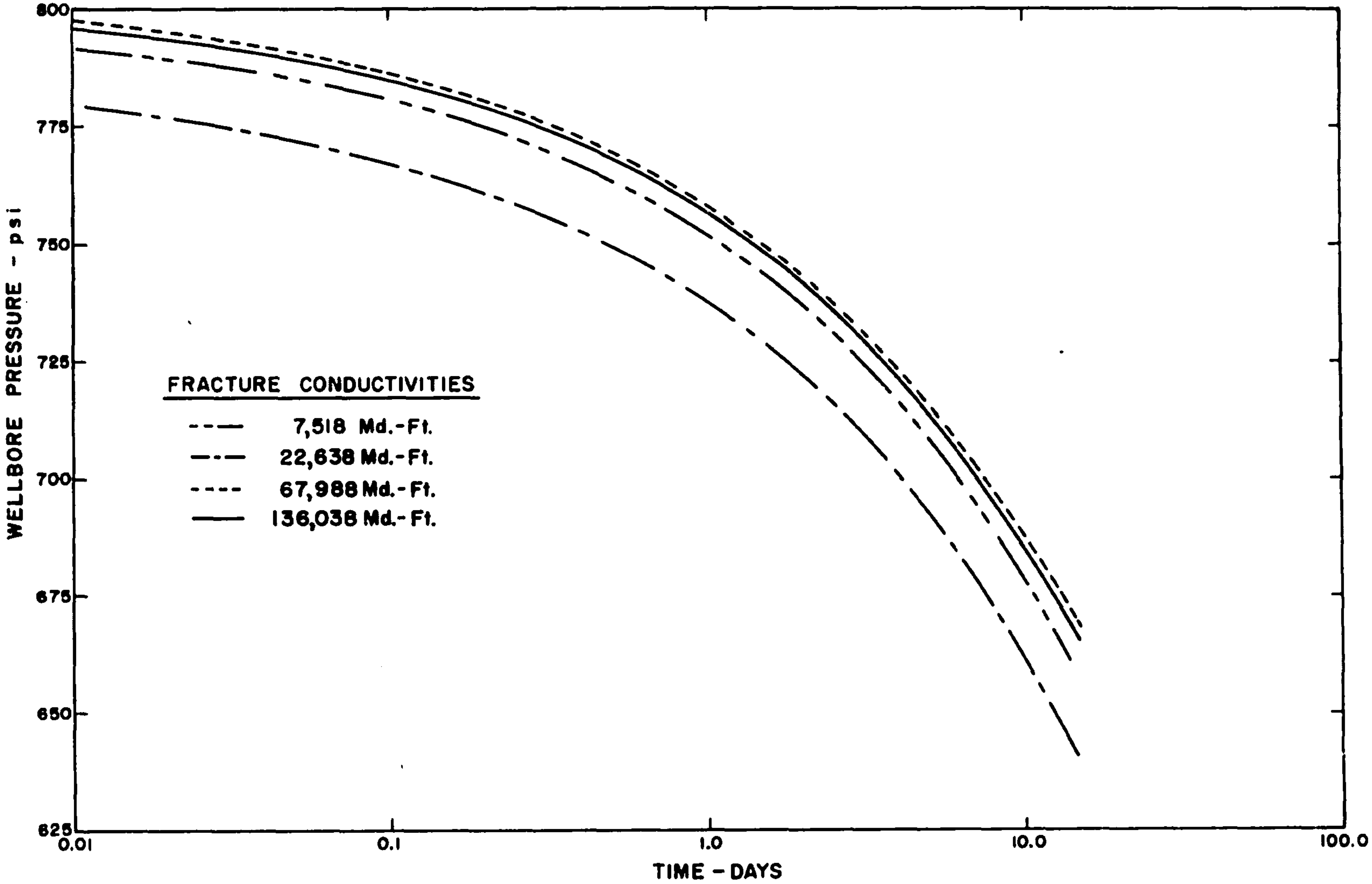

FIGURE 43 EFFECTS OF INCREASING FRACTURE CONDUCTIVITY ON THE CALCULATED WELLBORE PRESSURE

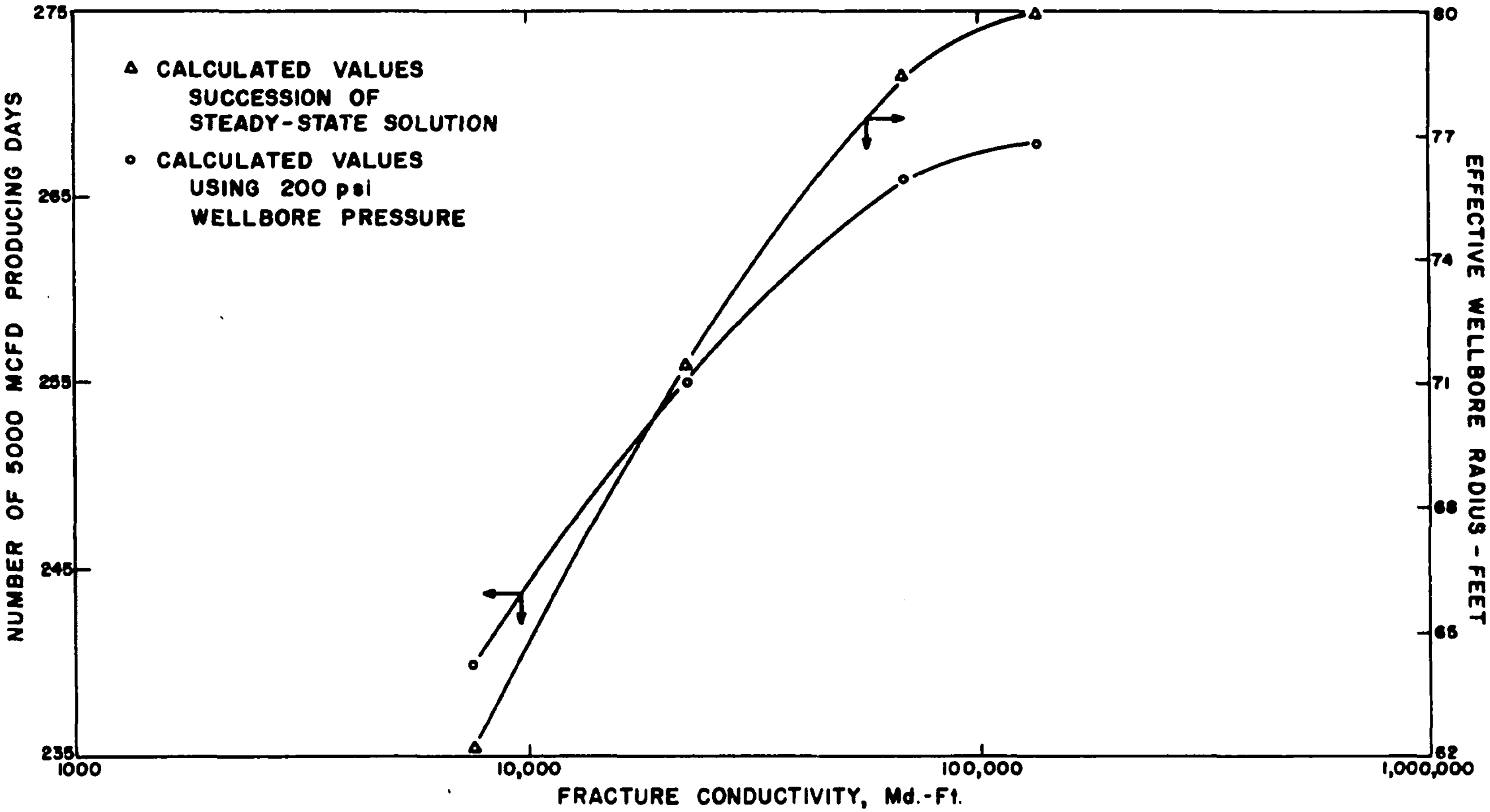

FIGURE 44 EFFECT OF FRACTURE CONDUCTIVITY ON EFFECTIVE WELLBORE RADIUS AND LENGTH OF CONSTANT-RATE PRODUCTION

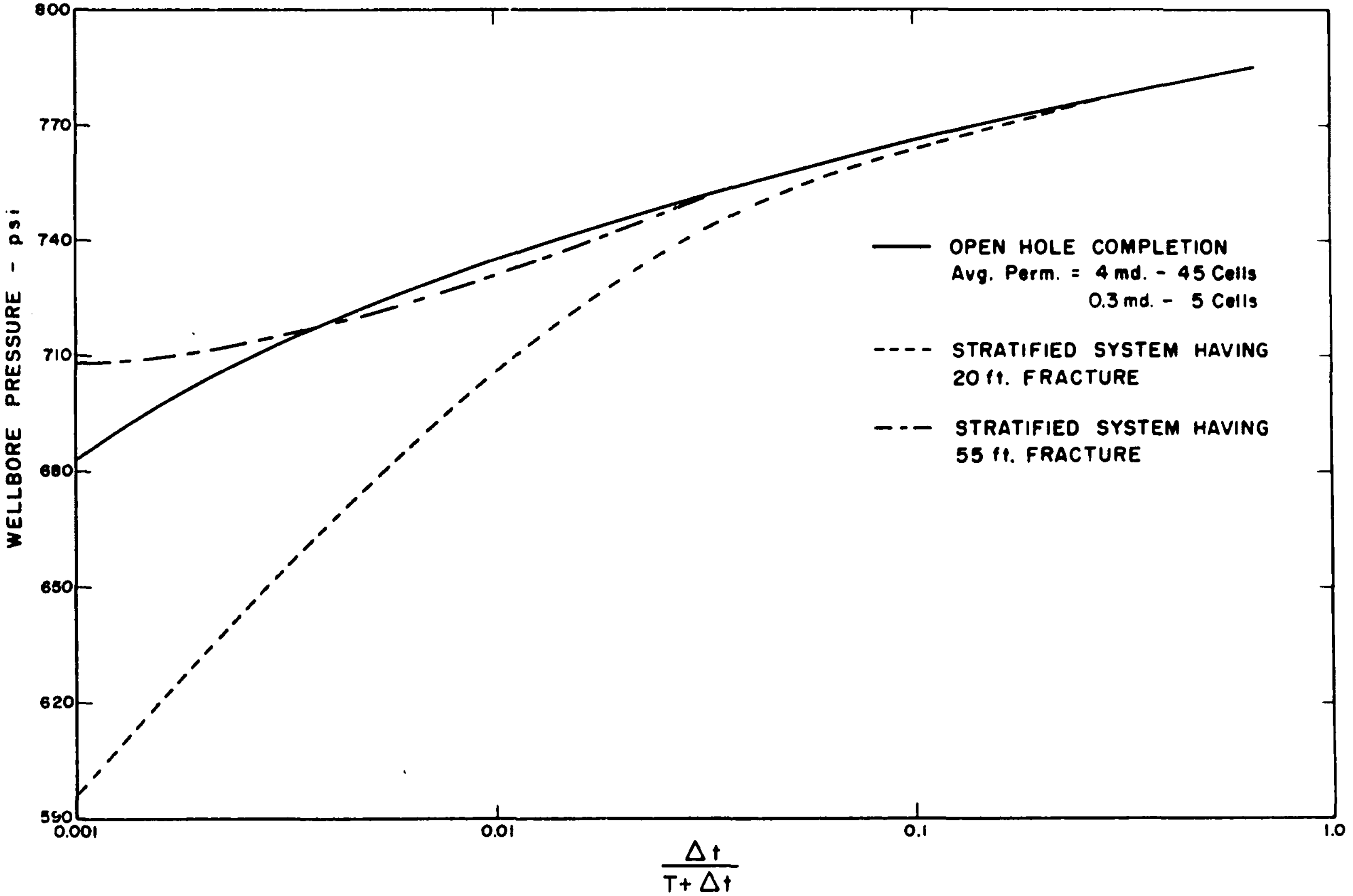

FIGURE 45 EFFECT OF FRACTURE SIZE ON PRESSURE BUILD-UP COMPARED WITH OPEN-HOLE COMPLETION

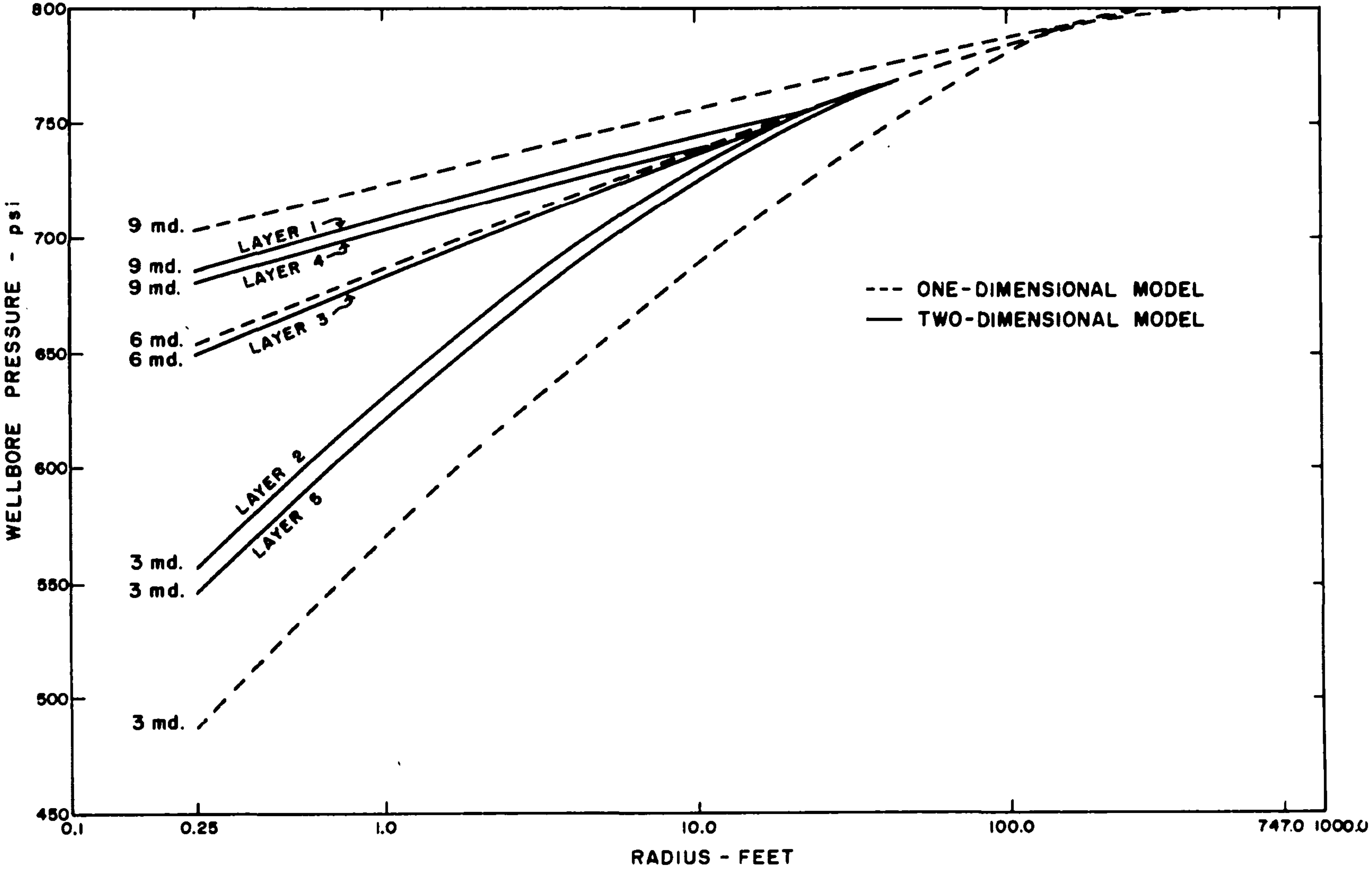

FIGURE 46 MODEL COMPARISONS SHOWING HIGH-PERMEABILITY LAYERS SERVE AS TRANSPORTS FOR GAS FROM OTHER LAYERS

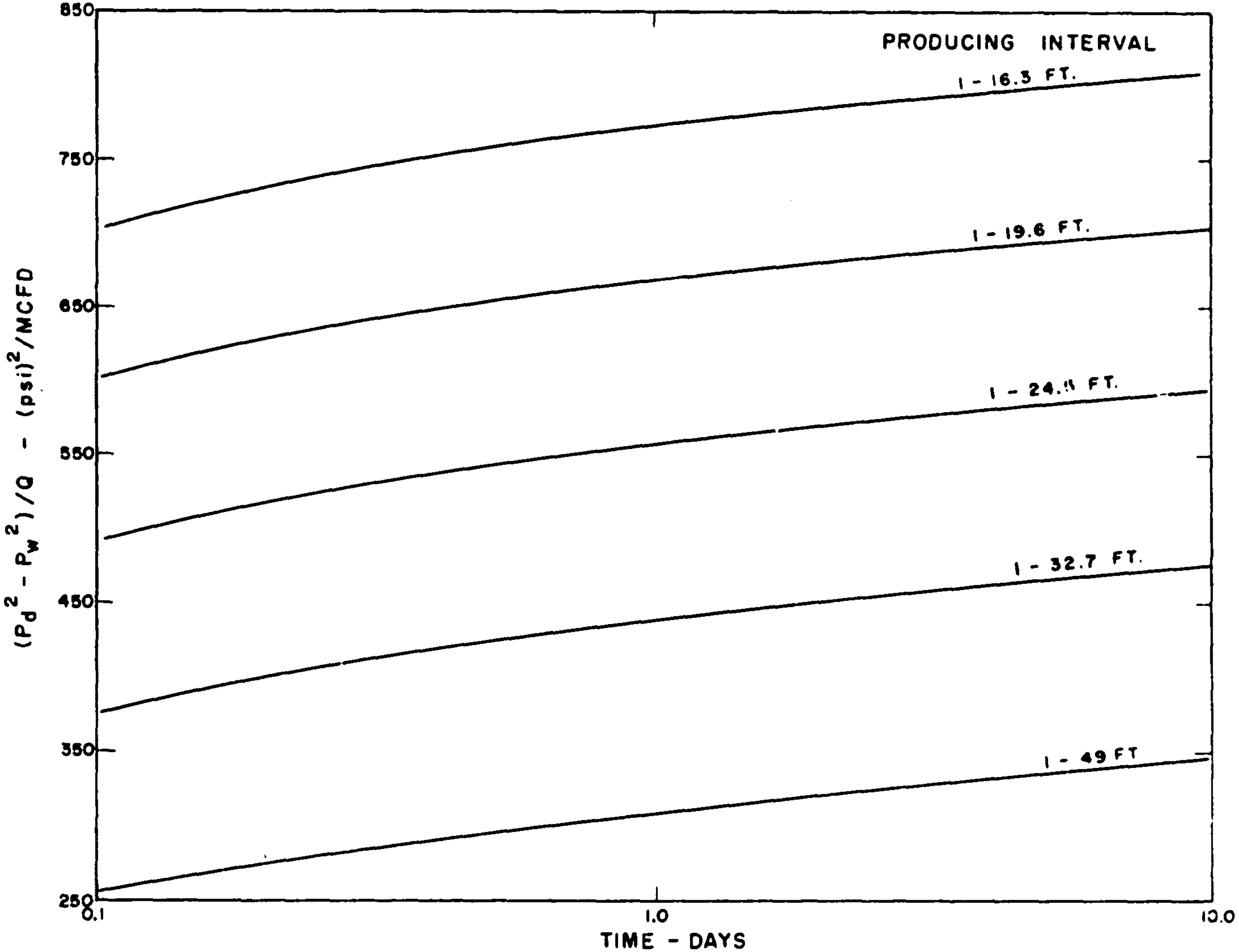

FIGURE 47 EFFECT OF RESTRICTED OPENINGS ON THE PRESSURE-DROP NECESSARY TO MAINTAIN A GIVEN FLOW RATE IN A UNIFORM SYSTEM 98 FEET THICK

TABLE X

FORMATION PROPERTIES USED TO ILLUSTRATE THE EFFECTS OF COMPLETION INTERVAL LOCATION UPON RESULTING PRESSURE BUILD-UP MEASUREMENTS

	Run 1	Run 2	Run 3
Formation Pressure, psi	800	800	800
Standard Pressure, psia	15.025	15.025	15.025
Flow Rate, MCFD	1670	1670	1670
Formation Thickness, ft	98	98	98
Horizontal Permeability, md			
1st 40 cells			
Layer 1	4	4	4
2	2	2	2
3	6	6	6
4	4	4	4
5	2	2	2
6	4	4	4
7	6	6	6
Last 10 cells	0.3	0.3	0.3
Vertical Permeability, md	0.3	0.3	0.3
Completion Interval, ft	85-98	43-56	29-42
Production Time, Days	35.0	35.0	35.0
Pressure Build-Up, Days	62.8	65.0	44.9
Fracture Capacity, md-ft	1,624	1,624	1,624
Fracture Radius, ft	20	20	20
Gas Viscosity, cp.	.012	.012	.012
Formation Temperature, °F	90	90	90
Standard Temperature, °F	60	60	60
Porosity, per cent	40	40	40

CHAPTER VII

CONCLUSIONS

1. An acceptable finite-difference approximation has been developed which is capable of handling large discontinuities in the permeability coefficients without creating calculational instabilities.

2. An iterative scheme which is a variation of an existing line method has been developed for solving these equations.

3. The early transient effects have been thoroughly analyzed. Calculated effects of each geometrical parameter such as completion interval location and vertical permeability on transient time are compatible with current knowledge of fluid-flow, thereby substantiating the validity of the model.

4. The duration of the period in which the vertical component of variable capacity is significant can exceed the relatively short flow-test periods currently used. However, this period is usually insignificant compared to the expected producing life in a constant-rate system. With each change in flow rate, another period follows in which the vertical component of variable capacity is significant.

5. Use of one-dimensional predictive techniques for analyzing data taken during the time period, wherein the vertical component of variable capacity is significant, will give erroneous results. If the early data are ignored, then data taken beyond this time interval

may be properly interpreted using one-dimensional techniques.

6. The proper permeability value to be used in one-dimensional techniques is the average obtained from dividing the sum of the capacity values for each layer by the total thickness.

7. Skin-effect representations in the form of zones of increased (or reduced) permeability or increased (or decreased) effective wellbore radii are shown to be equivalent.

8. After the vertical component of variable capacity has disappeared, the effects of vertical permeability, completion interval location, fracture radius, fracture conductivity, and layered horizontal permeability can be grouped as an equivalent skin effect for all systems other than those containing a very large fracture. In systems with large fractures, the radial component of variable capacity may outlast the vertical component. The performance of these systems may be described by adding the fracture conductivity to the formation conductivity.

9. The succession of steady-states approximation solution gives reliable answers for predicting long-term deliverability performance if the proper data are used. Erroneous answers of large magnitude can result from neglecting the vertical (or radial) component of variable capacity. In fractured systems, the results generally will be too optimistic. In systems with partially penetrating wells (or short perforated intervals), the results will be pessimistic.

10. One constant flow rate test period should be long enough to verify the disappearance of variable capacity. Succeeding tests at different rates should extend 4 hours beyond that point determined in

the first test.

11. The economical applications for the model are limited to short-term analyses such as pressure draw-down and build-up tests and optimum well completions. However, this was shown to be quite satisfactory for all constant flow-rate applications.

12. This model has the capability of providing answers for many other single-well transient problems heretofore necessarily simplified. Abbreviated descriptions of some of the problems have been illustrated.

BIBLIOGRAPHY

1. Aronofsky, J. S., and Jenkins, R. "A Simplified Analysis of Unsteady Radial Gas Flow," Trans. AIME (1954), vol. 201, p. 149.

2. Brian, P. L. T. "A Finite Difference Method of Higher-Order Accuracy for the Solution of Three-Dimensional Transient Heat Conduction Problems," AIChE Journal (September 1961) vol. 7, no. 3, p. 267.

3. Brons, F., and Marting, V. E. "The Effect of Restricted Fluid Entry on Well Productivity," Trans AIME (1961), vol. 222, p. 172.

4. Bruce, G. H., Peaceman, D. W., and Rachford, H. H., Jr. "Calculations of Unsteady-State Gas Flow Through Porous Media," Trans. AIME (1953), vol. 198, p. 79.

5. Carter, R. D. "Solutions of Unsteady-State Radial Gas Flow," J. Pet. Tech. (May 1962), p. 549.

6. Carter, R. D., Miller, S.C., and Riley, H. G. "Determination of Stabilized Gas Well Performance From Short Flow Tests," SPE Paper No. 400 presented at Fall Meeting of AIME, 1962.

7. Crank, J., and Nicholson, P. "A Practical Method for the Numerical Evaluation of Solutions of Partial Differential Equations of the Heat Conduction Type," Proc. Camb. Phil. Soc. (1947), vol. 43, pp. 50-67.

8. Cullender, M. H. "The Isochronal Performance Method of Determining the Flow Characteristics of Gas Wells," Trans. AIME (1955), vol. 204, p. 137.

9. Darin, S. R., and Huitt, J. L. "Effect of a Partial Monolayer of Propping Agent on Fracture Flow Capacity," Trans. AIME (1960), vol. 219, p. 31.

10. Douglas, J., Jr. "On the Numerical Integration of $U_{xx} + U_{yy} = U_t$ by Implicit Methods," J. Soc. Ind. Appl. Math. (1955), vol. 3, p. 52.

11. Douglas, J., Jr., and Peaceman, D. W. "Numerical Solution of Two-Dimensional Heat Flow Problems," AIChE Journal (December 1955), p. 505.

12. Douglas, J., Jr., Peaceman, D. W., and Rachford, H. H., Jr. "A Method for Calculating Multi-Dimensional Immiscible Displacement," Trans. AIME (1959), vol. 216, p. 297.

13. Douglas, J., Jr., Peaceman, D. W., and Rachford, H. H., Jr. "Calculation of Unsteady-State Gas Flow within a Square Drainage Area," Trans. AIME (1955), vol. 204, p. 190.

14. Douglas, J., Jr., and Rachford, H. H., Jr. "On the Numerical Solution of Heat Conduction Problems in Two and Three Space Variables," Trans. Am. Math. Soc. (1956), vol. 82, p. 421.

15. Dupuy, M. "Modelēs Mathematiques A Penetration Partielle et A Permeabilities Variees Realises Pour Le Bureau Reservoir de la C.F.P.A.," Revue de L'Institut Francais du Petrole (October 1961), vol. XVI, no. 10, p. 1067.

16. Hartsock, J. H., and Warren, J. E. "The Effect of Horizontal Hydraulic Fracturing on Well Performance," Trans. AIME (1961), vol. 222, p. 1050.

17. Huckaba, C. E., and Dickert, C. E. "Transient Heat Conduction in a Multilayer Multicomponent System," Chem. Eng. Symp. Series (1962), vol. 58, no. 37, pp. 91-106.

18. Jones. L. G. "An Approximate Method for Computing Non-Steady State Flow of Gases in Porous Media," Trans. AIME (1961), vol. 222, p. II-264.

19. Katz, M. L., and Tek, M. R. "A theoretical Study of Pressure Distribution and Fluid Flux in Bounded Stratified Porous Systems with Crossflow," SPE Journal (March 1962), vol. 2, no. 1, p. 68.

20. Korn, G. A., and Korn. T. M. Mathematical Handbook for Scientists and Engineers, McGraw-Hill Book Company, Inc., New York, 1961.

21. Lefkovits, H. C., Hazebrook, P., Allen, E. E., and Matthews, C. S. "A study of the Behavior of Bounded Reservoirs Composed of Stratified Layers," Trans. AIME (1961) vol. 222, p. II-43.

22. Matthews, C. S. "Analysis of Pressure Build-Up and Flow Test Data," J. Pet. Tech. (September 1961), p. 862.

23. McCarty, D. G., and Barfield, E. C. "The Use of High-Speed Computers for Predicting Flood-Out Patterns," Trans. AIME (1958), vol. 213, p. 139.

24. Moran, J H., and Finklea, E. E. "Theoretical Analysis of Pressure Phenomena Associated with the Wireline Formation Tester," J. Pet. Tech. (August 1962), p. 899.

25. Muskat, Morris. Physical Principles of Oil Production, McGraw-Hill Book Co., Inc., New York (1949), pp. 206-219.

26. Nisle, R. G. "The Effect of Partial Penetration on Pressure Build-Up in Oil Wells," Trans. AIME (1958), vol. 213, p. 85.

27. Nisle, R. G. "The Effect of a Short-Term Shut-in on a Subsequent Pressure Build-Up Test on an Oil Well," Trans. AIME (1956), vol. 207, p. 320.

28. Peaceman, D. W., and Rachford, H. H., Jr. "The Numerical Solution of Parabolic and Elliptic Differential Equations," J. Soc. Ind. Appl. Math. (1955), vol. 3, p. 28.

29. Pendergrass, J. D., and Berry, V. J., Jr. "Pressure Transient Performance of a Multilayered Reservoir with Crossflow," SPE Journal, (December 1962), vol. 2, No. 4, p. 347.

30. Pickering, C. H., Cotman, N. T., and Crawford, P. B. "A Study of Flow in Stratified Reservoirs by Use of the Thermal Analogy," Trans. AIME (1961), vol. 222, p. II-215.

31. Poettman, F. H., and Schilson, R. E. "Calculation of the Stabilized Performance Coefficient of Low Permeability Natural Gas Wells," Trans. AIME (1959), vol. 216, p. 240.

32. Rawlins, E. L., and Schellhardt, M. A. "Back Pressure on Natural Gas Wells and Their Application to Production Practices," Monograph 7, U.S.B.M. (1936).

33. Rowan, G., and Clegg, M. W. "An Approximate Method for Transient Radial Flow," SPE Journal (September 1962), p. 225.

34. Russell, D. G., and Pratts, M. "Performance of Layered Reservoirs with Crossflow Single-Compressible-Fluid Case," SPE Journal (March 1962), vol. 2, No. 1, p. 53.

35. Sheldon, J. W., Harris. C. D., and Bavly, D. "A Method for General Reservoir Behavior Simulation on Digital Computers," SPE Paper No. 152, presented at Fall Meeting of AIME, 1960.

36. Swift, G. W., and Kiel, O. G. "The Prediction of Gas Well Performance Including the Effect of Non-Darcy Flow," J. Pet. Tech. (July 1962), p. 79.

37. Tek. M. R. Coats, K. H., and Katz, D. L. "The Effect of Tubulence on Flow of Natural Gas Through Porous Reservoirs," J. Pet. Tech. (July 1962), vol. XIV, No. 7, p. 799.

38. Tek, M. R., Grove, M. L., and Poettman, F. H. "Method for Predicting the Bak Pressure Behavior of Low Permeability Natural Gas Wells," Trans. AIME (1957), vol. 210, p. 302.

39. Thomas, G. B., "Analysis of Pressure Build-Up Data," Trans. AIME (1953), vol. 198, p. 125.

40. Vacher, J. P., et Cazabat, V. "Ecoulement des Fluides Dans Les Millieux Pormeux Stratifies Resultats Obtenus Sur Le Modele Du Bicouche Avec Communication," Revue de L'Institut Francias du Petrole (October 1961), vol. XVI, No. 10, p. 1147.

41. Van Everdingen, A. F. "The Skin Effect and Its Influence on the Productive Capacity of a Well," Trans. AIME (1953), vol. 198, p. 171.

42. Wachspress, E. L. "Optimum Alternating Direction Implicit Interations Parameters for a Model Problem," J. Soc. Ind. and Appl. Math. (June 1962), pp. 339-350.

43. Warren, J. E., and Price, H. S. "Flow in Heterogeneous Porous Media," Trans AIME (1961), vol. 222, p. II-153.

44. West, W. J., Garvin, W. W., and Sheldon, J. W. "Solution of the Equations of Unsteady State Two-Phase Flow in Oil Reservoirs," Trans. AIME (1954), vol. 201, p. 217.

APPENDIX A

DISCARDED MATHEMATICAL APPROACHES TO SOLVING FINITE-DIFFERENCE EQUATIONS

The first finite-difference approximation used for a normalized form of equation (12) was an ordinary forward central-difference scheme. Starting with equation (12)

$$\frac{1}{r_e^2 e^{2v}} \frac{\partial}{\partial v}\left(K_v \frac{\partial p^2}{\partial v}\right) + \frac{1}{H^2} \frac{\partial}{\partial y}\left(K_y \frac{\partial p^2}{\partial y}\right) = 2\phi\mu \frac{\partial p}{\partial t} \tag{A-1}$$

we first multiplied through by $r_e^2 e^{2v}$ and normalized the equation by letting

$$\begin{aligned} P &= p/P_o \\ K_v &= K_v/K_{AVG} \\ K_y &= K_y/K_{AVG} \\ \theta &= \frac{P_o K_{AVG}\, t}{2\phi\mu r_e^2} \end{aligned} \tag{A-2}$$

Substituting equations (A-2) into equation (A-1) we get

$$\frac{\partial}{\partial v}\left(K_v \frac{\partial P^2}{\partial v}\right) + \left(\frac{r_e}{H}\right)^2 e^{2v} \frac{\partial}{\partial y}\left(K_y \frac{\partial P^2}{\partial y}\right) = e^{2v} \frac{\partial P}{\partial \theta} \tag{A-3}$$

The central difference representation of equation (A-3) at the grid point (i.j) is

$$\begin{aligned} &\left[K_{v_{i,j-1/2}}\left(P^2_{i,j-1} - P^2_{i,j}\right) + K_{v_{i,j+1/2}}\left(P^2_{i,j+1} - P^2_{i,j}\right)\right]/\overline{\Delta v}^2 \\ &\quad + \left(\frac{r_e}{H}\right)^2 e^{2v_j}\left[K_{y_{i-1/2,j}}\left(P^2_{i-1,j} - P^2_{i,j}\right) + K_{y_{i+1/2,j}}\left(P^2_{i+1,j} - P^2_{i,j}\right)\right]/\overline{\Delta y}^2 \\ &\quad = e^{2v_j}\left(P_{i,j,n+1} - P_{i,j,n}\right)/\Delta\theta \end{aligned} \tag{A-4}$$

The boundary conditions at the upper and lower boundaries and at the wellbore are the same as those given in equations (15). However, the equation used for the outer boundary was that developed by Bruce (4)

$$P^2_{i,m+1,n+1} - P^2_{i,m,n+1} = \left(P_{i,m+1,n+1} - P_{i,m+1,n} + P_{i,m,n+1} - P_{i,m,n}\right)\overline{\Delta V}^3/24\Delta\theta \tag{A-5}$$

The iterative scheme selected was the Alternating-Direction Implicit Method (28). A finite-difference equation must be written for each interior point (i,j) implicit in the v-direction. These pressures are calculated, one row at a time, for the time step (n+1) using the known pressures at time step n. The finite-difference equation at the grid point (i,j) in the v-direction is:

$$\left[Kv_{i,j-\frac{1}{2}}\left(P^2_{i,j-1,n+1} - P^2_{i,j,n+1}\right) + Kv_{i,j+\frac{1}{2}}\left(P^2_{i,j+1,n+1} - P^2_{i,j,n+1}\right)\right]/\overline{\Delta V}^2$$
$$= e^{2V_j}\left(P_{i,j,n+1} - P_{i,j,n}\right)/\Delta\theta - e^{2V_j}\left(\frac{r_e}{H}\right)^2\left[Ky_{i-\frac{1}{2},j}\left(P^2_{i-1,j,n} - P^2_{i,j,n}\right) + Ky_{i+\frac{1}{2},j}\left(P^2_{i+1,j,n} - P^2_{i,j,n}\right)\right]/\overline{\Delta y}^2 \tag{A-6}$$

Equation (A-6) is further rearranged into the form of equation (66) through use of the approximation scheme given in equation (58). The Thomas method was used to solve these equations. As soon as a satisfactory convergence was obtained in the v-direction, the pressure at the next time step was obtained from writing an implicit equation in the y-direction at each grid point (i,j) and solving the equations, one column at a time. The equation for the y-direction is

$$e^{2V_j}\left(\frac{r_e}{H}\right)^2\left[Ky_{i-\frac{1}{2},j}\left(P^2_{i-1,j,n+2} - P^2_{i,j,n+2}\right) + Ky_{i+\frac{1}{2},j}\left(P^2_{i+1,j,n+2} - P^2_{i,j,n+2}\right)\right]/\overline{\Delta y}^2 = e^{2V_j}\left(P_{i,j,n+2} - P_{i,j,n+1}\right)/\Delta\theta$$
$$- \left[Kv_{i,j-\frac{1}{2}}\left(P^2_{i,j-1,n+1} - P^2_{i,j,n+1}\right) + Kv_{i,j+\frac{1}{2}}\left(P^2_{i,j+1,n+1} - P^2_{i,j,n+1}\right)\right]/\overline{\Delta V}^2 \tag{A-7}$$

This equation also has a form analogous to that discussed for equation (A-6). These equations were never made to work satisfactorily. After searching until an initial time step was found that would satisfy the convergence criteria, each successive time step that satisfied the criteria would be smaller. Therefore, the solution degenerated before it got started.

The next method tried was the Crank-Nicholson (7) approach to the central-difference representation of equation (A-3). That is, the second partial derivative with respect to v evaluated at time steps n and n+1 replaced the left-hand side of equation (A-6). Similarly, for the implicit equation in the y-direction, the second partial with respect to y evaluated at time steps n+1 and n+2 replaces the left-hand side of equation (A-7).

The trouble encountered with this method was the minute time-step sizes for which convergence in the system selected could be maintained. The physical parameters of this 15-layer system can be found in Table XI. A total of 98 time steps were calculated, the maximum time-step size was 0.0000043 days. This maximum occurred on the 52nd, 53rd, and 54th time steps and then had decreased to 0.0000013 days by the time the calculations were terminated. The total producing time calculated for this run was 0.0001676 days. These calculations, with intermittent matrix print-outs and associated diagnostic information, required approximately 5 minutes IBM 7090 computer time. Examination of the pressure matrix indicated pressure reversals along the wellbore (matrix columns 1-2) and pressures exceeding the original reservoir pressure in rows above and below the completion interval. Additionally, a few trials wherein time-step sequences such as tabulated in Table XI were generated indicated that no economical solutions to problems of practical interest would be forthcoming from this approach. However, modifications of the finite-difference equations were made to remove the noted discrepancies in hopes that this would yield a satisfactory solution.

The equations were re-derived to include higher-order derivatives $\frac{\partial^4 p^2}{\partial v^4}$, $\frac{\partial^6 p^2}{\partial v^6}$, $\frac{\partial^8 p^2}{\partial v^8}$, and $\frac{\partial^3 p^2}{\partial v \partial y^2}$ for the iterative equation in the v-direction. The equation can be written in the form

$$A_{i,j} P_{i,j-1,n+1} + B_{i,j} P_{i,j,n+1} + C_{i,j} P_{i,j+1,n+1} = D_{i,j,n} \tag{A-8}$$

where:

$$A_{i,j} = T_j - Z_j - Kv_{i,j-\frac{1}{2}} \left(P_{i,j-1,n+\frac{1}{2}} + P_{i,j,n+\frac{1}{2}} \right) \tag{A-9}$$

$$C_{i,j} = T_j + Z_j - Kv_{i,j+\frac{1}{2}} \left(P_{i,j,n+\frac{1}{2}} + P_{i,j+1,n+\frac{1}{2}} \right) \tag{A-10}$$

$$B_{i,j} = X_{i,j} - A_{i,j} - C_{i,j} \tag{A-11}$$

$$\begin{aligned} D_{i,j,n} = & \left[X_j + Z_j - T_j - P_{i,j,n} \left(Kv_{i,j-\frac{1}{2}} + Kv_{i,j+\frac{1}{2}} \right) \right] P_{i,j,n} \\ & + \left(Z_j + T_j + Kv_{i,j+\frac{1}{2}} P_{i,j+1,n} \right) P_{i,j+1,n} + \left(Kv_{i,j-\frac{1}{2}} P_{i,j-1,n} + T_j \right. \\ & \left. - Z_j \right) P_{i,j-1,n} + \frac{2}{\Delta y^2} \left(N_j + \frac{M_j}{\Delta v} \right) \left[Ky_{i+\frac{1}{2},j} \left(P^2_{i+1,j,n} - P^2_{i,j,n} \right) \right. \\ & \left. - Ky_{i-\frac{1}{2},j} \left(P^2_{i,j,n} - P^2_{i-1,j,n} \right) \right] - \left[Ky_{i+\frac{1}{2},j+1} \left(P^2_{i+1,j+1,n} - P^2_{i,j+1,n} \right) \right. \\ & \left. - Ky_{i-\frac{1}{2},j+1} \left(P^2_{i,j-1,n} - P^2_{i-1,j-1,n} \right) \right] \left(2M_j / \Delta y^2 \Delta v \right) \end{aligned} \tag{A-12}$$

$$N_j = \left(\Delta v^2 + \frac{\Delta v^4}{3} + \frac{\Delta v^6}{22.5} + \frac{\Delta v^8}{315} \right) e^{2v_j} \left(\frac{r_a}{H} \right)^2 \tag{A-13}$$

$$M_j = \left(\frac{\overline{\Delta V}^4}{3} + \frac{\overline{\Delta V}^6}{11.25} + \frac{\overline{\Delta V}^8}{105}\right) e^{2V_j} \left(\frac{r_e}{H}\right)^2 \tag{A-14}$$

$$T_j = \left(\frac{\overline{\Delta V}^2}{6} + \frac{\overline{\Delta V}^4}{7.5} + \frac{\overline{\Delta V}^6}{42}\right) e^{2V_j} / \Delta\theta \tag{A-15}$$

$$X_j = 2\left(\overline{\Delta V}^2 + \frac{\overline{\Delta V}^4}{3} + \frac{\overline{\Delta V}^6}{22.5} + \frac{\overline{\Delta V}^8}{315}\right) e^{2V_j} / \Delta\theta \tag{A-16}$$

$$Z_j = \left(\frac{\overline{\Delta V}^4}{3} + \frac{\overline{\Delta V}^6}{11.25} + \frac{\overline{\Delta V}^8}{105}\right) e^{2V_j} / \Delta V \Delta\theta \tag{A-17}$$

The iterative equation in the y-direction was re-derived to include $\frac{\partial^3 p}{\partial y^2 \partial \theta}$ and $\frac{\partial^3 p^2}{\partial y \partial v^2}$. When written in the form of equation (A-8), the coefficients are

$$A_{i,j} = \frac{\overline{\Delta y}^2}{\Delta\theta}\left(\frac{H}{r_e}\right)^2 - K_{y_{i-\frac{1}{2},j}}\left(P_{i-1,j,n+\frac{1}{2}} + P_{i,j,n+\frac{1}{2}}\right) \tag{A-18}$$

$$C_{i,j} = \frac{\overline{\Delta y}^2}{\Delta\theta}\left(\frac{H}{r_e}\right)^2 - K_{y_{i+\frac{1}{2},j}}\left(P_{i+1,j,n+\frac{1}{2}} + P_{i,j,n+\frac{1}{2}}\right) \tag{A-19}$$

$$B_{i,j} = 2\,\frac{\overline{\Delta y}^2}{\Delta\theta} - A_{i,j} - C_{i,j} \tag{A-20}$$

$$\begin{aligned} D_{i,j,n+1} = {} & 2\frac{\overline{\Delta y}^2}{\Delta\theta}\left(\frac{H}{r_e}\right)^2 P_{i,j,n+1} + \left[\frac{\overline{\Delta y}^2}{6\Delta\theta}\left(\frac{H}{r_e}\right)^2 + K_{y_{i+\frac{1}{2},j}}\left(P_{i+1,j,n+1}\right.\right. \\ & \left.\left. + P_{i,j,n+1}\right)\right]\left(P_{i+1,j,n+1} - P_{i,j,n+1}\right) + \left[\frac{\overline{\Delta y}^2}{6\Delta\theta}\left(\frac{H}{r_e}\right)^2\right. \\ & \left. + K_{y_{i-\frac{1}{2},j}}\left(P_{i-1,j,n+1} + P_{i,j,n+1}\right)\right]\left(P_{i-1,j,n+1} - P_{i,j,n+1}\right) \\ & + \frac{2}{e^{2V_j}}\left(\frac{\Delta y}{\Delta V}\right)^2\left[K_{v_{i,j+\frac{1}{2}}}\left(P^2_{i,j+1,n+1} - P^2_{i,j,n+1}\right)\right. \\ & \left. - K_{v_{i,j-\frac{1}{2}}}\left(P^2_{i,j,n+1} - P^2_{i,j-1,n+1}\right)\right] \end{aligned} \tag{A-21}$$

When these equations were applied to a 27-layer system, the pressure gradients were inverted near the wellbore. That is, the pressure at the top of the formation would be slightly above the original pressure. The pressures would increase in magnitude in the vertical direction until the completion interval was reached. There it would drop sharply. The pressure gradient in t . vertical direction became corrected after the first 6 columns (equivalent to 0.6 feet from the wellbore). The pressure gradient in the completion interval appeared normal. As the calculations progressed, these abnormal pressure values about the wellbore became more unrealistic. Therefore, the equations were altered in an attempt to correct this condition.

The iterative equation in the v-direction was altered to include the $\frac{\partial^{10} p^2}{\partial v^{10}}$ and correct the expression for $\frac{\partial^3 p^2}{\partial v \partial y^2}$. This entailed changing the coefficients

$$N_j = \left(\overline{\Delta V}^2 + \frac{\overline{\Delta V}^4}{3} + \frac{\overline{\Delta V}^6}{22.5} + \frac{\overline{\Delta V}^8}{315} + \frac{\overline{\Delta V}^{10}}{7087.5}\right) e^{2v_j} \left(\frac{r_e}{H}\right)^2 \tag{A-22}$$

$$M_j = \left(\frac{\overline{\Delta V}^4}{3} + \frac{\overline{\Delta V}^6}{11.25} + \frac{\overline{\Delta V}^8}{105} + \frac{\overline{\Delta V}^{10}}{1771.9}\right) e^{2v_j} \left(\frac{r_e}{H}\right)^2 \Big/ \Delta v\, \overline{\Delta y}^2 \tag{A-23}$$

$$T_j = \left(\frac{\overline{\Delta V}^2}{6} + \frac{\overline{\Delta V}^4}{7.5} + \frac{\overline{\Delta V}^6}{42} + \frac{\overline{\Delta V}^8}{506.3}\right) e^{2v_j} \Big/ \Delta\theta \tag{A-24}$$

$$X_j = 2\left(\overline{\Delta V}^2 + \frac{\overline{\Delta V}^4}{3} + \frac{\overline{\Delta V}^6}{22.5} + \frac{\overline{\Delta V}^8}{315} + \frac{\overline{\Delta V}^{10}}{7087.5}\right) e^{2v_j} \Big/ \Delta\theta \tag{A-25}$$

$$Z_j = \left(\frac{\overline{\Delta V}^4}{3} + \frac{\overline{\Delta V}^6}{11.25} + \frac{\overline{\Delta V}^8}{105} + \frac{\overline{\Delta V}^{10}}{1771.9}\right) e^{2v_j} \Big/ \Delta v \Delta\theta \tag{A-26}$$

$$D_{i,j,n} = \left[X_j + Z_j - T_j - P_{i,j,n}\left(Kv_{i,j+\frac{1}{2}} + Kv_{i,j-\frac{1}{2}}\right)\right] P_{i,j,n} + \left(Z_j + T_j + Kv_{i,j+\frac{1}{2}} P_{i,j+1,n}\right) P_{i,j+1,n} - \left(Z_j - T_j - Kv_{i,j-\frac{1}{2}} P_{i,j-1,n}\right) P_{i,j-1,n}$$
$$+ \frac{2}{\Delta y^2} N_j \left[Ky_{i+\frac{1}{2},j}\left(P^2_{i+1,j,n} - P^2_{i,j,n}\right) - Ky_{i-\frac{1}{2},j}\left(P^2_{i,j,n} - P^2_{i-1,j,n}\right)\right]$$
$$+ M_j \left[Ky_{i+\frac{1}{2},j+1}\left(P^2_{i+1,j+1,n} - P^2_{i,j+1,n}\right) - Ky_{i+\frac{1}{2},j-1}\left(P^2_{i+1,j-1,n} - P^2_{i,j-1,n}\right) - Ky_{i-\frac{1}{2},j+1}\left(P^2_{i,j+1,n} - P^2_{i-1,j+1,n}\right) + Ky_{i-\frac{1}{2},j-1}\left(P^2_{i,j-1,n} - P^2_{i-1,j-1,n}\right)\right] \qquad \text{(A-27)}$$

The iterative equation in the y-direction was altered to drop the term $\frac{\partial^3 p}{\partial y^2 \partial \theta}$ in hopes of eliminating the inverted pressure gradient. The coefficients of equation (A-8) are

$$A_{i,j} = -Ky_{i-\frac{1}{2},j}\left(P_{i-1,j,n+\frac{1}{2}} + P_{i,j,n+\frac{1}{2}}\right) \qquad \text{(A-28)}$$

$$C_{i,j} = -Ky_{i+\frac{1}{2},j}\left(P_{i,j,n+\frac{1}{2}} + P_{i+1,j,n+\frac{1}{2}}\right) \qquad \text{(A-29)}$$

$$B_{i,j} = \frac{\overline{\Delta y}^2}{\Delta \theta}\left(\frac{H}{r_a}\right)^2 - A_{i,j} - C_{i,j} \qquad \text{(A-30)}$$

$$D_{i,j,n+1} = \frac{\overline{\Delta y}^2}{\Delta \theta}\left(\frac{H}{r_a}\right)^2 P_{i,j,n+1} + \left[Kv_{i,j+\frac{1}{2}}\left(P^2_{i,j+1,n+1} - P^2_{i,j,n+1}\right) - Kv_{i,j-\frac{1}{2}}\left(P^2_{i,j,n+1} - P^2_{i,j-1,n+1}\right)\right]\left(\frac{\Delta y}{\Delta v}\right)^2\left(\frac{H}{r_a}\right)^2 \frac{1}{e^{2v_j}} \qquad \text{(A-31)}$$

The improvement resulting from the addition of the term $\frac{\partial^{10} p^2}{\partial v^{10}}$ to the iterative equation in the v-direction was a noticeable reduction in the error build-up around the wellbore during the first iteration. Iterating in the v-direction in subsequent time-steps resulted in the same pressure inversions found through use of the previous set of equations. Negative pressures were calculated for columns one and two when using the equations for the y-direction. This indicated the possibility that the second partial derivatives with respect to v in column one were being evaluated inproperly. Another possibility to be checked was the validity of the boundary equations at the wellbore. Because of the troubles encountered, the number of model divisions in the vertical direction was reduced to 11 in order to conserve computer time. The immediate effect noticed was the size of the initial time-step for which the convergence criteria was satisfied; it increased. This was the first indication that stability of the attempted method was dependent upon the ratio $\Delta v/\Delta y$.

The averaging of $\left(\frac{\partial^2 p^2}{\partial v^2}\right)_{i,j,n}$ and $\left(\frac{\partial^2 p^2}{\partial v^2}\right)_{i,j,n+1}$ was deleted. This entailed changing the coefficients

$$N_j = \left(\overline{\Delta v}^2 + \frac{\overline{\Delta v}^4}{3} + \frac{\overline{\Delta v}^6}{22.5} + \frac{\overline{\Delta v}^8}{315} + \frac{\overline{\Delta v}^{10}}{7087.5}\right) e^{2v_j} \left(\frac{r_e}{H}\right)^2 \Big/ 2 \tag{A-32}$$

$$M_j = \left(\frac{\overline{\Delta v}^4}{3} + \frac{\overline{\Delta v}^6}{11.25} + \frac{\overline{\Delta v}^8}{105} + \frac{\overline{\Delta v}^{10}}{1771.9}\right) e^{2v_j} \left(\frac{r_e}{H}\right)^2 \Big/ 2\Delta v \overline{\Delta y}^2 \tag{A-33}$$

$$T_j = \left(\frac{\overline{\Delta v}^2}{6} + \frac{\overline{\Delta v}^4}{7.5} + \frac{\overline{\Delta v}^6}{42} + \frac{\overline{\Delta v}^8}{506.25}\right) e^{2v_j} \Big/ 2\Delta\theta \tag{A-34}$$

$$X_j = \left(\overline{\Delta v}^2 + \frac{\overline{\Delta v}^4}{3} + \frac{\overline{\Delta v}^6}{22.5} + \frac{\overline{\Delta v}^8}{315} + \frac{\overline{\Delta v}^{10}}{7087.5}\right) e^{2v_j} \Big/ \Delta\theta \tag{A-35}$$

$$Z_j = \left(\frac{\overline{\Delta V}^4}{3} + \frac{\overline{\Delta V}^6}{11.25} + \frac{\overline{\Delta V}^8}{105} + \frac{\overline{\Delta V}^{10}}{1771.9}\right) e^{2V_j} / 2\Delta V \Delta\theta \qquad \text{(A-36)}$$

$$\begin{aligned} D_{i,j,n} = {} & (X_j + Z_j - T_j) P_{i,j,n} + (Z_j + T_j) P_{i,j+1,n} - (Z_j \\ & - T_j) P_{i,j-1,n} + \frac{2}{\Delta y^2} N_j \Big[Ky_{i+\frac{1}{2},j} (P^2_{i+1,j,n} - P^2_{i,j,n}) \\ & - Ky_{i-\frac{1}{2},j} (P^2_{i,j,n} - P^2_{i-1,j,n}) \Big] + M_j \Big[Ky_{i+\frac{1}{2},j} (P^2_{i+1,j+1,n} \\ & - P^2_{i,j+1,n} - P^2_{i+1,j-1,n} + P^2_{i,j-1,n}) - Ky_{i-\frac{1}{2},j} (P^2_{i,j+1,n} \\ & - P^2_{i-1,j+1,n} - P^2_{i,j-1,n} + P^2_{i-1,j-1,n}) \Big] \end{aligned} \qquad \text{(A-37)}$$

The first two time-steps, one in the v-direction and the other in the y-direction, yielded perfect results. There were no oscillations. The pressure terms were symmetrical about the completion interval. After 4 time-steps, there were pressure reversals along the upper and lower boundaries amounting to a maximum of 0.9 psi (original pressure 800 psi) out for a distance of 2.5 feet from the wellbore. At a distance of 8 feet, there was a slight increase in the pressure within the completion interval compared to that of the contiguous cells above and below. This indicated the expression of the derivatives in the y-direction needed improvement. After nine time-steps, the reversal along the boundaries had disappeared. However, the slight inversion of pressures (0.0005 psi) in the vertical direction in columns 21 to 29 marred an otherwise acceptable solution. The system was expanded to include 25 layers in the vertical direction. Again, the time-step sizes for which the convergence criteria was satisfied were smaller. There were slight pressure reversals along the upper and lower boundaries that damped out as the solution progressed. However, at the end of 19 time-steps there were reversals in columns 1 and 2 at the upper and lower boundaries and pressure inversions (0.0008 psi) in columns 21 to 29. This pressure inversion in the y-direction indicated trouble with that equation. Therefore, the $\frac{\partial^3 p}{\partial y^2 \partial \theta}$ was added.

The necessary changes to the equations for the iteration in the y-direction were

$$A_{i,j} = \frac{\overline{\Delta y}^2}{12\Delta\theta}\left(\frac{H}{r_e}\right)^2 - K_{y_{i-1/2,j}}\left(P_{i-1,j,n+1/2} + P_{i,j,n+1/2}\right) \tag{A-38}$$

$$C_{i,j} = \frac{\overline{\Delta y}^2}{12\Delta\theta}\left(\frac{H}{r_e}\right)^2 - K_{y_{i+1/2,j}}\left(P_{i+1,j,n+1/2} + P_{i,j,n+1/2}\right) \tag{A-39}$$

$$\begin{aligned} D_{i,j,n+1} = {} & \frac{\overline{\Delta y}^2}{\Delta\theta}\left(\frac{H}{r_e}\right)^2 P_{i,j,n+1} + \left(\frac{\Delta y}{\Delta v}\right)^2\left(\frac{H}{r_e}\right)^2\Big[K_{v_{i,j+1/2}}\left(P^2_{i,j+1,n+1}\right. \\ & \left. - P^2_{i,j,n+1}\right) - K_{v_{i,j-1/2}}\left(P^2_{i,j,n+1} - P^2_{i,j-1,n+1}\right)\Big] / e^{2v_j} \\ & + \frac{\overline{\Delta y}^2}{12\Delta\theta}\left(\frac{H}{r_e}\right)^2\Big[K_{y_{i+1/2,j}}\left(P^2_{i+1,j,n+1} - P^2_{i,j,n+1}\right) \\ & - K_{y_{i-1/2,j}}\left(P^2_{i,j,n+1} - P^2_{i-1,j,n+1}\right)\Big] \end{aligned} \tag{A-40}$$

The reversals along the wellbore were improved but the pressure inversions along the completion interval starting in cell 20 did not. Failure to meet the convergence criteria was predominately located in the matrix row containing the producing interval in some column beyond the initial inversion point. Several attempts to reduce the contribution of the vertical derivative were made by applying a constant, or automatically decreasing, multipliers. This only moved the instability in toward the wellbore.

Additional experience obtained from making calculations using the one-dimensional model indicated that the boundary equation (A-5) was not stable for very small time-steps. Since some of the runs where the pressure gradient reached the drainage had instability problems at that point, the outer boundary equation was changed

$$P^2_{i,m+1,n+1} - P^2_{i,m,n+1} = 0 \tag{A-41}$$

Still the instability problems remained.

Other methods were tried including iterating in both directions to calculate the pressure at each time-step. None of these methods yielded suitable time-step sizes for a reasonable convergence criteria. Because of the predominant trouble in iterating in the vertical direction, the method presented in Chapter II was developed.

TABLE XI

SYSTEM USED IN CALCULATING PRESSURES BY THE ALTERNATING-DIRECTION-IMPLICIT METHOD

Area of Drainage, acres	640
Formation Thickness, ft	26
Porosity, per cent	12
Horizontal Permeability, md	1
Vertical Permeability, md	1
No. Model Cells, radial	36
No. Model Cells, vertical	15
Total Number Model Cells	540
Producing Rate, MCFD	100
Wellbore Radius, ft	0.3
Initial Reservoir Pressure, psi	800
Standard Pressure, psia	15.025
Formation Temperature, °F	100
Standard Temperature, °F	60

Time Step Sequence No.	Time-Step Size (10^{-5}) Days									
1-10	.00	.00	.00	.00	.01	.01	.01	.01	.01	.01
11-20	.02	.02	.02	.03	.03	.03	.05	.05	.05	.08
21-30	.08	.08	.12	.12	.12	.20	.20	.20	.32	.32
31-40	.32	.22	.14	.14	.14	.14	.23	.23	.23	.37
41-50	.37	.37	.26	.26	.17	.17	.17	.17	.27	.27
51-60	.27	.43	.43	.43	.20	.20	.20	.20	.31	.21
61-70	.21	.21	.21	.14	.14	.14	.14	.23	.23	.23
71-80	.37	.37	.24	.24	.16	.16	.16	.16	.25	.25
81-90	.25	.41	.18	.18	.18	.18	.28	.28	.18	.18
91-93	.18	.18	.13							

APPENDIX B

CALCULATION PROCEDURE FOR DETERMINING THE EFFECTIVE PERMEABILITY, EFFECTIVE WELLBORE RADIUS, AND LONG-TERM PREDICTIONS USING SUCCESSION OF STEADY-STATES APPROXIMATION SOLUTION

The predictive equation for Darcy flow was derived (36) and shown to be

$$Q = \frac{B\left[P_d^2 - P_w^2\right]}{\frac{1}{2}\ln t + \frac{1}{2}\ln A} \tag{B-1}$$

where:

$$B = 1.987(10^{-5})(HkT_b)/(\mu P_b T) \tag{B-2}$$

$$A = \frac{0.0139\, k^{+} P_b}{\mu \phi r_w^2} \tag{B-3}$$

$$P_d^2 = \left[\frac{V_t P_o}{V_{t=0}}\right]^2 \tag{B-4}$$

$$V_{t=0} = \pi r_e^2 H \phi P_o T_b/(1000 P_b T) \tag{B-5}$$

$$V_t = 1 - Qt \tag{B-6}$$

Since we have chosen to plot the data on $\log_{10}$ paper, equation (B-1) converted to that base is

$$\frac{2.303}{2B}(\log t + \log A) = (P_d^2 - P_w^2)/Q \tag{B-7}$$

The slope of the curve is

$$\frac{d\left[(P_d^2-P_w^2)/Q\right]}{d(\log t)} = \frac{2.303}{2B} \tag{B-8}$$

In order to evaluate B between times t_1 and t_2, we use the equation

$$\frac{\left[(P_d^2-P_w^2)/Q\right]_2-\left[(P_d^2-P_w^2)/Q\right]_1}{\log t_2 - \log t_1} = \frac{2.303}{2B} \tag{B-9}$$

Where the points 1 and 2 are taken off the best straight line through the data, all other factors being equal, more weight should be given the later points.

From B we obtain the effective permeability from equation (B-2) as all other parameters are known. In order to find the effective wellbore radius, we must first find A by evaluating equation (B-4) at a specific time in the interval t_1-t_2 using the slope determined from equation (B-9). The effective wellbore radius can then be determined from equation (B-3).

For predictive purposes, two forms of equation (B-1) are required. Equation (B-1) is the correct form for times less than or equal to stabilization time. Stabilization time (36) is calculated by the equation

$$\ln(t_s) = 2\ln\left(\frac{0.5\,r_e}{r_w}\right) - \ln\left(\frac{0.0139\,k\,P_o}{\mu\,\phi\,r_w^2}\right) \tag{B-10}$$

For times larger than the stabilization time, the denominator of equation (B-1) must be replaced by the term 2.303 log $\left(\frac{0.5r_e}{r_w}\right)$ to give

$$2.303\log\left(\frac{0.5\,r_e}{r_w}\right) = (P_d^2 - P_w^2)/Q \tag{B-11}$$

Repeated use of equation (B-11) permits continuance of the calculations until a pre-determined cut-off wellbore pressure or elapsed time period has been reached.

APPENDIX C

NOMENCLATURE

A = constant defined by equation (B-3)

$A_{i,j}$ = constant coefficient of $P_{i,j-1}$ term in equation (66) at every (i,j) grid point, defined by equation (61) for every iteration (time step n+1/2)

B = constant defined by equation (B-2)

$B_{i,j}$ = constant coefficient of $P_{i,j}$ term in equation (66) at every (i,j) grid point, defined by equation (62) for every iteration (time step n+1/2)

C_1 = coefficient defined by equation (1); $MCFD/(psi^2)^n$

$C_{i,j}$ = constant coefficient of $P_{i,j+1}$ term in equation (66) at every (i,j) grid point defined by equation (63) at every iteration (time step n+1/2)

$D_{i,j,n}$ = constant coefficient at every (i,j) grid point defined by equation (57) at every time step n

$D_{i,j,n+1/2}$ = constant coefficient at every (i,j) grid point defined by equation (65) at every iteration (time step n+1/2)

E_1 = convenience term for separating long equation into two parts

e = base of natural logarithms

$f(r,z)$ = radial permeability function—two spatial dimensions, md

$g(r,z)$ = vertical permeability function—two spatial dimensions, md

$g_{i,j}$ = constant coefficients at every (i,j) grid point, defined by equation (75) at every iteration (time step n+1/2)

H = thickness of formation, ft

h_1 = upper limit of completion interval, ft

h_2 = lower limit of completion interval, ft

k = equivalent one-dimensional radial permeability, md

k_r = radial permeability of producing formation, md

$(k_{r_w})_{h_1-h_2}$ = permeability at the wellbore in the interval h_1-h_2, md

k_v = radial permeability in logarithmically transformed coordinates, md

k_y = linearly transformed vertical permeability, md

k_z = vertical permeability, md

K_{avg} = average radial permeability, md

K_v = dimensionless radial permeability

K_y = dimensionless vertical permeability

M = constant multiplier for convergence criteria, dimensionless

M_j = coefficient of term $\frac{\partial^3 P^2}{\partial y^2 \partial v}$ as defined by equations (A-14), (A-23), and (A-33)

n = dimensionless number, nth term in series expansion

N_j = coefficient of term $\frac{\partial^3 P}{\partial y^2 \partial \Theta}$ as defined by equations (A-13), (A-22), and (A-32)

n_p = exponent of equation (1)

p = pressure, psia

P = dimensionless pressure, p/P_o

P_b = pressure base, psia

P_d = mid-formation average bulk pressure of reservoir defined by equation (B-4)

P_o = original reservoir pressure, psia

P_w = pressure at the wellbore, psia

Δp = convergence criteria, dimensionless

q = producing rate, MCFD measured at P_b and T_b

Q = producing rate, MCFD

$\overline{Q}$ = dimensionless flow rate defined by equation (16)

r = radius, ft

R = ideal gas constant, 10.73 psia (cu ft)/lb mol)(°R)

r_e = radius of drainage area, ft

R_{ml} = remainder obtained from combining terms according to equation (35)

R_m = remainder obtained from Taylor's Series expansion

r_w = wellbore radius, ft

T_R = formation temperature °R

t = time, days

Δt = time measured from shut-in, days

T = total producing time prior to shut-in for pressure build-up, days

T_b = temperature base °F

T_f = formation temperature °F

$T_{i,j}$ = constant coefficients at every (i,j) grid point, defined by equation (53)

T_s = standard temperature °F

t_s = time at which well stabilizes, days

v = logarithmically transformed spatial dimension defined by equation (10)

Δv = incremental dimensionless distance in radial direction

V = volume of gas contained in drainage area of well initially, MSCF measured at P_b and T_b

$\bar{v}_r$ = superficial velocity in r direction, ft/sec

$\bar{v}_\theta$ = superficial velocity in θ direction, ft/sec

$\bar{v}_z$ = superficial velocity in z direction, ft/sec

$W_{i,j}$ = constant coefficients at every (i,j) grid point, defined by equation at every iteration (time step n+1/2)

$X_{i,j}$ = constant coefficients at every (i,j) grid point, defined by equation (51)

y = dimensionless vertical spatial variable, y = x/H

Δy = incremental dimensionless distance in vertical direction

z = vertical distance, ft

$Z_{i,j}$ = constant coefficients at every (i,j) grid point, defined by equation (52)

γ = density of gas, lb/cu ft

ϵ = error residual at any matrix point (i,j)

θ = dimensionless time, $\theta = (P_o K_{avg} t)/(2\phi\mu)$

$\Delta\theta$ = incremental change in dimensionless time

μ = gas viscosity, cp

π = pure number, 3.1416

σ = function (or constant) for separating equation (14) into 2 parts

ϕ = porosity (effective), dimensionless

$\nabla = \frac{\partial}{\partial x} + \frac{\partial}{\partial y} + \frac{\partial}{\partial z}$